FABRICATION OF DOUBLE MESA STRUCTURES FROM SUPERCONDUCTING $Bi_2Sr_2CaCu_2O_{8+d}$ BY E-BEAM LITHOGRAPHY FOR TERAHERTZ EMISSION

A Thesis submitted to
the Graduate School of Engineering and Sciences of
İzmir Institute of Technology
in Partial Fulfillment of the Requirements for the Degree of

MASTER OF SCIENCE

in Physics

by
Yasemin DEMİRHAN

July 2011
İZMİR

We approve the thesis of **Yasemin DEMİRHAN**

Assoc. Prof. Lütfi ÖZYÜZER
Supervisor

Prof. Ekrem YANMAZ
Committee Member

Prof. Dogan ABUKAY
Committee Member

7 July 2011

Prof. Nejat Bulut
Head of the Department of Physics

Prof. Durmuş Ali Demir
Dean of the Graduate School of Engineering and Sciences

ACKNOWLEDGEMENTS

First of all, I would like to express my deepest gratitude to Assoc. Professor Lütfi Özyüzer for giving me the possibility of carrying out this work under his supervision. I appreciate him, for his endless patient, encouragement, understanding and supporting me not only during master education but also during undergraduate education. I learnt a lot from him and I could not have finished this thesis without his inspiring suggestions and constant guidance, and I hope that I also have acquired some of his scientific thinking along the way.

I would like to acknowledge Prof. Kazuo Kadowaki for providing us high quality Bi2212 single crystals.

I wish to extend my thanks to İzmir Institute of Technology for providing Research Assistantship throughout my graduate study.

I would like to thank also the members of my thesis defense committee Prof. Ekrem Yanmaz and Prof. Dogan Abukay for helpful comments and giving suggestions.

As teamwork is essential, I am very thankful to my lab mates, Zeynep Meriç, Hilal Sağlam, Mutlu Devran Yaman, Mehmet Ali Olgar and Hakan Alaboz for their kindness, support while studying together, especially Zeynep Meriç for her encouragement and creating a nice and funny environment in laboratory studies.

Also I am greatly indebted to my friends who are Fulya Köseoğlu and Hasan Köseoğlu for their helps and for their warm friendship during the past eight years.

Personally, my special thanks go to my precious old friends, Melis Ünal and Seda Gürer for their encouragement and friendship.

Thanks to each of my friends at Izmir Institute of Technology for providing a great atmosphere and a wonderful workplace. We have unforgettable memories at the end of three years and now each of them is very important for me. Especially, Atike İnce, Nesli Yagmurcukardes and Gözde Tunusoğlu have always been by my side.

Last, but not least I want to thank my family for their unconditional love, unending support and understanding me during my whole life and providing me with more than I can ever repay them for.

ABSTRACT

FABRICATION OF DOUBLE MESA STRUCTURES
FROM SUPERCONDUCTING $Bi_2Sr_2CaCu_2O_{8+d}$
BY E-BEAM LITHOGRAPHY
FOR TERAHERTZ EMISSION

Terahertz radiation is part of the electromagnetic spectrum lying between microwaves and the far-IR. This region has frequencies ranging from 0.1 – 10 THz and wavelengths from 3 mm to 0.03 mm. We work on a frequency tunable solid state device to meet the needs of continuous, coherent, powerful terahertz emission sources that fill practically important terahertz gap. Among the cuprates, single crystal of $Bi_2Sr_2CaCu_2O_{8+\delta}$ (Bi2212) is a potential candidate of compact solid state devices designed for generating electromagnetic waves in terahertz frequency range. Bi2212 crystals are consisting of natural arrays in the form of identical layers called intrinsic Josephson junctions (IJJ). In this study, under optimized doping conditions we aimed to investigate powerful terahertz emission. THz emission in the μW range can be obtained fabricating rectangular-shaped mesa structures on the Bi2212 crystal. In the experimental procedure, in order to obtain various doping levels, we annealed the high temperature superconducting Bi2212 single crystals at various temperatures in vacuum or under argon flow. By using the thermal evaporation, optic and electron beam lithography, ion beam etching techniques single and double mesa structures were fabricated. For the e-beam lithography process, we optimized and improved the required parameters. After the mesa fabrication, the exact dimensions of the mesas were obtained using surface profilometer and atomic force microscope. In order to characterize the Bi2212 mesas, by three probe contact *c*-axis resistance versus temperature (*R–T*), and current–voltage behavior (*I –V)* were measured in a He flow cryostat. Some of the hysteretic quasiparticle branches are seen in the I–V characteristics of Bi2212 crystals.

ÖZET

TERAHERTZ IŞIMASI İÇİN E-DEMETİ LİTOGRAFİ İLE SÜPERİLETKEN $Bi_2Sr_2CaCu_2O_{8+d}$'DEN ÇİFT MESA YAPILARIN ÜRETİMİ

Terahertz ışıması, elektromagnetik spektrumun mikrodalgalar ile uzak-IR arasında yer alan bölümüdür. Bu bölge 0,1 – 10 THz frekans aralığına ve 3 mm den 0,03 mm ye dalga boyu aralığına sahiptir. Uygulamada önemli terahertz boşluğunu dolduracak sürekli uyumlu ve güçlü terahertz ışıma kaynaklarının gereksinimi karşılayan, frekansı ayarlanabilir katıhal aygıtları üzerinde çalışıyoruz. Kupratler arasında, $Bi_2Sr_2CaCu_2O_{8+\rho}$ (Bi2212)nin tek kristali terahertz frekans bölgesinde elektromagnetik dalgalar oluşturması için tasarlanan kompakt katı hal aygıtlarına potansiyel bir adaydır. Bi2212 kristalleri, özgün Josephson eklemleri (ÖJK) olarak adlandırılan özdeş tabakalar şeklinde doğal dizilimlerden oluşmaktadırlar. Bu çalışmada, optimize edilmiş doping koşulları altında, güçlü terahertz emisyonunu araştırmayı amaçladık. μW mertebesinde THz emisyonu, dikdörtgensel şekillendirilmiş mesa yapılarının Bi2212 kristalleri üzerine fabrikasyonu ile elde edilebilirler. Deneysel prosedürde, farklı doping seviyelerini elde etmek için, yüksek sıcaklık süperiletkeni Bi2212 kristallerini farklı sıcaklıklarda vakum veya argon akımı içinde tavladık. Termal evaporasyon, optik ve elektron demet lithografi, iyon demet aşındırma teknikleri kullanılarak tek ve ikişerli mesa yapıları üretildi. e-demet lithografi yöntemi için gerekli parametreleri optimize ettik ve geliştirdik. Mesa fabrikasyonundan sonra, mesaların gerçek boyutları, yüzey profilometresi ve atomik kuvvet mikroskobu kulanılarak elde edildi. Bi2212 mesalarını karakterize etmek için üç prob kontağı ile c-ekseni direncine karşı sıcaklık (R-T) ve akım-voltaj (I – V) davranışları He akım kriyostatında ölçüldü. Bazı histeretik kuaziparçacık dallanmaları Bi2212 kristallerinin I – V karakteristiklerinde görülmektedir.

TABLE OF CONTENTS

LIST OF FIGURES

Figure **Page**

LIST OF TABLES

Table **Page**

CHAPTER 1

TERAHERTZ WAVES

1.1. Introduction

The electromagnetic spectrum is defined as the region of all observed frequencies of electromagnetic radiation. The characteristic distribution of electromagnetic radiation emitted or absorbed by any particular object is named as the "electromagnetic spectrum" of that object. Starting from low frequencies where modern radio to gamma radiation at the short-wavelength end is taking place, the electromagnetic spectrum extends to wavelengths from thousands of kilometers down to a fraction of the size of an atom. In this spectrum, the upper limit is the size of the universe, where as the short wavelength limit is in the neighborhood of the Planck length, however the spectrum is considered to be infinite and continuous.

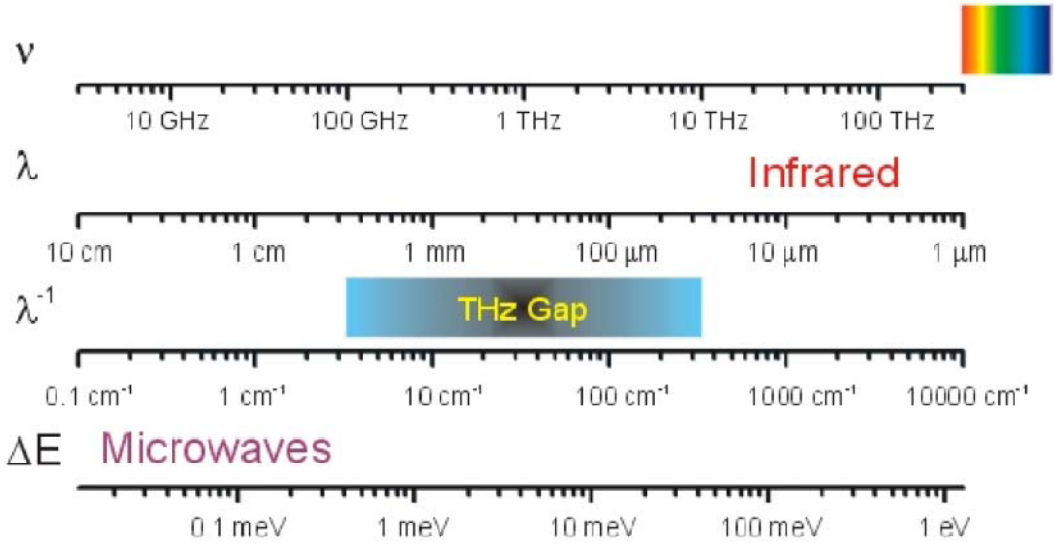

Figure 1.1. The electromagnetic spectrum with THz gap

In principal, Electromagnetic (EM) waves are defined by one of the three physical properties; namely frequency f, wavelength λ, or energy E(photon energy). In this description, range of the frequencies starts from 2.4×10^{23} Hz (i.e. 1 Get gamma rays) going down to the local plasma frequency of the ionized interstellar medium (~1 kHz). As it is well known, wavelength is inversely proportional to the frequency,

consequently gamma rays have very short wavelengths which are on the order of atomic size. However, wavelengths can be as long as the size of the universe. On the other hand, there is a direct proportionality between the photon energy and the wave frequency which leads to the fact that gamma rays have the highest energy (about a billion electron volts) mean while radio waves have very low energy (around feta electron volts). The classification of EM radiation is usually given by using the wavelength namely; radio waves, microwaves, infrared region, visible region (light), ultraviolet region, X-rays and finally gamma rays. Where terahertz radiation is taking part in the spectrum is a region between far infrared and microwaves.

1.2. THz radiation

Electromagnetic radiation which is in the frequency range of 300 gigahertz = 3×10^{11} Hz to 3 terahertz = 3×10^{12} Hz is named as terahertz radiation. In this definition, 1 THz = 1012 Hz = 1 ps, λ = 300 μm = 0.3 mm, which reveals the fact that this radiation is between the microwave region and the infrared region. Consequently, this region is a transition region from electronics to the optics where the photon energy corresponding to 1 THz (10^{12} Hz) is 4.1 meV (33.33 cm^{-1}). There exists other definitions for terahertz radiation namely submillimeter radiation, terahertz waves, terahertz light, T-rays, T-light, T-lux and THz. In the literature, this spectral region where terahertz radiation is taking place has been considered as the last remaining region in the electromagnetic spectrum. In the last decade, scientists have paid much more attention to this newly explored region ("THz gap") which has scientific and technological importance. This region, namely 'terahertz gap' requires new scientific work to develope convenient and inexpensive sources, detectors, other components for the manipulation of terahertz waves.

1.3. Applications of the THz Radiation

Some of the many areas where terahertz radiation is used are; imaging pills in pharmaceuticals, scientific research conducted in material characterization in the universities, and defense related issues for the government. Some other commercial related areas are; T-ray imaging, dentistry (detection of tooth decay), terahertz time

domain spectroscopy, medical diagnostics (early detection of skin cancer), pharmaceutical process control (pill inspection).

Terahertz radiation has a unique characteristic which is not found in other regions of the spectrum. THz waves have low photon energies (1 THz = 4.1 meV, one million times weaker than X-rays) and do not cause harmful photoionization in biological tissues (Kawase 2004). Moreover Terahertz radiation is absorbed by water, thus it can also be used to detect differences in water content and density of a tissue. Interaction of terahertz waves with living tissues gives us the chance to detect the early signs of tooth decay and skin or breast cancer, or understanding dynamical properties of cell using a safer and less in painful system with the help of imaging. Terahertz radiation has the ability to penetrate into materials that are usually opaque with both visible and infrared radiation. This property makes these waves very interesting for the scientists.

Terahertz waves can pass through the materials such as fog, clothing, fabrics, plastics, wood, paper and ceramic. The frequency of Terahertz waves matches with the frequency of the motion of a great number of molecules in many chemical and biological materials.

In these materials, the transmitted and reflected THz spectra contain THz absorption informations characterizing the THz vibrational modes and provide important spectroscopic information (Fischer, et al. 2005). Terahertz spectroscopy technique is particularly useful for pharmaceutical applications where the structure of drugs has to be rapidly and precisely identified. Considering these advantages, THz technologies are nowadays very important methods in searching for hidden explosives, chemical/biological threats and defects in defense and security applications (Arnone, et al. 1999). Moreover, there exists a potential application in ultra-high bandwidth wireless communication networks, vehicle control, atmospheric pollution monitoring and inter-satellite communication (Tonouchi 2007).

In this technology arena, lots of application areas are envisioned which is discussing below is listed as a summary. These are;

Airport screening of passengers for weapons, explosives, drugs or other contraband

- Secure wireless communications
- Cancer detection
- Imaging in dentistry

- Biochip analysis of DNA, proteins and other biological materials
- Detection of chemical and biological warfare agents
- Detection of land mines and buried explosive devices
- Measuring the water content of food to detect spoilage
- Inspecting finished products through packaging
- Determining the thickness of a layer of paint while it is still wet
- Quality control of insulated wires during manufacture
- Inspecting semiconductor wafers for defects

Some images about the some part of the applications of THz radiation area shown in the Figure 1.2.

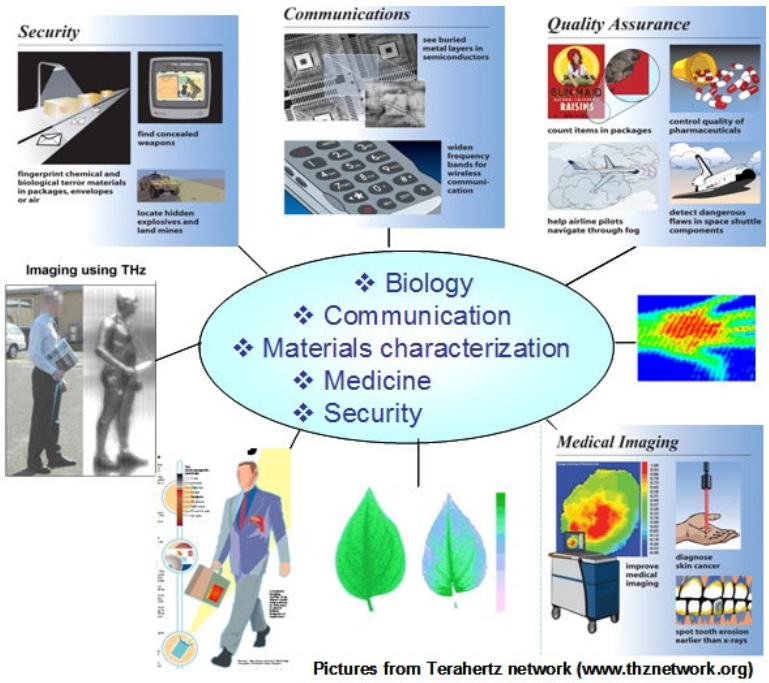

Figure 1.1. Some of the applications of THz radiation

1.3. Terahertz Radiation from High Temperature Superconductors

Far-infrared studies have occurred since the invention of the bolometer in 1881 by astronomer Samuel Langley. Much of the early far-infrared work was done by Rubens, who discovered reststrahlen sources enabling measurements crucial to Planck's blackbody radiation theory. At the begining of 1960s, important advantages of working

with the THz radiation was well understood by the scientists however adequate radiation sources and suitable detectors for the scientific investigations did not exist since the terahertz technology has not been developed up to that time. In the next decade, the word 'Terahertz' had been frequently used in scientific papers and some research workers started to introduce microwave and optical techniques in their THz experiments. Far-infrared transmission studies of superconductors confirmed the energy gap predicted by Bardeen, Cooper, and Schrieffer's superconductivity theory. In the practical applications, solid-state terahertz wave sources are required which emission power. Quantum cascade lasers used as CW sources which operate only above 1.2 THz are available (Wade, et al. 2009). Gunn diodes have low output powers. At higher frequencies, backward wave oscillators are bulky and have also low output power.

On the other hand, THz gas lasers which are optically-pumped are bulky but not tunable. Free THz gas lasers electron lasers are the most powerful sources available, producing either CW or pulsed beams of coherent THz waves (Saldin, et al. 2000). However, their size and high cost do not allow them to be used in practical applications. Schottky diodes are compact devices but their frequency agility is not so good and again not suitable for practical applications since cost is very high. The solution is high temperature superconductor Bi2212 single crystals which could provide us to overcome the limitations met in the other sources.

These crystals are made up of stacks of Josephson junctions which exhibit a unique electrical property namely, the Josephson Effect. When an external voltage is applied, an alternating current will flow back and forth across the junctions at a frequency proportional to the strength of the voltage. These alternating currents in turn produce electromagnetic fields and the frequency is tuned by the applied voltage. A voltage even as small two mVs per junction can induce frequencies in the terahertz range.

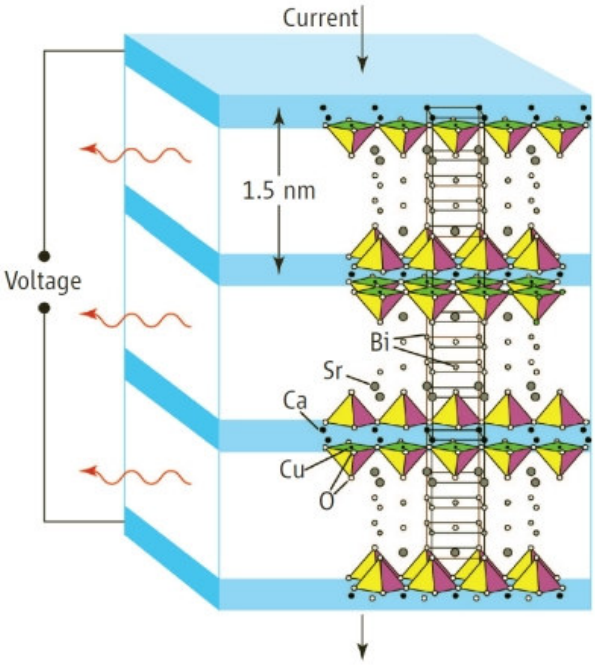

Figure 1.3. Schematic view of high temperature superconductor Bi2212 single crystals (Source: Kleiner, et al. 2007)

1.4. THz Waves Generation from $Bi_2Sr_2CaCu_2O_{8+\delta}$

There is a growing interest in and technology of electromagnetic waves in terahertz frequency region (0.1-10 THz) due to their variety of application areas in the physical, astronomical, medical and biological sciences, including imaging, spectroscopy, information technology, environmental monitoring and medical diagnosis (Tonouchi, et al. 2007). However, these applications have been limited by the scarcity of inexpensive compact solid-state sources of powerful continuous wave (CW) THz radiation.

The ac Josephson effect occurring between two superconducting electrodes separated by a thin insulating layer provides a unique way to develop voltage-tunable generators of electromagnetic radiation in the terahertz frequency range. When a bias voltage is applied to a Josephson junction, it behaves as a source of high-frequency electromagnetic radiation whose frequency is governed by the ac Josephson relation $f_{Jos}= V/\Phi_0$, where V is the voltage across the junction and Φo is flux quantum. Therefore, 1 mV corresponds to 0.483 THz. However, the operation frequency is restricted by the superconducting gap so it cannot exceed several hundred gigahertz for the devices made of conventional superconductors (Ozyuzer, et al. 2007). Radiation

from a Josephson junction directly in the microwave frequency range has been detected a long time ago (Yanson, et al. 1996; Langenberg, et al. 1965). However, radiation power is limited to the pW range (Langenberg, et al. 1965; Dmitrenko, et al. 1965) and it is too small for practical applications. Since a significant effort has been devoted to develop JJ arrays as coherent sources of radiation (Jain et al. 1984, Lukens 1990; Barbara, et al. 1999). A major challenge is to force all JJs in array to emit coherently, so that total emitted power increases proportionally to the square of the total number of junctions in the array (Jain, et al. 1984). Artificial junctions always have slightly different junction parameters, especially the Josephson critical current. This leads to desynchronization and dramatic drop in emission power. Therefore, the major challenge is to synchronize Josephson oscillations in all junctions. Also, as the maximum frequency is limited by the superconducting gap, it cannot exceed several hundred gigahertz for structures fabricated out of conventional superconductors.

Demonstration of intrinsic Josephson effect in layered high temperature superconductors (Kleiner, et al. 1992 and Kleiner and Muller 1994), such as $Bi_2S_2CaCu_2O_{8+d}$ (BSCCO), opened a completely new route to developing electromagnetic sources. Large values of superconducting gap up to 60 meV allow to bring the Josephson frequency into the practically important terahertz range. Moreover, intrinsic JJs (IJJs) have much closer parameters than artificial ones as these parameters are controlled by the atomic crystal structure rather than by amorphous dielectric layer in artificial JJs. Also, layered superconductors provide a very high density of IJJs (1 per 1.56 nm along the c-axis) and thus it is easy to reach super-radiation regime with many junctions on the scale of radiation wave length. There have been many attempts to obtain THz radiation from layered superconductors using IJJ properties. Nevertheless, the same challenge to synchronize oscillations in all junctions also remains for this system.

High-frequency emission of unsynchronized intrinsic junctions has been observed up to 0.5 THz from Bi2212 with a weak power (Batov, et al. 2006). Numerous approaches for synchronizing the junctions have been considered, such as applying a magnetic field to induce coherent Josephson vortex flow (Irie, et al. 1998), inserting the BSCCO crystal into a microwave cavity (Madsen, et al. 2004), the use of shunting elements in parallel to small sized stacks (Wang, et al. 2000), the excitation of Josephson plasma oscillations via heavy quasiparticle injection (Kume, et al. 1999) or the investigation of stimulated emission due to quantum cascade processes (Krasnov

2006). The strategy perhaps investigated most intensively considered the generation of collective Josephson oscillations by a lattice of moving Josephson vortices, exciting electromagnetic cavity resonances inside the stack (Kadowaki, et al. 2006 and Bae, et al. 2007) in order to generate noticeable radiation oscillations induced by the moving lattice have to be in phase in different layers, which is realized only if the moving vortices form a rectangular lattice. However, such a rectangular lattice is usually unstable in most of parameter space (Koshelev and Aranson 2001). In other words, the vortex–vortex interaction favors the triangular lattice that can produce only weak noncoherent radiation.

L. N. Bulaevskii and A. E. Koshelev proposed that mesa with small lateral size and a very large number of junctions (about 10^4) in zero magnetic field can provide high radiation power and efficiency in the THz frequency range (Bulaevskii and Koshelev 2007). They show that in such a design oscillations in different junctions are synchronized by the external electromagnetic radiation field generated by the oscillations them-selves (Bulaevskii and Koshelev 2007). Fabrication of a mesa with such a large number of almost identical junctions is technological challenge of this design.

An experimental breakthrough was achieved in 2007. Ozyuzer et al. succeeded in generating intense, coherent, continuous and monochromatic electromagnetic waves in the THz frequency region emitted from rectangular mesa structures of intrinsic Josephson junctions (IJJ) in $Bi_2Sr_2CaCu_2O_{8+d}$ (Bi2212). The fundamental frequencies of the observed emission were as high as 0.85 THz and radiation power was up to 0.5 μW. In contrast to previous studies, the radiation was detected outside the cryostat after traveling through ambient space. This is only possible since the power emitted from this device is several orders of magnitude stronger than the previous ones. Another striking contrast to the previous results is that emission does not require the application of a magnetic field, considerably simplifying the design of superconducting THz sources. In fact, a single applied dc current leads to the efficient excitation of continuous coherent THz radiation.

The general mechanism for the emission is as follows, when an external current is applied along the c-axis, the ac Josephson current in the resistive state excites a cavity resonance mode of Josephson plasma wave and converted to a terahertz wave at the mesa surfaces.

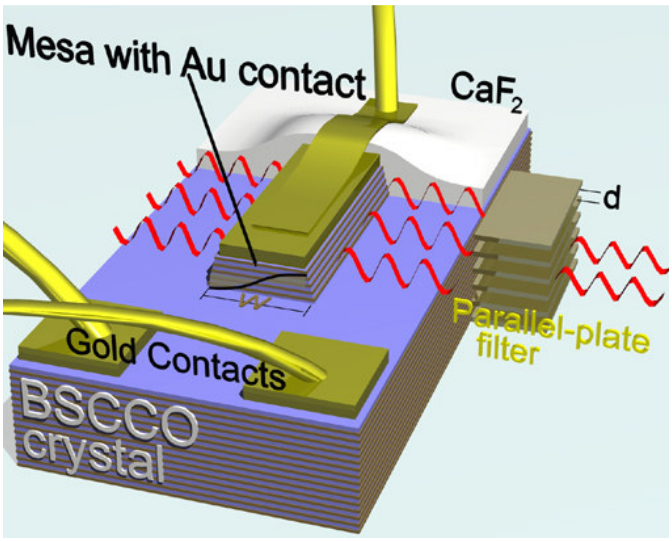

Figure 1.4. Schematic of mesa and electrical contacts on Bi2212 for emission of THz radiation (Source: Ozyuzer, et al. 2007)

The operation of the THz-source is based on the propagation of electromagnetic waves inside the layered BSCCO structure as Josephson plasma modes (Kleiner, et al. 1994). The mode with the highest velocity is the in-phase mode in which all junctions oscillate in-phase and the mode with the lowest velocity is the anti-phase mode in which neighboring junctions oscillate out-of-phase (Figure 2.10a and b). Only the in-phase mode produces noticeable emission because the average electric field on the side surfaces cancels in other modes. In the in-phase mode, the coherent superposition of the electromagnetic waves from each junction creates a macroscopic coherent state in which the radiation power increases as the square of the number of junctions. In mesas with lateral dimensions that are smaller than the propagation distance of the Josephson plasma modes, multiple reflections at the side faces of the mesa create a standing wave pattern and Fabry-Perot type cavity resonances, or Fiske resonances. A resonance condition occurs whenever the Josephson frequency, f_{Jos}, equals the cavity frequency, fcav= $V/(N\Phi_0)$. Here, w is the width of the cavity, V is the voltage applied across the junction stack, Φ_0 is magnetic flux quantum, and N is the number of active junctions in the stack. As the resonance condition is approached, for example by scanning the applied voltage, energy is pumped into the cavity resonance. As the cavity field builds up it entrains the oscillations of more junctions leading to a further increase of the cavity field until (almost) all the junctions are synchronized into a coherent in-phase oscillation accompanied by a large cavity field. This process resembles the emergence

of coherence in a laser cavity. Furthermore, the resonance condition implies that the emission frequency can be controlled by the mesa width according to f~1/w.

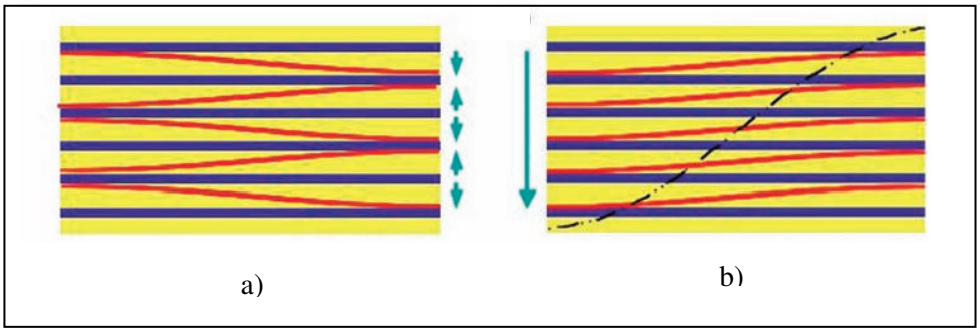

Figure 1.5. Schematics of the anti-phase (a) and of the in-phase (b) mode (Source: Ozyuzer, et al. 2007)

These studies stimulated further work on THz generation from intrinsic Josephson junctions in Bi2212 mesas and recently one order of magnitude larger radiation power (5 μW) and higher harmonics (up to fourth order, corresponding to 2.5 THz) have been obtained (Kadowaki, et al. 2008). Tunability of the THz emission and local temperature properties have also been studied (Gray, et al. 2009, Kurter, et al. 2009 and Wang, et al 2009). Furthermore dependence of the characteristics of the mesa structures on the oxygen doping level of Bi2212 crystals are also discussed (Ozyuzer et al. 2009). Using low temperature scanning laser microscopy, Wang, et al. 2009 imaged electric field distributions in the junction stack of $Bi_2Sr_2CaCu_2O_{8+d}$. They observed standing electromagnetic waves (cavity resonances), thus provided a direct confirmation of cavity modes observed in the previous experiments. In high bias region where the IV curve is back bending, the authors observed that hot spots with temperature higher than T_c are created, and their positions vary with the external current. It is argued that these hot spots can be used to tune the cavity size, and thus the radiation frequency (Wang, et al. 2009). They reported that as in the low bias regime, also at high bias cavity modes are important for synchronizing the Josephson currents (Wang, et al. 2010). Experimental results clearly demonstrate the validity of the cavity resonance model for the fundamental frequency mode of thin square and cylindrical mesas (Tsujimoto, et al.2010). For cylindrical and rectangular stacks of intrinsic Josephson junctions the primary source of the coherent radiation has been identified as the non linear ac Josephson current, its uniform part acts as electric current density source and the non

uniform part excites one of the linear cavity modes, which sets the wavelength of the fundamental ac Josephson frequency to the appropriate sample dimension and acts as a magnetic surface current density source (Kadowaki, et al.2010). As the synchronized operation of Josephson junctions has been reported previously, for the improvement of the applications synchronized operation between two mesas is also demonstrated (Kadowaki, et al.2010).

CHAPTER 2

THEORETICAL BACKGROUND

In this section, I intend to present a brief background on superconductivity. In solid state physics, superconductivity which is a very interesting phenomenon has a special importance and provides a great interest on the scientists. Soon after the superconductivity is discovered, both theoretical and experimental physicists are engaged in the effort of explaining this phenomenon. As a result of these efforts a great number of materials exhibiting superconductor behavior at high temperatures above 77 K (the boiling point of liquid Nitrogen) were realized. In various areas of technology these materials have very important applications. Basic characteristic properties of superconductivity are: zero resistance, Meissner effect, magnetic flux quantization, Josephson effect and gaps in elementary excitation energy spectra. Superconductivity is refered as a “macroscopic quantum phenomenon”.

2.1. Discovery of Superconductors

Materials which have no resistance to the flow of electric current are known as Superconductors and the discovery of these materials is one of the important occasions in the scientific discovery. It is worth while to note at this point that ; the limits of superconductivity has not yet been reached and the theories that try to explain superconductor behavior has been constantly under progress. Historically, superconductivity was first observed in mercury by Dutch physicist Heike Kamerlingh Onnes of Leiden University in the year 1911. In the experiment carried out by Kamerlingh Onnes, he cooled mercury to the temperature of liquid helium namely to 4 degrees Kelvin (-452F, -269C), he observed that its resistance suddenly disappeared. As it is well known , the Kelvin scale represents an "absolute" scale of temperature and therefore Onnes had to come within 4 degrees of the coldest temperature that is theoretically attainable to observe the phenomenon of superconductivity. Not so long,this important experimental achievement brought Kamerlingh Onnes a Nobel Prize in physics in the year 1913.

The following milestone took place in 1933 when German physicists Walther Meissner and Robert Ochsenfeld discovered that a superconducting material will repel a magnetic field which brought an understanding how matter behaves at extreme cold temperatures. It is well known that, a magnet moving by a conductor induces currents in the conductor and this is the principle which explains how the electric generator operates. However , in a superconductor the induced currents exactly mirror the field that would have otherwise penetrated the superconducting material and surprisingly causing the magnet to be repulsed. This new phenomenon is known as strong diamagnetism and nowadays is given the name "Meissner effect". This effect has such a strength that it can levitate a magnet over a superconductive material.

Other superconducting metals, alloys and compounds were discovered in the following decades. In 1941 it was discovered that niobium-nitride exhibits superconductive behavior at 16 K. In 1953 it was observed that vanadium-silicon displayes superconductive properties at 17.5 K. In 1962 scientists at Westinghouse developed the first commercial superconducting wire which is an alloy of niobium and titanium (NbTi). Later on, at the Rutherford-Appleton Laboratory in the UK, high-energy, particle-accelerator electromagnets were developed in the 1960s which were made of copper-clad niobium-titanium.

In the USA, in the year 1987 they were first employed in a superconducting accelerator at the Fermilab Tevatron .

The first successful theoretical study on superconductivity was advanced in 1957 by the physicists John Bardeen, Leon Cooper, and John Schrieffer and their Theory of Superconductivity is know as the BCS theory (derived from the first letter of each physicists' last name) . Later in 1972, John Bardeen, Leon Cooper, and John Schrieffer won the Nobel prize. The BCS theory which is mathematically-complex in its content, has given an understanding of superconductivity at temperatures close to absolute zero for elements and simple alloys. However, at higher temperatures and with different superconductor systems, the BCS theory has subsequently become inadequate to fully explain how superconductivity is occurring.

Another significant theoretical advancement occured in 1962. Brian D. Josephson, a graduate student at Cambridge University, predicted that electrical current would flow between two superconducting materials (even when they are separated by a non-superconductor or insulator). This prediction was later confirmed and this tunneling phenomenon is known as the "Josephson effect" which has been applied to

electronic devices such as the SQUID, an instrument capabable of detecting even the weakest magnetic fields. (Below SQUID graphic courtesy Quantum Design). Let us mention also that Brian D. Josephson shared the Nobel Prize in Physics in the year 1973. In 1964, at Stanford University Bill Little had suggested the possibility of organic (carbon-based) superconductors. In the historical progress of superconductivity, the 1980's were a decade of great importance.

In 1980, The first of these theoretically suggested superconductors was successfully synthesized by Danish researcher Klaus Bechgaard of the University of Copenhagen together with his three French colleagues. $(TMTSF)_2PF_6$ had to be cooled to an incredibly cold 1.2K transition temperature (known as Tc),

Then, in 1986, a breakthrough discovery was made by Alex Müller and Georg Bednorz. They are researchers, working at the IBM Research Laboratory in Rüschlikon, Switzerland. Alex Müller and Georg Bednorz created a brittle ceramic compound that superconducted at the highest temperature then known: 30 K. This discovery was so remarkable since ceramics are normally insulators and thus they do not conduct electricity well at all. For this reason, researchers had not considered them as candidates of possible high-temperature superconductors. The Lanthanum, Barium, Copper and Oxygen compound that Müller and Bednorz synthesized, behaved in a way which has not as yet understood. (Original article printed in Zeitschrift für Physik Condensed Matter, April 1986). In the following year, Müller and Bednorz won a Nobel Prize for their discovery of this first of the superconducting copper-oxides (cuprates). However it is even more noteworthy, later it was discovered that tiny amounts of this material were actually superconducting at 58 K, due to a small amount of lead having been added as a calibration standard.

After Müller and Bednorz' discovery a flurry of activity in the field of superconductivity has started. All over the world physicists began preparing ceramics of every possible combination in a quest for higher and higher Tc's. In January of 1987 a group of physicists at the University of Alabama-Huntsville substituted Yttrium for Lanthanum in the Müller and Bednorz molecule and achieved an incredible 92 K Tc. This is an important point in the historical developement of superconductivity since for the first time a material (today referred to as YBCO) had been found that exhibits superconductive behavior at temperatures warmer than liquid nitrogen. There are additional milestones in superconductivity history; exotic - and often toxic - elements in the base perovskite ceramic are also used. At the present, a class (or "system") of

ceramic superconductors with the highest transition temperatures are the mercuric-cuprates. In 1993 at the University of Colorado and by a group of physicists at Zurich, Switzerland namely, A. Schilling, M. Cantoni, J. D. Guo, and H. R. Ott, these compounds were synthesized for the first time. The world record T_c of 138 K is now held by a thallium-doped, mercuric-cuprate comprised of the elements Mercury, Thallium, Barium, Calcium, Copper and Oxygen. In 1994, Ron Goldfarb at the National Institute of Standards and Technology-Colorado confirmed the T_c of this ceramic superconductor. This T_c can be coaxed up even higher (approximately 25 to 30 degrees more) under extreme pressure. Illinois Superconductor (today known as ISCO International), founded in 1989 was the first company to capitalize on high-temperature superconductors.

In the following years , discoveries about the novel nature of superconductivity have been made.

In 1997 it was found that at a temperature very near absolute zero an alloy of gold and indium was both a superconductor and a natural magnet. It was believed up to then that a material with such properties could not exist. However, up to now , over a half-dozen such compounds have been found. In the last decade, the first high-temperature superconductor that does NOT contain any copper (2000), and the first all-metal perovskite superconductor (2001) were discovered..

Again in 2001 a material that had been known for decades was found to be an extraordinary new superconductor. Japanese physicists measured the transition temperature of magnesium diboride at 39 Kelvin - far above the highest Tc of any of the elemental or binary alloy superconductors. Although 39 K is still well below the T_c's of the "warm" ceramic superconductors, later on they made refinements in the fabrication of MgB_2 and have opened the way for its use in industrial applications. Laboratory testing led to the conclusions that MgB_2 are superior to and will replace NbTi and Nb_3Sn wires in high magnetic field applications such as MRI.

A theory to explain high-temperature superconductivity has not been achived yet but clues occasionally appear that contribute to our understanding of the nature of this phenomenon. An example is , in 2005, Superconductors.ORG discovered that when the weight ratios of alternating planes within the layered perovskites are increased then often T_c significantly increases. This achievement has led to the discovery of more than 45 new high-temperature superconductors, including a candidate for a new highest T_c.

"Pnictides" are discovered as the most recent "family" of superconductors . They are iron-based superconductors and were first observed by a group of Japanese physicists in 2006. Similar to the high-T_c copper-oxides, the exact mechanism how the superconductivity in these materials initiates is not known yet. However, with T_c's over 50 K, their discovery has given rise to a great deal of interest.

2.2. Basic Characteristics of Superconductors

One of the important properties of superconductors is the critical temperature T_c at which the resistivity of the material vanishes. Thus researches try to discover new superconducting materials with high critical temperatures. Another important property of superconductors is their critical magnetic field (H_c). The importance of this parameter is due to the fact that; superconducting state cannot exist in the presence of an applied magnetic field greater than a critical value called H_c even at absolute zero. This critical magnetic field which is a characteristic of the material has a strong correlation with the critical temperature of the superconductor. When critical magnetic field (H_c) increases then critical temperature T_c decreases.

According to Meissner effect, when the material is in a superconducting state, the magnetic field lines are expelled from the sample . The external field penetrates into the bulk from the surface of the sample, on the other hand the magnitude of the magnetic field that penetrates decreases and this decrease is in an exponential form. Superconductors are divided into two groups in terms of to their diamagnetic properties namely type I and type II. In type I superconductors, H_c is a limiting factor because with an increase in applied magnetic field, the magnetization which balances this magnetic field also increases until H_c is reached. Thus, if the applied external magnetic field surpasses H_c then the material is no longer in the superconducting state.When the applied magnetic field is lower then H_c, the material is in the Meissner state and all magnetic flux is expelled from the sample. Type I superconductors which are mostly pure metals have limited practical usefulness because their critical magnetic fields are so small and the superconducting state disappears suddenly at that temperature.

On the other hand in Type II Superconductors, passing from the normal state to superconducting state Meissner effect does not occur immediately but goes through a transitional state in which the applied field is able to penetrate through certain local

regimes of the sample. This transitional state is called the vortex state. The vortices of superconducting currents surround cores of normal material and it shows the properties of a mixed state of normal and superconducting regions. If the applied magnetic field is increased until the lower critical field, $H_c(1)$, is reached, then the material expels all the magnetic flux that falls on it. Moreover if the applied magnetic field is kept on being increased, until upper critical field, $H_c(2)$, then the material is in the vortex state and magnetic flux lines can penetrate through the sample in some regions. The effect of these flux lines are cancelled out by the supercurrents circulating around the walls of vortices and the total magnetic flux is zero.

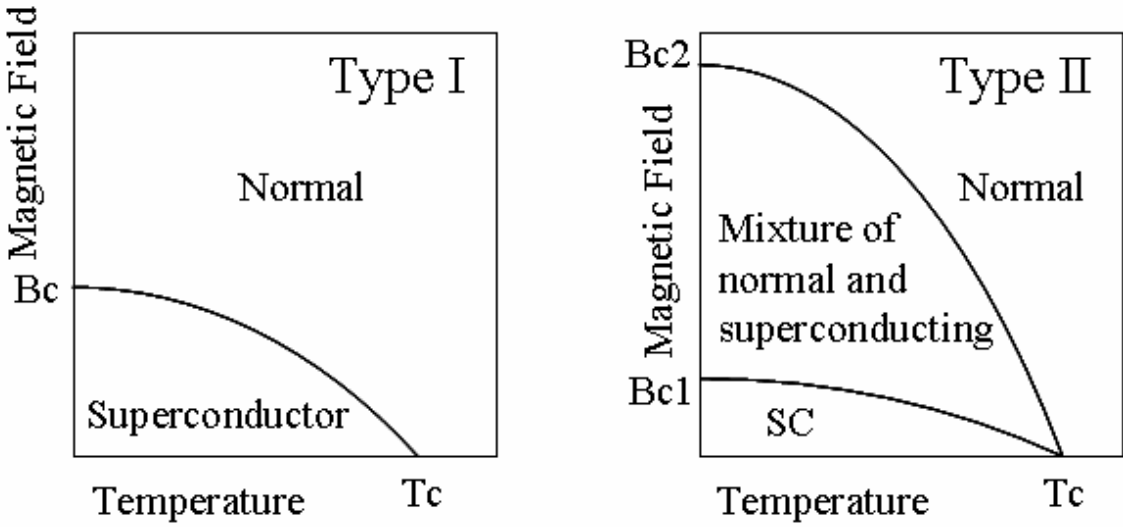

Figure 2.1. Schematic representation of Type I and Type II superconductors

Most of Type II superconductors are alloys and they show much higher critical magnetic fields. There is another important parameter which is called critical current density J_c, and it determines the quality of the superconductor. J_c is defined as the maximum current the material can carry per unit area and it is strongly dependent on temperature. With an increase in the current flowing through a superconductor, T_c will usually decrease.

When current is flowing through a superconductor, a magnetic field is created.In the case when the current density is high enough, the magnetic field at the surface of the sample becomes larger. This in turn gives rise to vanishing of the critical magnetic field ($H_{c)}$ and the superconductivity.

Since spin of the Cooper pairs is zero, Pauli's exclusive principle is not available any longer in the superconductors. Thus they can occupy the same quantum state and the occupation of energy state is described by Bose-Einstein distribution law. All Cooper pairs have same momentum, but it is not possible when energy resulting from applied electric field exceeds the energy gap of the Cooper pair. The expressing of energy gap (Δ) in a superconductor and a semiconductor is quite different from each other. In superconductor, the energy 2Δ can be defined as a binding energy of the Cooper pair and it is enough energy to break a cooper pair in a superconductor. After breaking of pairs, the single electrons occur and they are called quasi-particles.

Experimentally, the energy gap varies with temperature that is also predicted by BCS theory. At T=0, the ratio $2\Delta(0)/k_BT_c$ variation with superconductor elements are typically between 3.2 and 4.6 but this radio predicted by BCS theory is equal to 3.5 (Wesche 1998).

2.3. Low Temperature and High Temperature Superconductivity

In 1957, Bardeen, Cooper and Schrieffer proposed a theory (BCS theory) which was successful in explaining the superconductivity on microscopic origins. BCS theory could quantitatively predict the properties of superconductors (Bardeen et al. 1957). Their theory is based on an earlier discovery by Cooper (1956). In his study Cooper came to the conclusion that the ground state of a material is unstable with respect to pairs of 'bound' electrons. These pairs of electrons are formed by electron-phonon interactions and given the name Cooper pairs. Let us briefly describe the mechanism of the Cooper pairs; an electron in the cation lattice distorts the lattice around it and thus creating an area of greater positive charge density around itself. Another electron at some distance in the lattice is then attracted to this charge distortion (phonon) and this is called electron-phonon interaction. In this way, the electrons are indirectly attracted to each other and they form a Cooper pair. In other words, there is an attraction between two electrons mediated by the lattice which creates a 'bound' state of the two electrons. It is well known that electrons which are fermions obey the Pauli Exclusion Principle. However, pairs of electrons can behave very differently from single electrons namely they behave more like bosons which can condense into the

same energy level and have one single wave function describing the behaviours of all cooper pairs.

The BCS Theory is successful in explaing the mechanism of superconductivity in low temperature superconductors. According to BCS theory the highest T_c a superconductor can achieve is about 30 K and consequently the theory could not account for high temperature superconductors with much higher T_c values.

In the superconductor technology the most important problem is the cooling the system. A broad range of superconducting devices have been proposed but their widespread usage is possible only through a discovery of new superconducting materials with transition temperatures on the range of room temperature. Therefore the production of high temperature superconductors gives new hopes for many more technological applications. However , although an increase in the transition temperature with high T_c superconductors are achieved, cooling of the system is still a problem to be solved. There are three main regimes that superconductors are inclined to work in. These regimes are based on the zero resistance when superconducting state is maintained, transition between the superconducting state and normal state and Josephson Junctions.

2.3.1. High Temperature Superconductors

Usage of the liquid helium discovered by H. K. Onnes in 1911 in order to reach the very low temperatures led to find new superconducting materials with increasingtheir critical temperature (T_c) values in subsequent decades. Until 1986, physicists hadbelieved that BCS theory forbade superconductivity at temperatures between 30 K and 40 K due to thermal vibrations. However, a interesting research renewed superconductivity was published by Bednorz and Müller in that year and they discovered superconductivity in a ceramic compound material, lanthanum barium copper oxide ($La_{2-x}Ba_xCuO_4$), with transition temperature of 35 K (Bednorz and Müller 1986). Making this ceramic compound important discover in superconductivity was that it has not only high critical temperature but also was first cuprate in new class superconducting materials known as copper oxide superconductors. After a year, replacing the lanthanum with yttrium at LBCO materials, yttrium barium copper oxide compound, $YBa_2Cu_3O_{7-x}$ (YBCO), was found with T_c around 90 K (Wu, et al. 1987). It

was important commercially because liquid nitrogen produced cheaply could then be used as a refrigerant (at atmospheric pressure, the boiling point of nitrogen is 77 K). In the same year another superconducting compound including bismuth, strontium, calcium and copper (BSCCO) was discovered. Two superconducting phases were characterized as $Bi_2Sr_2CaCu_2O_{8+\delta}$ (Bi2212) and $Bi_2Sr_2Ca_2Cu_3O_{10+\delta}$ (Bi2223) with their T_c 95 K and 110 K respectively (Chu, et al. 1998). After a very short time, thallium barium calcium copper oxide compound, $Tl_2Ba_2Ca_2Cu_3O_\delta$ (Tl2223) which has around T_c 125 K was found in 1988 (Hazen, et al. 1988). The last superconductor compound $HgBa_2Ca_2Cu_3O_{8+\delta}$ (Hg1223) with maximum transition temperature T_c around 135 K was found in 1993 (Schilling, et al. 1993).

All of the HTSs have a layered crystal structure and include copper oxide layers providing superconductivity separated by non-superconductor layers. They are base on oxygen defect modification of a perovskite structure which is adopted by many oxides that have the chemical formula ABO_2. Its structure is a primitive cube, with the Acation in the middle of the cube, the B-cation in the corner and the anion, commonly oxygen, in the centre of the face edges. Because of these layered structures of HTSs, they have anisotropic behaviors at critical field, London penetration dept, coherence length and resistivity. They are extremely type II superconductors and only these superconductors can be used for magnet and energy applications which can be well defined by the Gindzburg-Landau theory (Ginzburg ; Landau 1950). In 1959, it has been showed that this theory can be derived from the BCS theory (Gor'kov 1959). Type I and type II superconductors are different with respect to critical fields, London penetration dept λ and coherence length ξ. While $\xi>\lambda$ shows the characteristic of type I superconductors, the situation of $\xi<\lambda$ is found in type II superconductors. If the ratio λ/ξ called the Ginzburg-Landau parameter (κ) is greater than $1/\sqrt{2}$, superconductor must be type II (Wesche 1998). Although the coherence length values ξ of HTSs are short, they have large critical magnetic field. Besides these different parameters, Shubnikov firstly found an unusual behavior of some superconductor in external magnetic field.

After 20 years in order to explain the Shubnikov's experiment, Abrikosov using the Gindzburg-Landau theory theoretically showed that there are two types of superconducting materials which are categorized as type-I and type-II superconductor.

For example, while type I superconductor materials expel magnetic flux completely from their interior until a critical magnetic field values, at the high presence of an applied external magnetic field, a mixed state in the type-II superconductor

material is characterized by the properties of the vortex that is formed at point where the magnetic field penetrates the superconductor in a flux tube through the sample. Due to penetration of magnetic flux, the region in which is near the core of the vortex acts as a normal metal. Type-II superconductors have two critical magnetic fields which are the lower critical magnetic field B_{c1} and the upper critical magnetic field B_{c2}. If applied field is less than B_{c1}, the superconductor completely expel the magnetic field as a type-I superconductor. Superconductor in magnetic field between B_{c1} and B_{c2} mixed state is formed and at B_{c2} material become normal state (Bourdillons 1993).

2.3.2. Crystal Structure of Bi2212

All HTSC can be considered as naturally stacked arrays of IJJ while keeping their periodicity along the crystal c-axis. A promising research area is the generic features of HTSC. A remarkable member of the HTSC group is Bi-2212 which has many experimental perspectives. It has been investigated widely in various studies so far, since it has superior properties compared to other high T_c superconductors. Bi-2212 single crystals can be easily grown with a high degree of quality. In these crystals, cleavage process creates atomically smooth and shiny regions to facilitate the patterning. After annealing in argon or oxygen media the doping level of this material can be altered easily. This property makes it an excellent candidate while investigating its physical characteristics over a large range of the doping.

The complicated HTSC series, $(BiO)_2Si_2Ca_{n-1}Cu_nO_{2+2n,}$ contains perovskite-type layers and $(BiO)_2$ layers of bismuth in the unit cell. Number of the perovskite units in other words the number of the consecutive copper oxide layers in the unit cell can be denoted by "n". There exits three phases for BSCCO namely, (n=1) $Bi_2Sr_2CuO_{6+\delta}$ (Bi2201) with $T_c \leq 20$ (Akimitsu, et al. 1987), $Bi_2Sr_2CaCu_2O_{8+\delta}$ (n=2, Bi2212 phase) with $T_c \approx 90$ K and $Bi_2Sr_2Ca_2Cu_3O_{10+\delta}$ (Bi2223 phase) with Tc= 110 K (Maeda, et al. 1988). All of these phases have layered atomic arrangement with planes of weak bonding, the $(BiO)_2$ (Romano et al. 1998). Among the cuprates, or more specifically within the BSCCO family, the Bi-2212 is the most widely studied material and many researchers have been working on it in the recent years. The optimally doped sample of Bi-2212 has an onset critical temperature of approximately 95 K which is the maximum value of T_c for this compound and its transition temperature can be reduced either by

additional oxygen content (overdoping) or by the removal of oxygen with vacuum annealing (underdoping). Thus, the phase diagram of this cuprate as well as its physical properties can be investigated by means of doping (Ozyuzer et al. 2000). There is an important advantage of this material namely, it can be grown in the way of single crystal without any macroscopic defects or dislocations. The abone mentioned parameter n also corresponds to the number of superconducting layers in the structure. For example, there are two CuO_2 layers separated by Ca layer in the structure of Bi2212 phase. The unit cell of Bi2212 has a pseudo-tetragonal symmetry with lattice parameter; a = b = 5.4 and c = 31 Å (Matsui, et al. 1988).

Sequence of its stacking atomic layers is like that, $(BiO)_2$ / SrO / CuO_2 / Ca / CuO_2 / SrO / $(BiO)_2$ / SrO / CuO_2 / Ca / CuO_2 / SrO / $(BiO)_2$. Taking into account to the structure types there exits two kinds of layers in crystal structure of Bi2212. One of which consisting SrO / CuO_2 / Ca / CuO_2 / SrO has a structure of perovskite type, while another consisiting SrO / $(BiO)_2$ / SrO has a structure of NaCl type. The layered structure of Bi2212 HTSs including IJJs makes the crystal anisotropic material. Consequently, Josephson tunneling occurs along the c axis between superconducting (Cu-O) layers separated by insulating layers unlike electrical behaviors of the crystal at a-b planes. On the other hand, layered HTSs have different coherence lengths and penetration depths at different directions. At a-b planes coherence length ξab (between 20 and 40 Å) is larger than coherence length ξc ($\approx$1 Å) along to c axis. Although the coherence lengths of Bi2212 is small, λ_{ab} is equal to 2000 Å. Accordingly Bi2212 with the Ginzburg-Landau parameter κ greater than 100 exhibits behaviors of type II superconductors (Ting Wei 1995). The crystal is fairly intricate and show excessively anisotropic properties due to its layered structure.

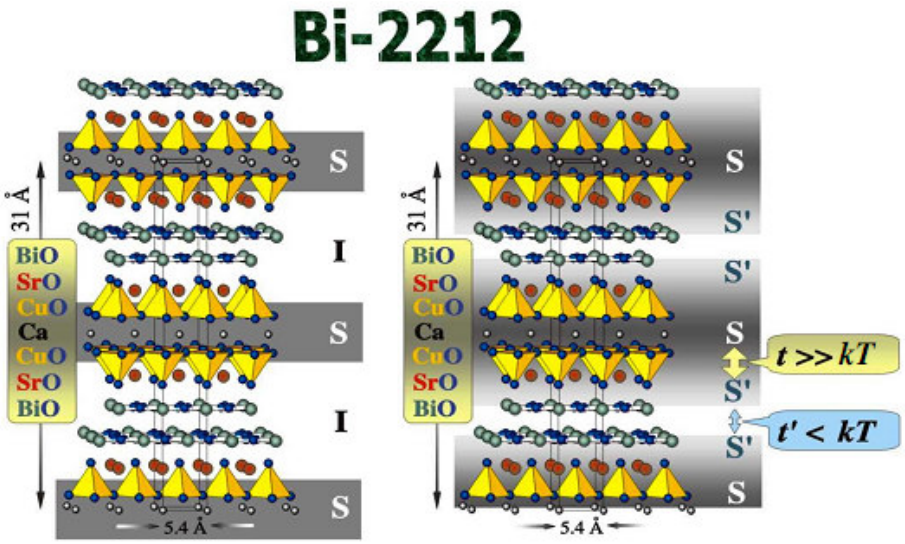

Figure 2.2. The crystal structure of Bi2212. The left image corresponds to basic multilayer model and the right image defines the proximity model (Yurgens, 1996a).

In order to be able to explain the mechanism of this material two models are developed namely, multilayer model and proximity model (Yurgens et al. 1996a) which are represented i n Figure 2.2. According to the multilayer model; Bi-2212 single crystals behave like stacks of Josephson coupled Cu-O double layers with the thickness of 3 A^0 separated by nonsuperconducting Sr-O and Bi-O layers of thickness 12 A^0. This configuration forms natural Josephson tunnel junctions array going on like SISIS... inside the single crystal and enables to observe both dc and ac Josephson effects. Superconducting properties of the multilayered high Tc superconductors stem mainly from the double CuO_2 layers in which coupling occurs, while the role of the other layers can not be defined exactly; it is commonly believed that Sr-O and Bi-O intermediate planes behave as passive spacers or charge reservoirs.

As stated in the preceding lines, the superconducting coherence length for Bi-2212 in the out of plane direction is approximately 0.1 A^0, which is relatively small when compared with the distance between two adjacent CuO_2 layers in the Bi-2212 unit cell. This point makes Josephson tunneling of Cooper pairs hard across the insulating layer (Yurgens, et al.1996a).

Another model namely proximity model is proposed ; where it is suggested that not only CuO2 layers but also Bi-O planes make contribution to superconductivity of the HTSC. It is shown by some other experiments that Bi-O layers exhibit metal-like

property or even superconducting features rather than insulating character. According to the proximity effect, there is a strong coupling between the Cu-O and Bi-O layers (S-S') with weak Josephson coupling between neighboring Bi-O layers (S'-S'). There are research workers who claim that the reduced energy gap value of Bi-2212 is the consequence of the proximity induced superconductivity of the Bi-O layers (Yurgens, et al. 1996a).

The current-voltage characteristics which are obtained by means of a current sweeping back and forth from zero to a some maximum values exhibit large hysteresis and multiple branches corresponding to IJJ inside the crystal. Each quasi-particle branch which belongs to a different IJJ has a well-developed gap structure.

2.4. Tunneling

In a superconductor , tunneling phenomena gives us very important information about superconducting materials namely, energy gap and other superconducting features. Josephson junctions is made up of two superconducting layers separated by a very thin insulating layer. They are called Josephson junction since Josephson theoretically predicted that, cooper pair tunneling across the insulating layers is taking place as well as single electron tunneling, (Josephson 1962). The insulating layer in SIS junctions can be such as cracks, grain boundaries and point contacts. The single electron tunneling is a well known phenomena but Josephson's theoretical prediction on pair tunneling presented a new and an important concept to superconductive theories. Josephson stated that the cooper pair tunneling current through the barrier is depended on the difference of phases of the effective wave functions on the two sides of the junction and the phase difference is both temporally and spatially variable. Leaving aside single electron tunneling, there are no excitation and bias across the junction. Cooper pair tunneling results in the flow of the Josephson current without resistance until the critical current value I_c of the SIS junction is exceeded. After the critical current value I_c, voltage and current jump to values exhibiting single electron (quasi-particle) tunneling characteristic on the I-V (Duzer and Turner 1999).

Using an ultra thin insulating layer and by intervening between two metals one could produce different kinds of tunnel junctions such as NIN, SIN, SIS (N: normal metal, I: insulator, S: superconductor).

In the independent particle approximation, the tunneling current from metal 1 to metal 2 is given by

$$I = c|T|^2 \int_{-\infty}^{\infty} N_1(E)N_2(E+eV)[f(E) - f(E+eV)]dE \qquad (2.1)$$

where c is a constant of proportionality, T is a constant tunneling matrix element, $N_1(E)$ and $N_2(E)$ are the density of states of the metals and f(E) is the Fermi-Dirac distribution function.

In the case when both electrodes are normal metals,using Eq. 2.1 one obtains the tunneling current as follows:

$$I_{nn} = c|T|^2 N_n(0)N_n(0)eV \equiv G_{nn}V : \; G_{nn}V = \frac{1}{R_{nn}}V \qquad (2.2)$$

there by the junction is ohmic.

Without an applied voltage, as shown in Figure 2.4a their Fermi levels become equal and consequently net charge transport can not occur. On the other hand when a small potential difference V is applied to the junction, there will be a shift in the Fermi levels of the metals on the order of eV with respect to each other as shown in Figure 2.4b. In this case , the electrons from the top of the conduction band of the fixed metal are now able to tunnel to the empty continuum levels of the positively biased metal.

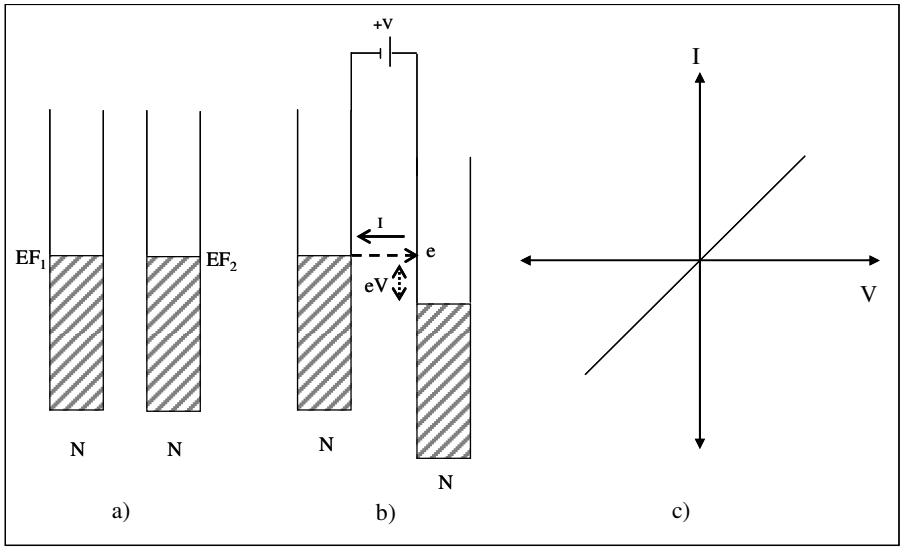

Figure 2.3. The NIN tunneling process and its current-voltage (I-V) characteristic at T= 0 K

Let us examine the energy level systems in superconductors before introducing SIN and SIS tunneling. There are two different representation of the energy levels associated with superconductors namely, semiconductor and Boson condensation representations. Semiconductor representation proposes that at absolute zero superconductors have an energy gap $E_g = 2\Delta$ between a lower energy band which is full of superelectrons and an upper energy band which is totally empty.

Above the 0 K, some of the electrons, which are given the name quasiparticles, are excited from the lower band to the upper band. In the Boson condensation representation, all the Cooper pairs are condensed into a level located at a distance Δ below the bottom of the conduction band at absolute zero, that is called ground state for superconductors. Meanwhile, above the 0 K, some of the Cooper pairs spilt up and consequently quasiparticles occur. The Boson condensation representation is merely more convenient than the semiconductor representation for analysis of the tunneling of super electrons.

2.4.1. NIS Tunneling

Current-voltage characteristics of Superconductor-Insulator-Normal Junction (SIN) deviate from straight line observed in NIN junctions which is due to the existence of energy gap in the electron density of states of superconductors (Giaver 1960b). Bose-condensation representation of SIN tunneling process at absolute zero is presented in Figure 2.5.

Tunneling does not occur in the unbiased case, since all the electrons within Δ of the Fermi energy have fallen into the superconducting state there are no electron states for the normal single electrons to tunnel. This is also valid for biases with in the range of $-\Delta/e<V<+\Delta/e$.

On the other hand, in the case of $V\geq\Delta/e$, the Fermi level of the normal metal is shifted up by the order of eV above the ground state of the superconductor. Consequently, electrons can tunnel from the conduction band of the normal metal to the empty states above the gap of the superconductor. In the case of a negative bias, $V\leq-\Delta/e$, tunneling involves the breakup of a Cooper pair, with one of the electrons of the pair tunneling down to the top of the normal metal conduction band and the other shifting upward to the quasiparticles energy band of the superconductor. Thus the

breaking up a pair creates a quasiparticle inside the superconductor and electrons passing through the insulating layer reach the normal metal (Poole, et al. 1995).

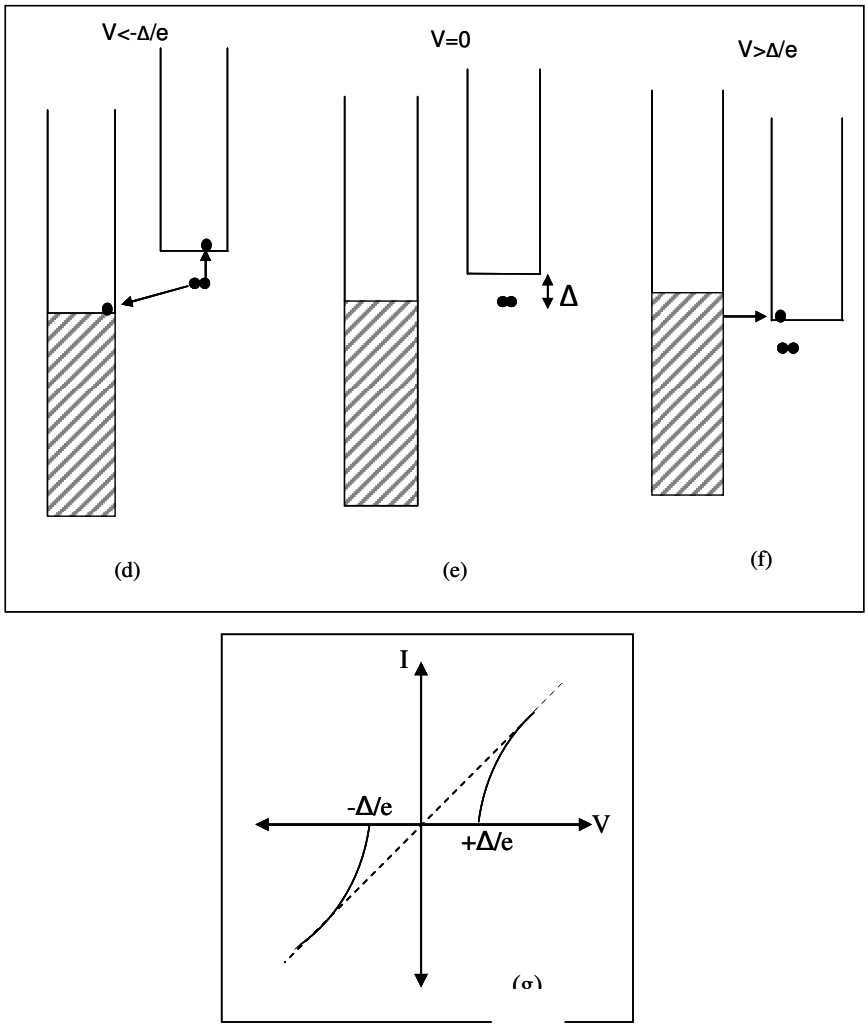

Figure 2.4. The SIN tunneling process with representation of Boson condensation and its current-voltage (I-V) characteristic at T= 0 K

The total tunneling current in an SIN junction which is introduced in Eq. 2.2 could be determined by the independent particle approximation as follows:

$$I(V) = c \int |T|^2 N_n(E) N_s(E + eV)[f(E) - F(E + eV)]dE \qquad (2.3)$$

In the case when one of the electrodes is a superconductor, many-body field theory proposes that the differential conductance is proportional to the density of states in the superconductor. One assumes that the normal metal electrode has a well-behaved almost constant density of states near the Fermi energy. When the gap opens up in a

superconductor, the quasiparticle states are pushed to the gap edge resulting in a singularity in the density of states:

$$\frac{N_s}{N_n} = \begin{cases} 0 & |E| < \Delta \\ \dfrac{E}{\sqrt{E^2 - \Delta^2}} & |E| \geq \Delta \end{cases} \tag{2.4}$$

There are no quasiparticle states within the gap i.e. E < Δ. At low temperatures, the differential conductance is directly a measure of the density of states:

$$G_{ns} \propto N_s(e|V|) \tag{2.5}$$

To derive this result it is necessary to go through rigorous many-body calculations. Thus, it is surprising that this correct result can be obtained from the equation for the current in the independent particle model (Eq. 2.1) by assuming a BCS density of states in the superconductor. This model was used by Giaever to explain his pioneering tunneling results on superconductors.

2.4.2. SIS Tunneling

In Figure 2.6 , Bose condensation representation of the S-I-S tunneling process is presented. At T=0 K, minimum voltage necessary to produce electron tunneling is V> $|\Delta_1+\Delta_2|/e$ where Δ_1 is the energy gap of the first superconductor and Δ_2 is the energy gap of the second superconductor. I the tunneling process, a Cooper pair breaks up in the first superconductor and one of the electrons belongs to pair tunnels to the empty (quasiparticle) energy state of second superconductor. Since energy released from pair breaking is equal and greater than the energy gap value of first superconductor, the second electron of broken pair is excited to the quasiparticle energy state of first superconductor (Schmidt 1997). At the voltage $V=-|\Delta_1+\Delta_2|/e$ direction of tunneling reversely changes. For temperature T>0 K, the tunneling current could also flow at lower voltages because of the availability of the thermally excited quasiparticles.

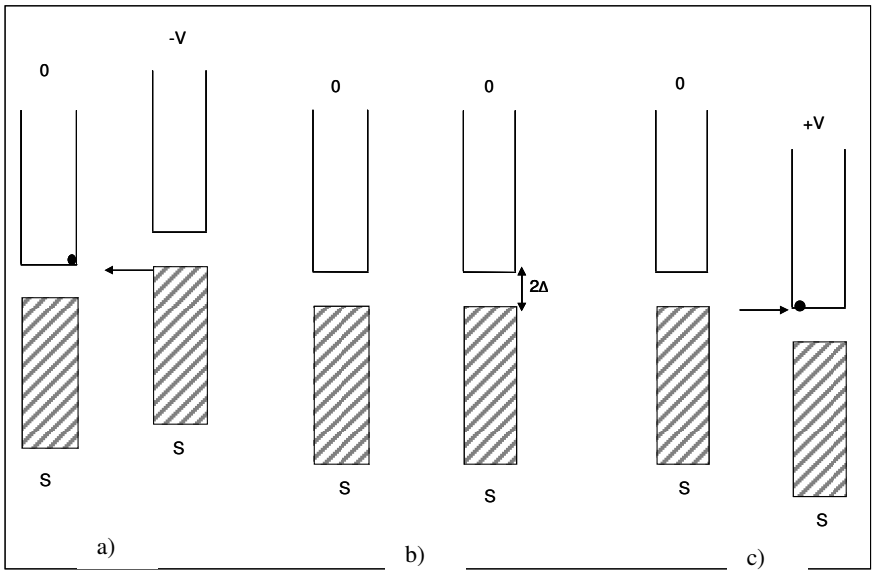

Figure 2.5 Bose condensation representation of single electron tunneling between two identical superconductors at absolute zero

The SIS tunneling current passing through the barrier is denoted as equation 2.5.

$$I(V) = c\int |T|^2 N_{1s}(E)N_{2s}(E+eV)[f(E)-F(E+eV)]dE \tag{2.6}$$

$$= c|T|^2 N_{1n}(0)N_{2s}(0)\int \left[\frac{|E|}{\sqrt{E^2-{\Delta_1}^2}}\frac{|E+eV|}{\sqrt{(E+eV)^2-\Delta^2}}(f(E)-F(E+eV))\right]dE$$

In the integration , the range of values of E such that $|E|<\Delta_1$ and $|E+eV|<\Delta_2$ are excluded

SIS junctions have a difference from other junction types since they exhibit supercurrent tunneling due to Cooper pair transfer between two superconductors which is called Josephson current apart from the quasiparticle tunneling. The existence of the Josephson current, I_c, depends on the junction resistance and given by Ambegaokar-Baratoff theory (Ambegaokar and Baratoff 1963) for BCS superconductors,

$$I_c R_n = \frac{\pi\Delta(0)}{2e} \tag{2.7}$$

where I_c is the Josephson current, R_n is the normal state resistance of the junction and $\Delta(0)$ is the energy gap at T=0 K.

Ideal current-voltage characteristics of a Josephson junction at T=0 K for identical superconductors is presented in Figure 2.7. The current at zero bias is a straight-forward result of the Cooper pair tunneling and is known as the Josephson current. One could apply a dc current to the junction and not develop a voltage drop across it. On the other hand, there is a limit to the amount of current that the tunneling Cooper pairs can carry. In the case when the applied current exceeds the critical current, the lossless current transport breaks down and the system switch from a zero voltage to a finite voltage state that corresponds to the double gap energy 2Δ. The binding energy of the Cooper pairs is also expressed by this gap energy. Then, the tunneling current is dominated by quasiparticles. If the current is increased further then the Ohms law at $V>2\Delta/e$ is merely displayed. While decreasing the current a hysteresis curve behavior is observed. The tunneling current remains to be carried by quasiparticles. For the zero temperature, the current should decrease to zero before the zero voltage state would be achieved again.

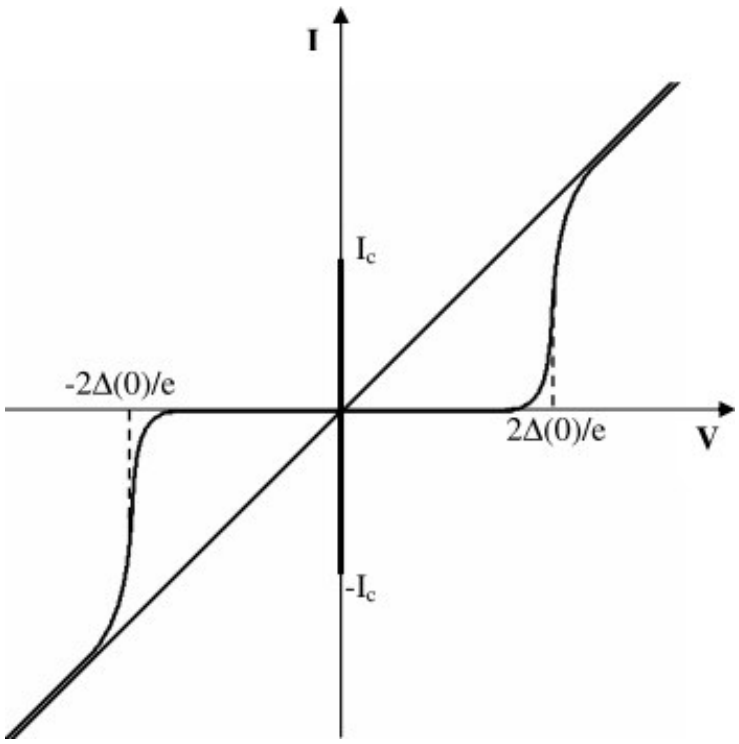

Figure 2.6. I-V characteristics of an SIS junction at T=0 K.

(Source: Wesche 1998)

I-V characteristic of layered HTSs along the natural IJJ stacks includes several branches due to individual switching of each junction from Josephson state to quasiparticle state when the bias current exceeds the individual critical current of each junction (Yurgens 2000). Thus each of the junctions acts as one of the single branch in large gap voltage of all junctions and the branches are almost vertical these voltages.

The poor thermal conductivity of Bi2212 single crystal results in a local overheating in superconductor structure. Overheating and nonequilibrium effects are the most encountered problems while obtaining I-V data and up to now various research groups have investigated this phenomena (Tanabe et al. 1996, Yurgens et al. 2004). By increasing the number of IJJs in the quasiparticle state, the overheating increases and leads to smaller voltage jump (conductance peak) in I-V curves. Furthermore the Non-equilibrium effect which is easy quasiparticle self injection through the high transmissive IJJ tunneling barrier (about 0.3 nm thickness in Bi2212) increases the heating effect in the structure. This effect also leads to back-bending of the I-V curve in the sub-gap region. One of the methods to eliminate heating problem is to use stacks of intrinsic junctions (mesas) with small dimensions in order to reduce I_c (Zhu, et al. 2006) However, since the same current per unit area through the junctions flows, the non-equilibrium effect still occurs and resuls in the Joule heating (Zasadzinski 2002). Thus this method is partly successful in observing the energy gap in I-V curves. Another method is to use the short current pulse tunneling measurements which provides free I-V characteristic different from gap suppression because of joule heating in IJJ (Suziki, et al. 1999). However, much of the interest of these measurements is in the behavior close to the energy gap, and high bias currents are required. Another alternative method is to intercalate the Bi2212 single crystals along the c axis with inert guest molecules such as $HgBr_2$, HgI_2 or I_2 molecules to reduce the coupling between CuO_2 layers. Due to intercalation, the intrinsic tunneling barriers are becoming wider which results in a drastic decrease of the c-axis critical current density. Therefore, Joule heating can be significantly suppressed.

2.4.3. Josephson Effect

Josephson Effect is a direct manifestation of the macroscopic quantum coherence of superconducting state. In 1962, Brian D. Josephson, then a graduate

student at Cambridge University made a remarkable prediction that the case of two superconductors weakly coupled by a thin insulating barrier that allows quantum mechanical tunneling of Cooper pairs without breaking up the pairs from one side to other side even with no potential difference (Josephson 1962). Before 1962 the general consensus related with Cooper pairs tunneling through a thin insulating layer was that such an event would not happen enough to be measurable. The reason was that as the tunneling of an electron has a very small change of occurring, the tunneling of electrons in a Cooper pair simultaneously crossing the insulator would be astronomically small. However Brian Josephson changed this common belief. From his calculations using BCS theory he discovered that probability of Cooper pair tunneling through the barrier was the same as that for a single electron.

The single electron tunneling is a well known phenomena and based on classical mechanics but his theoretical prediction on pair tunneling presented new important conception to superconductive theories. He predicted that the cooper pair tunneling current through the barrier is depended on the difference of phases of the effective wave functions on the two sides of the junction and the phase difference is both temporally and spatially variable. Apart from single electron tunneling, there are no excitation and bias across the junction. Cooper pair tunneling occurs the Josephson current flowing without resistance until the critical current value I_c of the SIS junction is exceeded. After the critical current value I_c, voltage and current jump to values exhibiting single electron (quasi-particle) tunneling characteristic on the I-V (Duzer and Turner 1999).

There are two principle phenomena in Josephson effect namely, DC and AC Josephson effects. When Josephson current flows at the absence of any electrical and magnetic field, DC Josephson effect takes place. The current resulting from cooper pair tunneling across the thin insulating layer at zero voltage depends on phase differences between two superconductors on either side of the junction. When a constant and nonzero voltage is applied across the insulating barrier, an alternating Josephson current occurs. This oscillating current which generates emission is explained by AC Josephson effect. Since the radiation frequency is proportional to the voltage, Josephson junctions are used such a voltage-frequency converter (Bourdillon and Bourdillon 1993).

2.5. Charge Doping

Antiferromagnetic Mott insulators with one hole per planar copper constitute the parent states of each family of cuprates (Taillefer, et al. 1997). A mott insulator is a material in which the conductivity vanishes as temperature tends to zero.

After doping with charge carriers these insulators are transformed into metals and then superconductors. Depending on the increasing carrier concentration, they all have an antiferromagnetic phase near zero doping then an insulating phase follows, consequently the superconducting transition temperature rises from zero to a maximum and finally drops to zero again. It is widely believed that all cuprates have the same phase diagrams which is schematically shown in Figure 2.7. There are two regions in the phase diagram, namely the antiferromagnetic insulating state (AF) with hole doping $p \leq 0.02$ and secondly the superconducting state (SC) where p is between 0.06 and 0.26. The insulating phase is generally given the name as undoped region. The materials are said to be underdoped where T_c is an increasing function of carrier concentration. They are called optimally doped where T_c reaches its maximum value and named as overdoped for larger carrier concentration. In the underdoped regime there exits variety of crossover phenomena which are observed at temperatures above T_c and are associated with the opening of a pseudo gap. By adding excess oxygen atoms or by reducing oxygen atoms without changing crystalline structure carrier concentrations of superconducting cuprates could be varied. Although hole-doping is the rule in high-T_c superconductors in some cases the mobile charges are electrons. The phase diagram of the electron-doped HTS is qualitatively similar to the phase diagram of the hole-doped HTS.

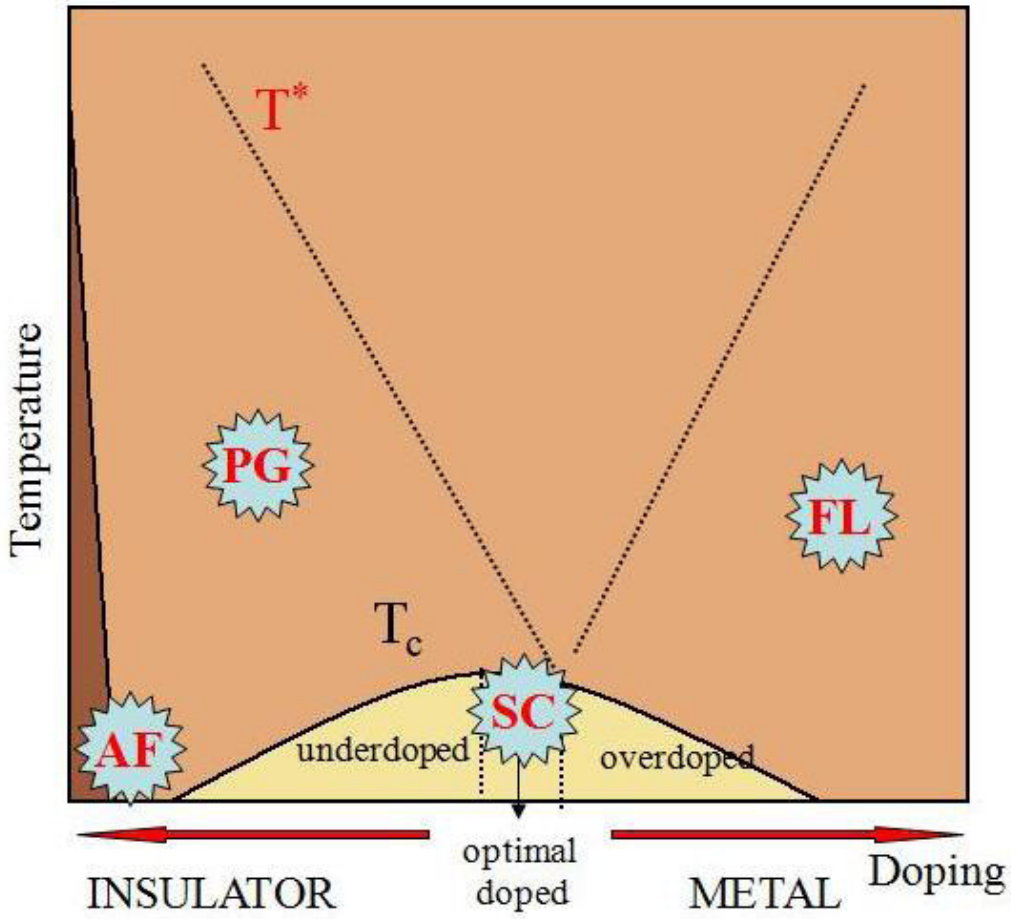

Figure 2.7. Typical overall phase diagram with doping in high-T_c cuprate Superconductors

The doping dependence of various superconducting properties of Bi2212 single crystal such as energy gap are widely studied. Superconducting energy gaps of the underdoped $Bi_2Sr_2CaCu_2O_{8+d}$ single crystals are larger than optimally doped crystals meanwhile the trend of decreasing energy gap with increasing hole doping proceed into the overdoped region (Miyakawa, et al. 1998). The optimally doped samples of Bi2212 have approximately an onset critical temperature of 95 K. In Figure 2.8 the temperature dependence of c-axis resistivity, T_c, of Bi2212 single crystal with various doping level are presented. As it could be observed in the figure, overall magnitude of c-axis resistivity of the crystal increases with decreasing doping level (Watanabe, et al. 1997). When the oxygen level varies from the optimally doped to overdoped, c-axis resistivity of the crystal gradually begins to exhibit metallic behavior. Furthermore, Josephson critical current density of the crystal increases significantly as the doping level increases (Suzuki, et al. 2009).

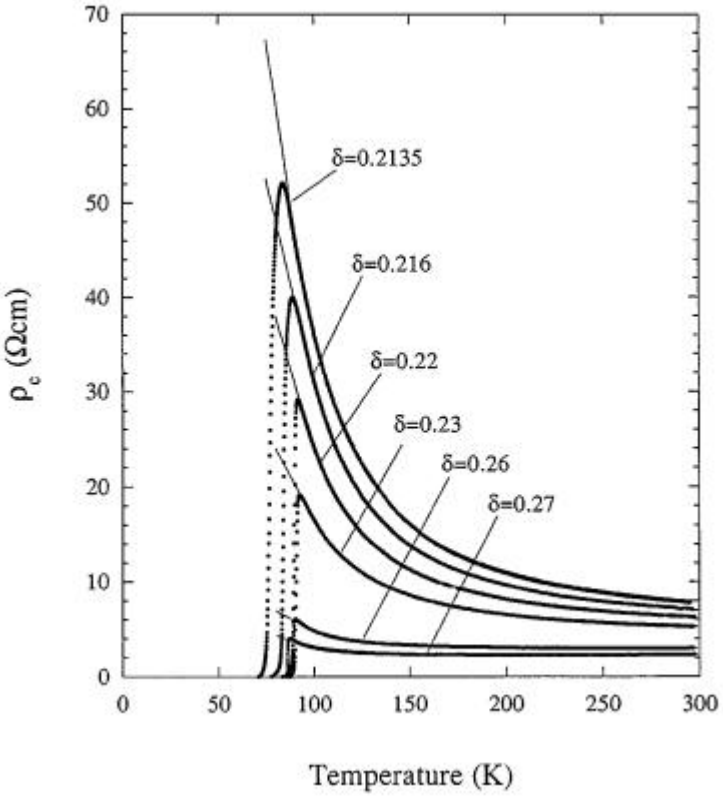

Figure 2.8. Out-of-plane resistivity (T_c) of a $Bi_2Sr_2CaCu_2O_{8+\rho}$ single crystal versus temperature for various oxygen contents (T) (Source: Watanabe, et al.1997)

2.6. Motivation

Among the cuprates, single crystal of $Bi_2Sr_2CaCu_2O_{8+\delta}$ (Bi2212) is a potential candidate of compact solid state devices designed for generating electromagnetic waves in terahertz frequency range. Bi2212 crystals are consisting of natural arrays in the form of identical layers called intrinsic Josephson junctions (IJJ). Since the IJJs are homogeneous in the atomic scale along the c-axis of Bi2212 single crystals highly-uniform junction arrays hold great potential for very high emission power. Each single junction has small emission power which is not enough for practical applications so we fabricate a terahertz oscillator in a rectangular mesa shaped containing large series arrays of IJJs. Therefore, they can provide much more power. Also fabricated mesa structures can operate at frequencies well exceeding those obtainable with low T_c superconductors due to the Josephson effect between these stacks, their large superconducting gap and other unique properties.

By using mesa-shaped samples of $Bi_2Sr_2CaCu_2O_{8+d}$ (Bi2212) intense, coherent, and continuous emission of terahertz electromagnetic waves can be obtained. In layered high temperature superconductors like Bi2212 superconductivity is controlled by carrier doping of the conducting CuO planes. By changing the doping level of the crystals critical temperature, c-axis resistivty and critical current of IJJs can be tuned in a range from underdoped to overdoped region. The result is hole doping of charge carriers. In the previous studies, it is also shown that, all of the THz emitting rectangular mesa structures are below a certain underdoped level of Bi2212 single crystal (Ozyuzer, et. Al.2009). In this study, we searched the possible optimum doping level for an intensive radiation. In the sample fabrication procedure, we first annealed the Bi2212 single crystals in vacuum or purified argon gas flow at various temperatures to study doping dependence of THz emission. For further processing, we pattern both single and double rectangular mesa structures by using electron beam lithography and argon ion milling on the cleaved surface of the crystal. After the mesa fabrication, the exact dimensions of the mesas were obtained using surface profilometer and atomic force microscopy. The number of Josephson junctions were determined which gives emission voltage.

We next performed the electrical characterizations from room temperature through low temperatures, c-axis resistance versus temperature (R-T) and current-voltage (I-V) tunneling characteristics were investigated. In the next chapter, all of the experimental processes will be described including, the annealing procedures, mesa fabrication and the characterization methods step by step.

CHAPTER 3

EXPERIMENTAL

This chapter concerns with experimental facilities used while preparing this thesis. The micron sized sample fabrication procedure of Bi2212 crystals are presented in the first part. The second part of this chapter is associated with characterization methods of the samples and in the following part, resistance versus temperature R-T and current versus voltage I-V characteristics are explained in details.

Recently, it is demonstrated that rectangular IJJ mesa structures of Bi2212 can be used as a source of continuous, coherent and polarized THz radiation. All THz emitting mesas are below a certain underdoped level, which has relatively small critical current in contrast to optimally doped and overdoped Bi2212. In the experimental procedure, in order to obtain various doping levels, we annealed the high temperature superconducting Bi2212 single crystals at various temperatures in vacuum or under argon flow. In the first annealing procedure, Argon gas is purified in the gettering furnace and flowed through the crystals at the rate of 100 sccm. Second system has a turbo molecular pump for high vacuum as 10^{-6} and under vacuum conditions we annealed the crystals for different time intervals. Then the single crystal having a smooth surface (the a-b plane) was glued onto a sapphire substrate by silver epoxy. Sapphire substrate and silver epoxy were preferred since they are good thermal conductors. In order to get a fresh and smooth surface on Bi2212, the crystal was mechanically cleaved with adhesive tape. After the cleaving process, gold layer with thickness of 100 nm is immediately deposited by a vacuum evaporation technique on fresh surface of the crystal in order to keep the surface against deterioration and to protect the crystal surface from water and chemicals during the experimental processes. We describe a mesa patterning process, which makes it possible to measure current–voltage characteristics along the c-axes of the films. To obtain natural IJJ stacks with various size and height, mesa on Bi2212 have been fabricated using e-beam lithography and argon ion beam etching techniques. After the mesa fabrication, in order to establish electrical contact to the gold layer on top of the mesa, CaF_2 layer was evaporated through a shadow mask onto the top part of the crystal including a small section of the mesa for the electrical isolation purpose. Subsequently, lift off technique is used for

fabrication of gold stripes by e-beam lithography onto the mesa and the CaF_2. Finally, a gold wire was attached to the strip over the CaF_2 and 2 pads with silver epoxy for the electrical connection of the mesa and two contact pads.

3.1. Material

Experiments were carried out on annealed Bi-2212 single crystals. In the unit cell, the complicated HTSC series, $(BiO)_2Si_2Ca_{n-1}Cu_nO_{2+2n}$, contains perovskite-type layers and $(BiO)_2$ layers of bismuth. Number of the perovskite units or in some other words the number of the consecutive copper oxide layers in the unit cell could be denoted by "n". There exists no calcium in the unit cell when n is equal to one, which results in formation of $Bi_2Sr_2CuO_6$ (Bi-2201) structure with Tc ranging from 8 K up to as high as 22 K. When n takes the value 2, then one could obtain $Bi_2Sr_2CaCu_2O_{8+d}$ (Bi-2212) phase.

Moreover, for n=3 there is another configuration namely $Bi_2Sr_2Ca_2Cu_3O_{10}$ (Bi-2223) whose transition temperature is around 110 K. All of the above configurations have layered atomic arrangement with planes of weak bonding, the $(BiO)_2$ (Romano et al. 1998). Among the cuprates, or more specifically within the BSCCO family, the Bi-2212 is the most studied material and a great number of researchers have focused on it in the recent years. The optimally doped sample of Bi-2212 has an onset critical temperature of approximately 95 K thereby the maximum value of Tc for this compound. The transition temperature of this sample could be reduced either by additional oxygen content namely overdoping or by the removal of oxygen with vacuum annealing (underdoping). Thus, the physical properties of this cuprate can be investigated by means of doping phase diagram (Ozyuzer et al. 2000). The most important advantage of this material is that it can be grown in the way of single crystal without any macroscopic defects or dislocations. Moreover, it could be cleaved easily in a simple manner; thus flat and convenient regions are able to be created for mesa fabrication. For Bi-2212 compound, the Ginzburg-Landau parameter k is greater than 100 ; which reveals the fact that it exhibits strong type II superconducting behavior. In accordance with this parameter, at low temperatures, it has an extremely short coherence length $\xi ab(0)$= 20-40 A^0 and $\xi ab(0) \cong 0.1\text{-}0.3$ A^0 and relatively large penetration depth λab=2000 A^0 (Ting Wei-Li 1995).

For the purpose of producing, the layered HTSs with high quality and c-axis aligned structure, the researchers use the melting processes including the KCl flux method (Katsui 1988), vertical Bridgman method (Ono, etal.1988) self-flux method (Shishido, et al. 1989, Tanaka, et al. 2001), melt-textured growth method (Jin, et al. 1988), the laser-heated pedestal growth method (Feigelson, etal. 1988) and travelling solvent floating zone method (TSFZ) (Takekawa, et al. 1988).

3.2. Annealing Procedure:

In layered high temperature superconductors like Bi2212, superconductivity is controlled by carrier doping of the conducting CuO planes. By changing the doping level of the crystals, critical temperature, c-axis resistivity and critical current of IJJs can be tuned in a range from underdoped to overdoped region. In previous studies, it is also shown that, all of the THz emitting rectangular mesa structures are below a certain underdoped level of Bi2212 single crystal (Ozyuzer, et al.2009). We fabricated a set of samples with various doping levels and sizes. The heat treatment duration is varied to change the T_c and critical current of crystals.

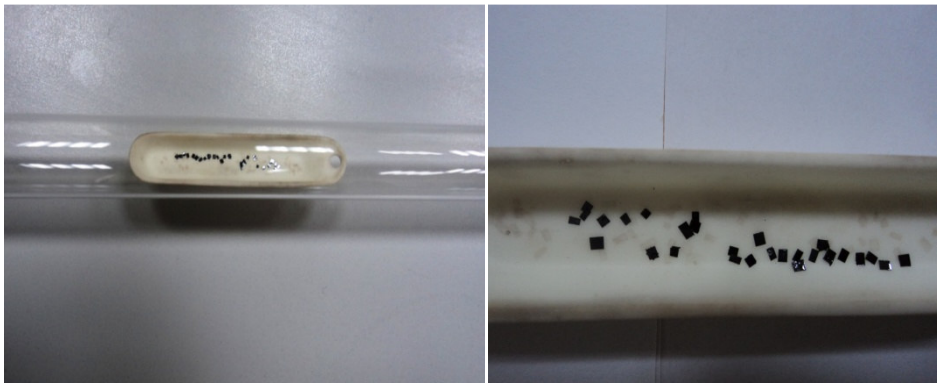

Figure 3.1. a) Crystals on crucible in quartz tube, b) Crystals on crucible

3.2.1. Annealing Procedure in Argon Atmosphere:

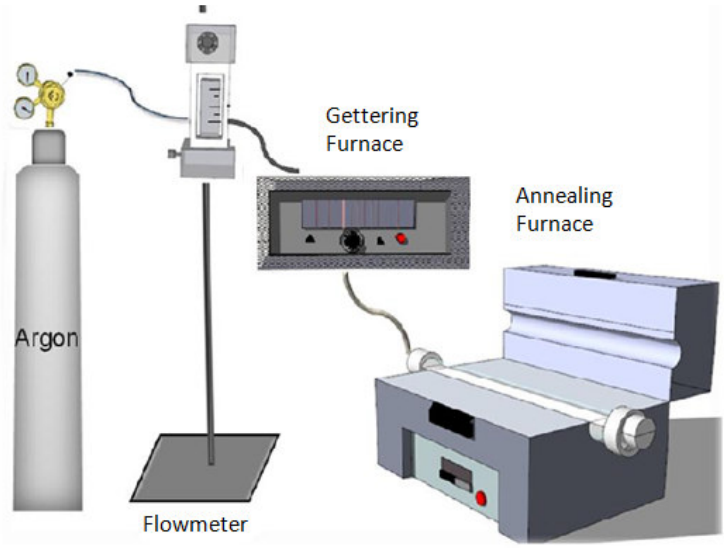

Figure 3.2. Our annealing system (in Argon atmosphere)

In the first set up which has been constituted from Argon gas,flowmeter, gettering furnace and annealing furnace, after placing the crucible inside the quartz tube ; 100sccm argon gas has been send to the annealing furnace right after purification.

3.2.2. Annealing Procedure in Vacuum:

In the second annealing set up (Figure 3.3) we have used only the vacuum pump and the furnace. At first we have reduced the the pressure of the quartz tube in which we have located the crystals up to 10^{-3} Torr using the turbomolecular pump. Afterwards we have operated the furnace which has been previously programmed to desired temperature and time in order to establish annealing at different temperatures.

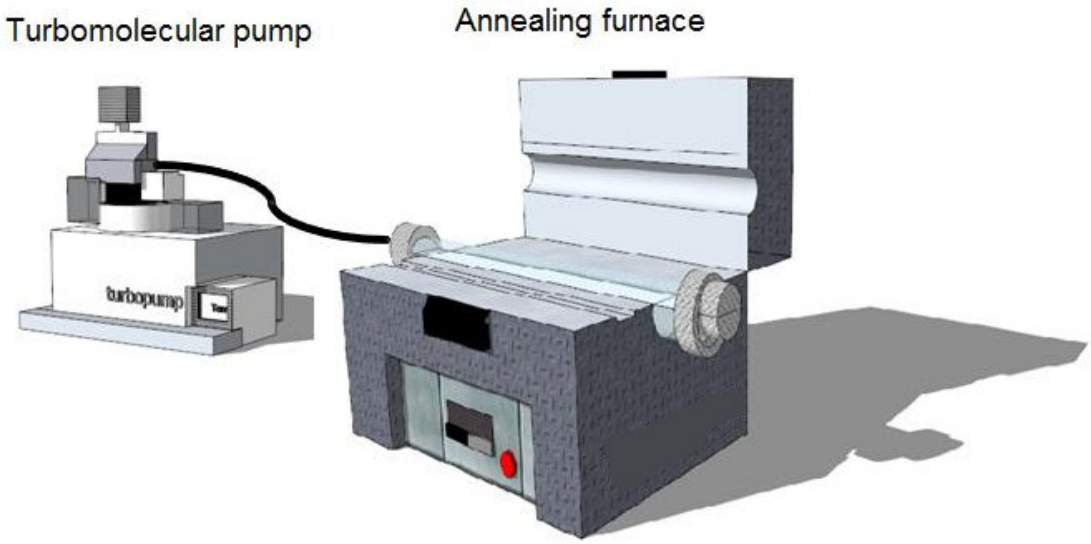

Figure 3.3. Our annealing system (under vacuum)

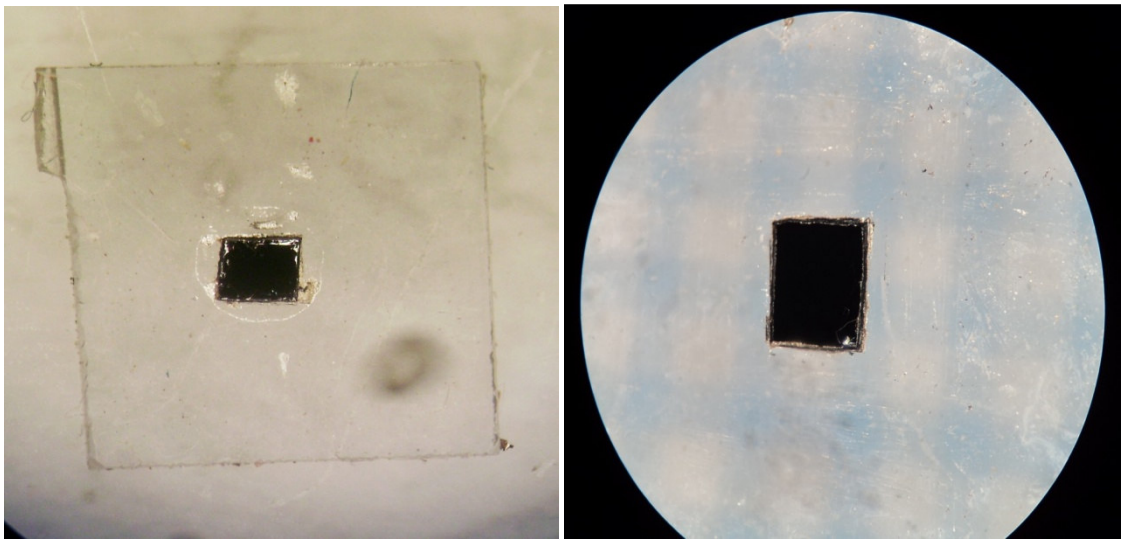

Figure 3.4. Image of the crystal after doping procedure on sapphire substrate

3.3. Mesa Fabrication

The vacuum thermal evaporation deposition technique is basically consists of the heating of the material to be deposited until evaporation. The material vapor finally condenses in the form of a thin film on the substrate surface and on the vacuum chamber walls. To avoid the reaction between the vapor and atmosphere, usually low

pressures are used, about 10^{-6} or 10^{-5} Torr. At these low pressures, the mean free paths of vapor atoms are at the same order of the vacuum chamber dimensions and consequently these particles travel in straight lines from the evaporation source towards the substrate. This gives rise to the 'shadowing' phenomena with 3D objects, especially in those regions not directly accessible from the evaporation source. In addition to this , in thermal evaporation techniques the average energy of vapor atoms reaching the substrate surface is generally low (order of kT, i.e. tenths of eV). This has a serious effect on the morphology of the films, in most cases resulting in a porous and little adherent material. In thermal evaporation techniques, different methods could be applied in order to heat the material namely , resistance heating (Joule effect) or bombardment with a high energy electron beam, usually several KeV, from an electron beam gun (electron beam heating).

In this work, experiments were performed on as-grown Bi2212 single crystals which were grown using floating zone method by Kazuo Kadowaki at University of Tsukuba, Japan. In order to produce single and double mesa structures on the smooth surface of as-grown Bi2212 single crystals, there exists many experimental processes which are needed to be attentiveness. At first, single crystal of Bi2212 is glued onto a sapphire substrate from its smooth a-b surface by silver epoxy (Figure 3.1a).In this process, using the silver epoxy and sapphire substrate is due to their perfect thermal conductors since the differences between crystal temperature and measured temperature on cold-head by sensor affect the electrical results on mesa.

With the purpose of obtaining fresh and flat regions, the crystal was then cleaved with the help of an adhesive tape and was immediately placed in vacuum chamber of the evaporator. A thin film of gold was deposited onto the cleaved crystal in order to protect the surface from chemicals such as photoresist, developer and water during the lithography and also to get electrical contacts for characterization.

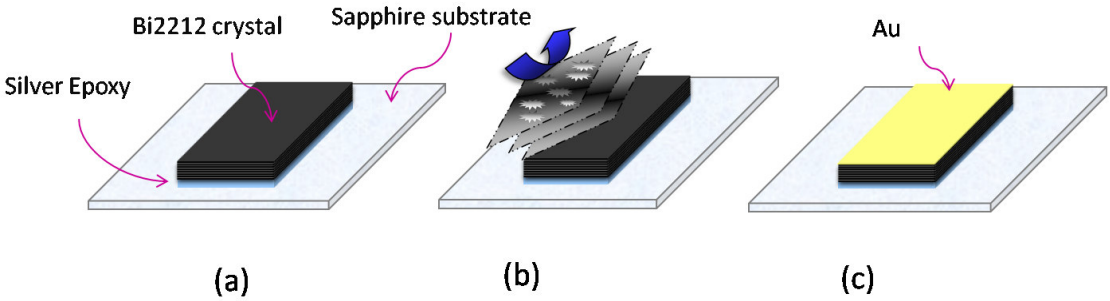

Figure 3.5. The steps in the beginning for the mesa fabrication a) Adhesion crystal on substrate b) Cleaving crystal c) Gold layer deposition on crystal

Schematic representation of our thermal evaporation system can be seen in the Figure 3.5. Thermal evaporation technique is fast and comparatively simple; it registers a low-energy impact on the Bi2212 surface; that is, no surface damage results. This technique includes evaporation of the material in filament boat heated by high current source and re-condensation of the heated material with vapor state onto cooler substrate in a vacuum. Generally it needs high temperatures to evaporate the material and in our system it is carried out by passing large current through the filament boat. The value of the current necessary for evaporation temperature changes with respect to filament boat resistance (its sizes). It is between 190 and 200 A for our filament boat. For the good quality film evaporation should be done in vacuum around 10^{-6} Torr. It is not only necessary to avoid reaction between the vapor and atmosphere but also to increase the mean free path of vapor atoms. Thus they do not undergo collisions with the surrounding gas molecules inside the evaporation chamber. In order to reach high vacuum, turbo molecular pump with back pumping is used in our system. Deposition and thickness of film on the substrate are controlled by shutter and it also provides to get good quality thin films which have not contamination coming from other materials in the boat at the starting of evaporation. Thickness of the deposition is measured by thickness monitor and shutter is closed when required thickness reaches.

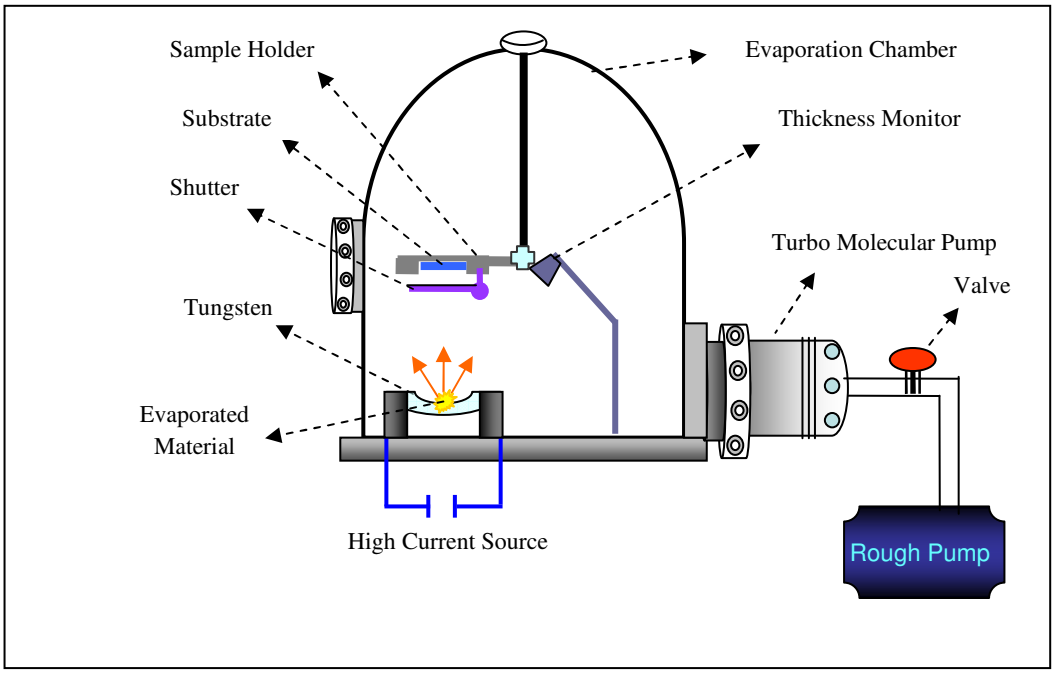

Figure 3.6. Schematic of our thermal evaporation system

3.4. Mesa fabrication with Lithography processes:

The next step in the mesa fabrication is patterning the mesa shape photoresist (PR) by standard optical photolithography or e beam lithography processes. Thus selective areas without regions protected by PR layer are etched down by ion beam while PR patterns protect mesa areas from etching. In the following, both lithography processes is described more in details, with reference to Figure 3.7 which shows an optical photolithography scheme, Figure 3.9 shows an e-beam lithography scheme.

3.4.1. Photolithography Process:

Optical lithography shares some fundamental principles with photography, in that the pattern in the etching resist is created by exposing it to light, either using a projected image or an optical mask.

The first step is that the crystal surface is covered with PR by spin coater. The spinner was rotated at 4.5 V by using power supply for 25 s giving a 1.5 µm layer of resist. The spin coating step is ended with a thermal treatment of the sample in an oven at 90^0C for 30 minutes in order to drive off the excess solvent of the PR solution. For

the third step, the exposure, a mesa shaped mask is placed between UV source and the sample. The resist is a sensitive solution which changes its chemical properties if exposed to a suitable radiation; in particular resist solubility is modified in an appropriate solution called developer which is sodium hydroxide (NaOH) with concentration of 0.2 M in our case. According to the desired pattern, some adsorbing and transparent regions are present on the mask; as a consequence only some regions of the sample are exposed by UV radiation. During the exposure, the solubility of the resist is changed only near the incident radiation, that is to say that only the exposed areas are chemically modified. Afterwards, in the development step, only the exposed resist is removed, thus producing a resist pattern that is a replication of the mask pattern. The sample was then rinsed in distilled water and dried with flow of N_2. Finally, the mesa shaped patterned samples were exposed UV light for 10 seconds for the blanket exposure and hard baked at the 115°C in the drying oven for 40 minutes, which solidifies the remaining PR to make more durable layer for the reactive ion beam etching. (In photolithographic processes I have benefited from previous thesis studies performed by (Türkoğlu 2010; Köseoğlu 2009).

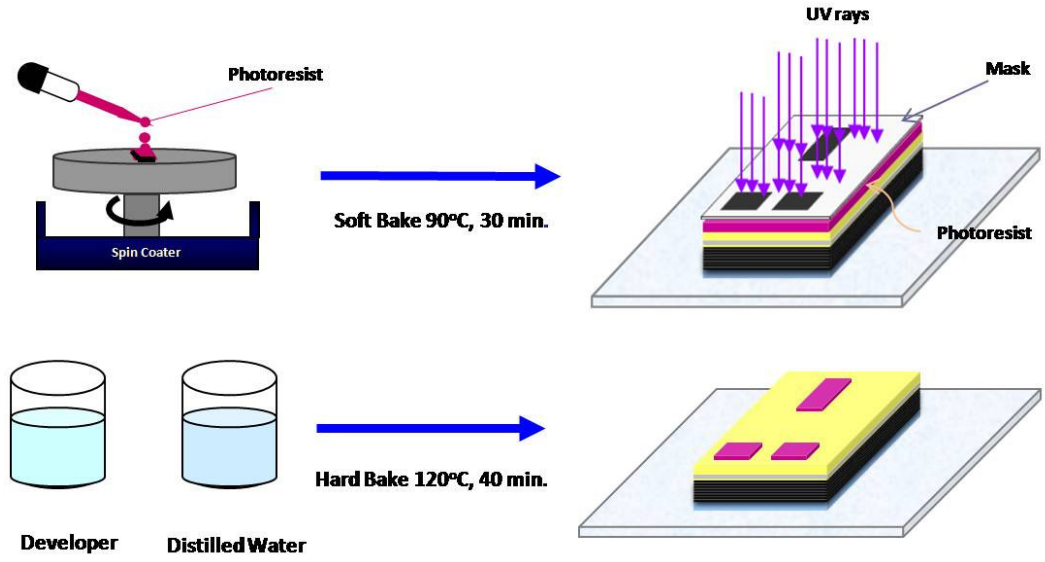

Figure 3.7. Schematic representation of photolithographic processes

3.4.2. E-beam Lithography Process :

Electron beam lithography (EBL) is a method used to determine a pattern on the surface of a thin film that is sensitive to electron impact and is given the name

electron beam resist. The positive photoresist, poly methyl methacrylate (PMMA) are used as the electron beam sensitive film in most of the applications. In order to describe briefly let us denote that, an electron beam exposes selected areas of the resist and a developer removes the exposed areas of the positive resists. On the other hand, in the case of negative resists, un- exposed regions are removed after developing the resist. The purpose of this procedure is to write very small features into the resist consequently these features could be transferred to the substrate material which is placed under the PMMA film.

The most important advantage of electron beam lithography is that ; it is able to create features below the diffraction limit of light i.e. features at the nanometer scale. This is possible due to the small spot size and the short wavelength of the electrons. Electron beam lithography is a maskless process and it could also be adopted to create photomasks which are used in photolithography. There exists a limitation of electron beam lithography that is the long exposure times for a large substrate area.Throughout the long exposure times, beam may drift or electron current from the source may become unstable.

For fabrication by e-beam lithography, we desing the double mesa structures with various dimensions by e-line program.

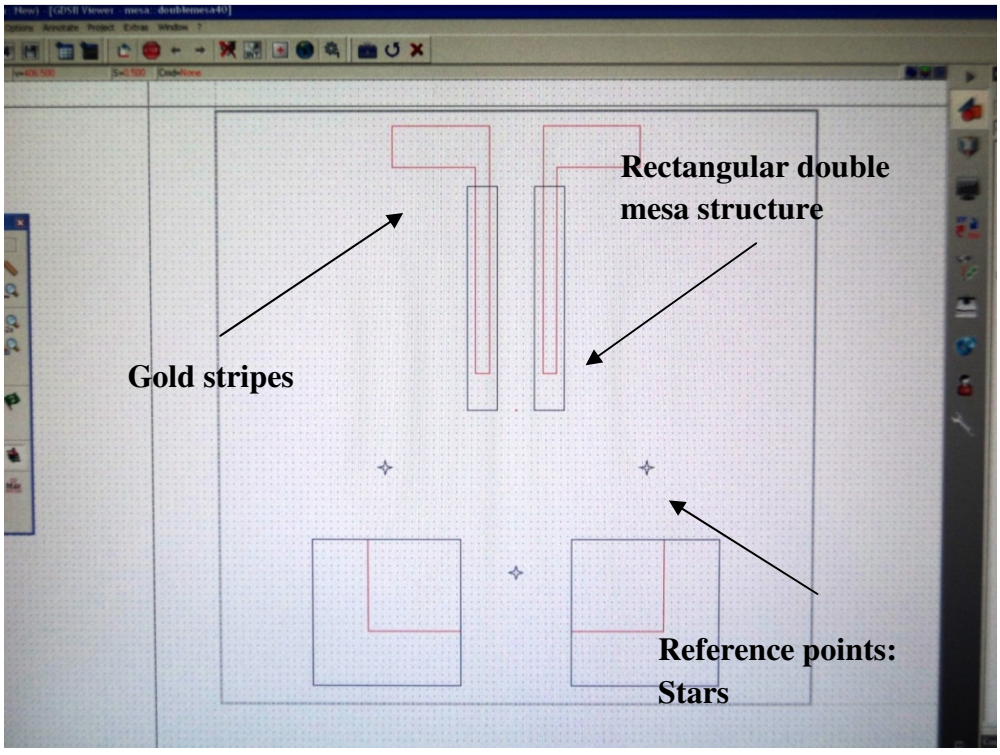

Figure 3.8. The design of the mesa structures by e-line program

The e-beam lithography procedure to create double mesa structures on a Bi2212 crystal is as follow:

- AZ5214 photoresist is spun onto the sample for 60 seconds at 3000 rpm and resulting in a thickness of about 1500 nm
- Sample is soft baked in a oven at 110° C for 30 minutes.
- Sample is exposed at 10kV to form designed mesa patterns
- (Dose = dwell time x electron current).
- Sample is placed in UV light for 10 seconds.
- Sample is developed in 2M NaOH solution for 20 seconds.
- Sample is checked under the microscope and if necessary, sample is developed for a longer time.
- Sample is hard baked in a oven at 110° C for 30 minutes.

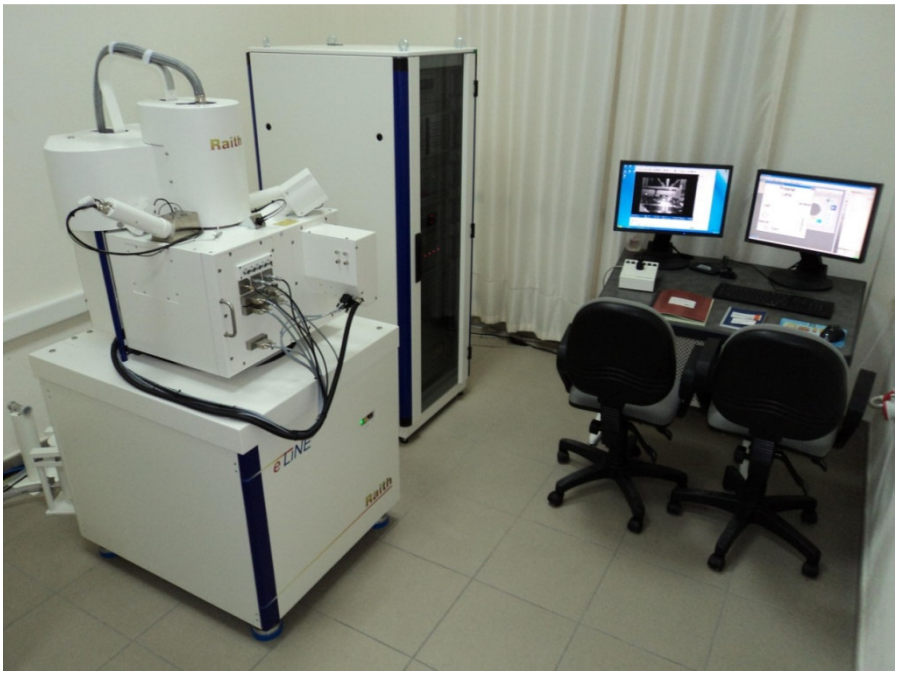

Figure 3.9. Picture of our electron beam lithography system

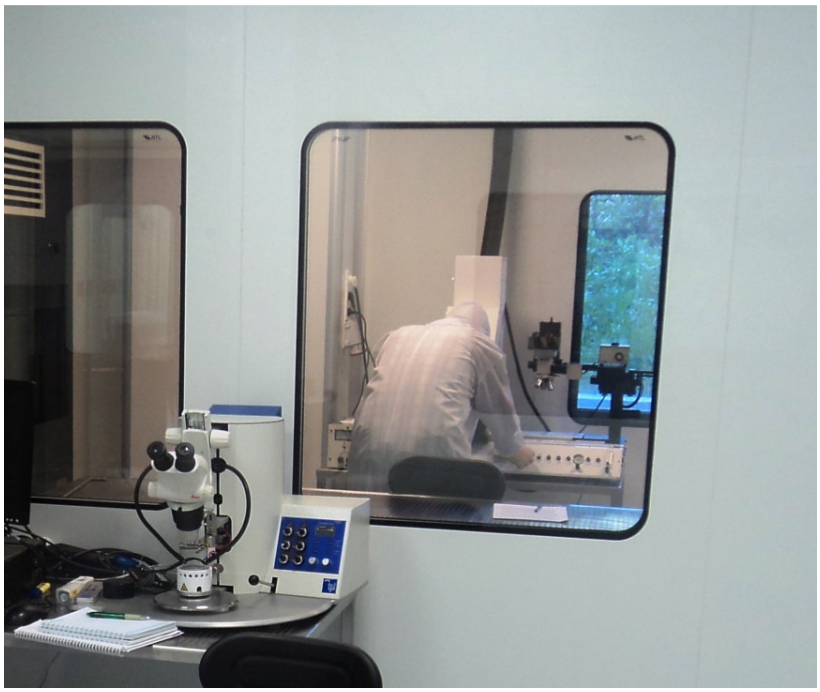

Figure 3.10. Picture of our photolithography system in our clean rooms

3.5. Ion Beam Etching:

To pattern the mesa or micro fabrication in the other research field, there are well known two processes such as, wet and dry etching. Disadvantage of wet etching is the undercutting caused by the isotropy of the etching. The purpose of dry etching is to create an anisotropic etching. It means that the etching is unidirectional. An anisotropic etching is critical for high-fidelity pattern transfer.

After the preparation of mesa shape photoresist pattern on 100 nm gold layer, sample is mounted in ion beam system that produces ion beam accelerated through the surface of sample to etch down some area unprotected by PR layer on crystal. Since the regions protected by PR layer are not etched, the mesa structure with required sizes on Bi2212 single crystal is obtained after the etching (Figure 3.11).

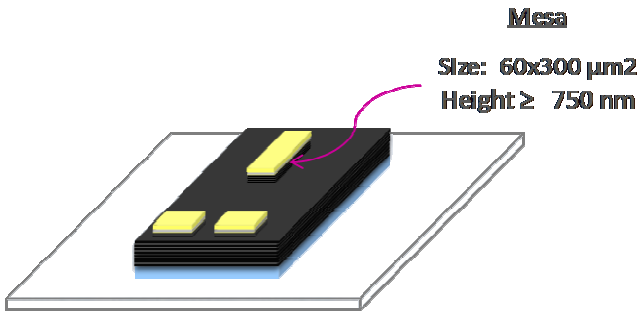

Figure 3.11. Schematic of mesa structure

The picture and top view schematic of our ion beam etching system is shown in figure 3.8 and 3.9, respectively. Samples were mounted to the sample holder and sample holder was placed into chamber with an angle of 67.5° with the direction of ion beam. High vacuum is necessary to increase mean free path of ion beam and it increases the possibility of etching on crystal without lost of their energies by colliding with each other and other atoms in the chamber. Therefore turbo molecular pump with back pump is used to reach the high vacuum that is 10^{-6} Torr for our system. After reached to base pressure, Argon gas was flowed to the chamber using a mass flow controller. Then, dc voltage is exploited to produce and to sustain plasma inside the chamber; the ions beam formed in the plasma are accelerated towards the sample. The parameters for Ar ion beam etching can be seen in table 3.1. During the etching, our sample holder was rotated with the rotary feed through to prevent the differences in lateral angles of mesa and obtain smooth rectangular mesa shape. Because of the collisions between ions and crystal atoms, heating occurs during the ion beam etching. Therefore sample holder was cooled by continuous flow water to prevent the heating on sample during the etching by liquid N_2.

Figure 3.12. Picture of our ion beam etching system

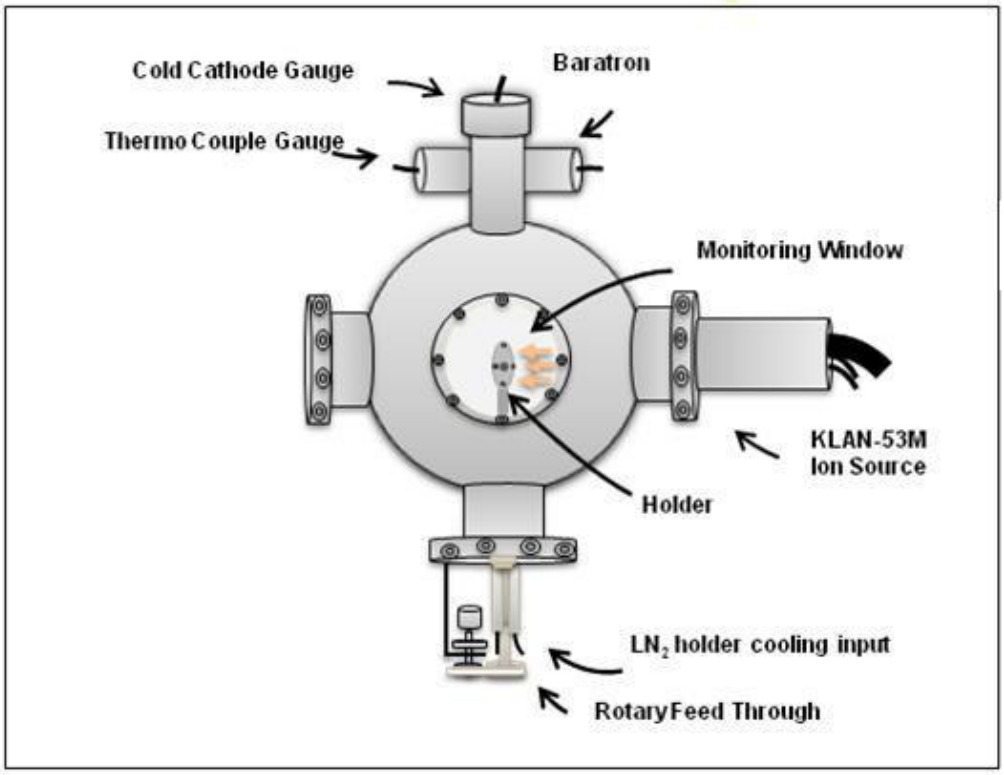

Figure 3.13. Top view schematic of our ion beam etching system

Table 3.1. Ion beam etching parameters for Ar

	Parameters for Ar etching
Discharge	50 V – 0.7 A
Cathode	320 V – 0.45 A
Acceleration	400 V – 1 mA
Ion Beam	300 V – 38 mA
Neutralizer	13 A – 38 mA
Gas Flow	2.7 sccm Ar
Cold Cathode Gauge	5 x10^{-4} Torr

3.6. Fabrication of Gold Stripes :

As it is difficult to make a contact on small area of the mesa, firstly we deposited an insulating layer CaF_2 by evaporation onto crystal and small area of the mesa (Figure 3.10a). After that, a gold stripe was created by lift-off technique on the mesa and CaF_2 layer (Figure 3.14b).

Finally three gold probe wires are connected to the two contact paths and mesa by silver epoxy. The final measurement configuration of mesa structure can be seen in the Figure 3.15.

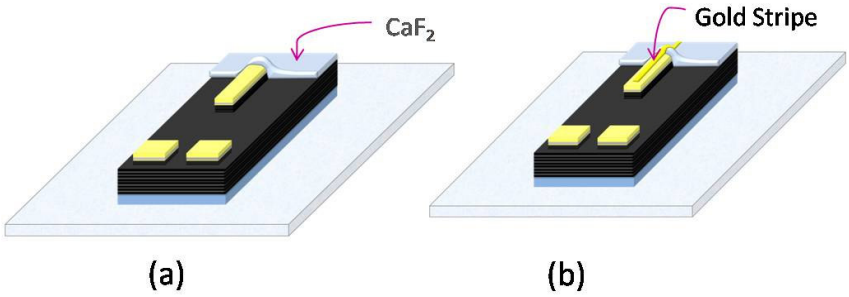

Figure 3.14. a) CaF_2 deposition onto crystal and small part of mesa b) Gold stripe deposition on mesa and CaF_2 layer

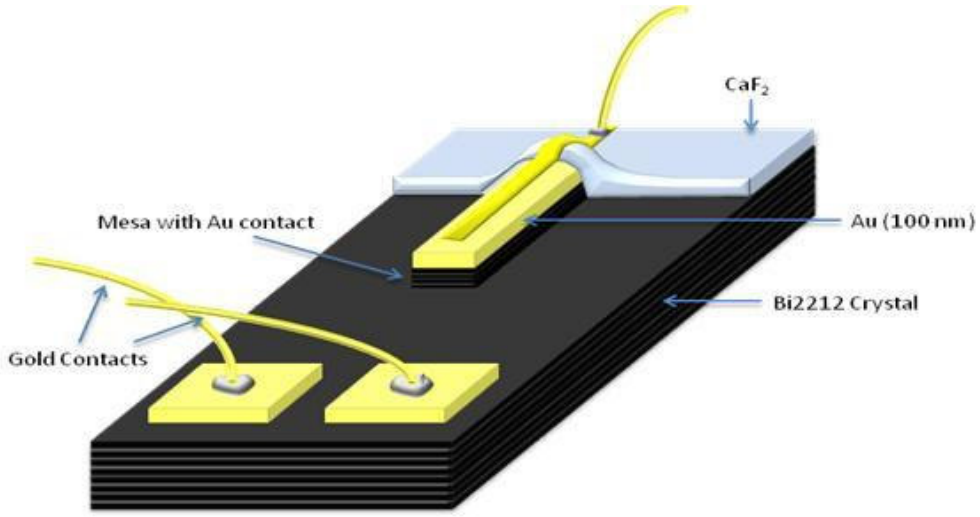

Figure 3.15. The final measurement configuration of mesa structure
(Fulya Turkoglu İYTE M.S. Thesis, 2010)

Steps of lift of technique by e- beam lithography:

- PMMA 200K is spun onto the sample for 45 seconds at 3000 rpm.
- Sample is soft baked in a convection oven at 170° C for 1 minutes.
- PMMA 950K is spun onto the sample for 45 seconds at 4000 rpm.
- Sample is soft baked on a hot plate at 170° C for 1 minutes.
- Sample is exposed at 10kV to form gold stripe patterns.
- Sample is developed in 1:2 MIBK:IPA (Methyl Isobutyl for 90 seconds.
- 200nm of gold is evaporated in the thermal evaporator.
- Sample is placed in acetone for 60 seconds to solve excess PMMA layer.
- Sample is washed with DI water for 60 seconds.

3.7. R-T, I-V Measurements

In order to obtain the characterization of the Bi2212 mesas, we have measured c-axis resistance versus temperature (R-T), and current-voltage behavior (I-V) in a He flow cryostat system which is equipped with an optical window as shown in figure 3.12. With the purpose of cooling the crystal, liquid He was transferred from external reservoir to copper cold finger inside cryostat. The temperature of the sample on cold finger was controlled by heater and temperature sensor that are interfaced by a

temperature controller. In the system there was a turbo molecular pumping system which operates between cold finger and shield of the cryostat until reaching ultra high vacuum. Owing to the good thermal isolation, temperature of sample could be reduced up to 4.2 K and also the influence of ambient temperature on measurement was reduced by using ultra high vacuum thermal isolation.

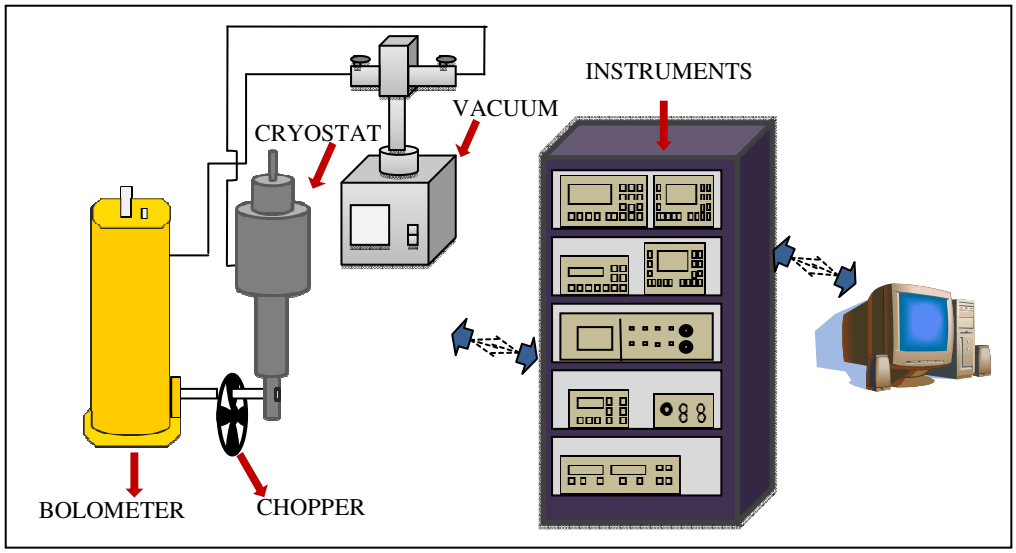

Figure 3.16. The schematic of our He flow cryostat system

For the R-T and I-V measurements the schematic representation of our experimental setups is presented in figure 3.14. The experimental setups are interfaced with a computer and controlled by Lab-view program which consists of serial instrument control, data analysis and data storage. In addition to this it has a graphical programming tool which provides to observe the drift of the experimental result during the measurement and moreover there is a block diagram form that allows creating program for the measurements.

During the phase where the temperature varies from room temperature to 20 K, simultaneously changing mesa resistance values with temperature are measured using the experimental setup given in figure 3.17a. This setup includes a current source, a voltmeter and a temperature controller and they are interfaced with a computer. The variations at voltage and temperature are measured by the voltmeter and the temperature controller respectively. During the measurement since applied current along to mesa height is constant , the experimental data is analyzed and stored such as

R-T by Lab-view program. With the purpose of obtaining accurate data, current with both positive and negative directions are rapidly applied by current source, resistance is measured twice for both direction of applied current and average of these resistances are used. There is a problem in thermal equilibrium between crystal and cooling head since a good thermal isolation with vacuum between cold head and shield at the cryostat cannot be well created.

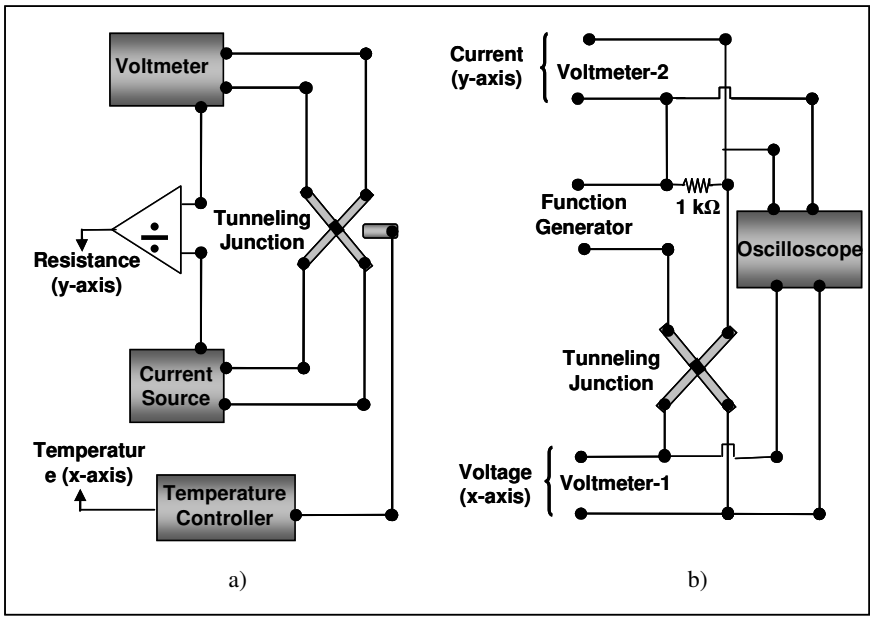

Figure 3.17. Schematic representations of a) R-T b) I-V measurement setups

In Figure 3.17b , I-V experimental setup interfaced with a computer is presented. This setup provides two voltmeters in order to measure the voltage of mesa including all junctions and applied current on resistance serially connected to circuit between function generator and mesa. On the other hand ,the function generator is used to apply current with required frequencies and amplitudes. During the I-V measurement, sample temperature is kept constant by temperature controller. In order to establish a perfect I-V measurement with hysterical behavior and much quasiparticle branches, current with low frequency (5 mHz) is applied while its amplitude is gradually increased until obtaining whole hysterical curve including normal state. The oscillator is provided in order to observe the voltage jump value and I-V drift before starting to measurement. Thereby the data including current versus voltage and constant temperature is obtained by Lab-view program. I-V measurements have been carried out at various temperatures.

CHAPTER 4

RESULTS AND DISCUSSION

This chapter begins with optical microscope images, scanning electron microscope images, electrical characterization consequences of Bi2212 mesa structures and this is followed by analysis and discussion of graphs.

4.1. Structural Characterizations:

4.1.1 Optic Microscope Images

For the each step of mesa fabrication, we take the optical photos of the crystals to have a general idea of surface roughness and condition of the mesa structures.

If we look at the Figure 4.1. we can see the rough and nonsmooth surface of the Bi2212 crystals which disappears after the cleaving process, the fresh, smooth and clear top layers are seen in Figure 4.2., structural quality is high in this case. During the annealing treatment, surface of the crystals are covered with a kind of contamination that's why we see a quite different, dirty layers.

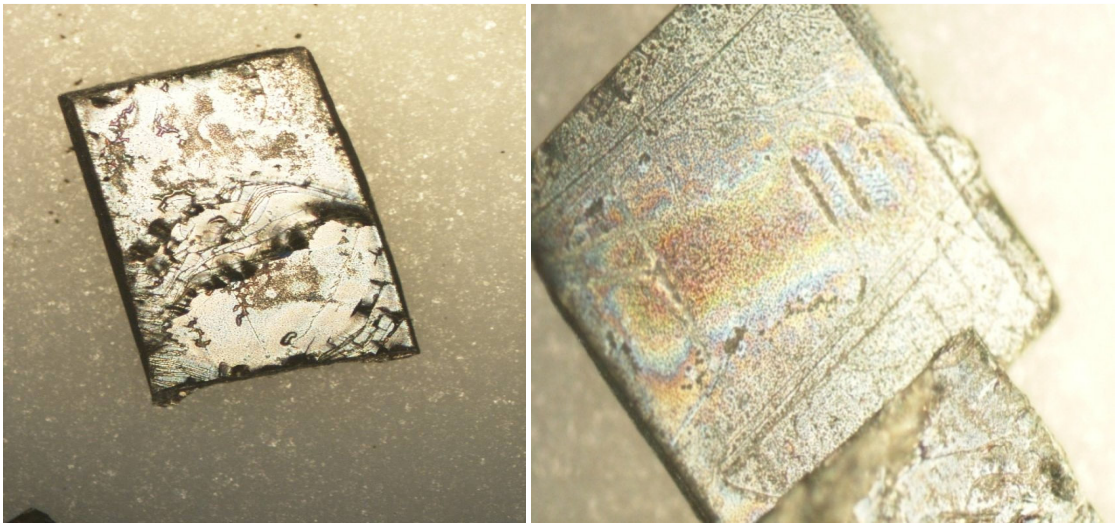

Figure 4.2. Optical image of crystals after annealing

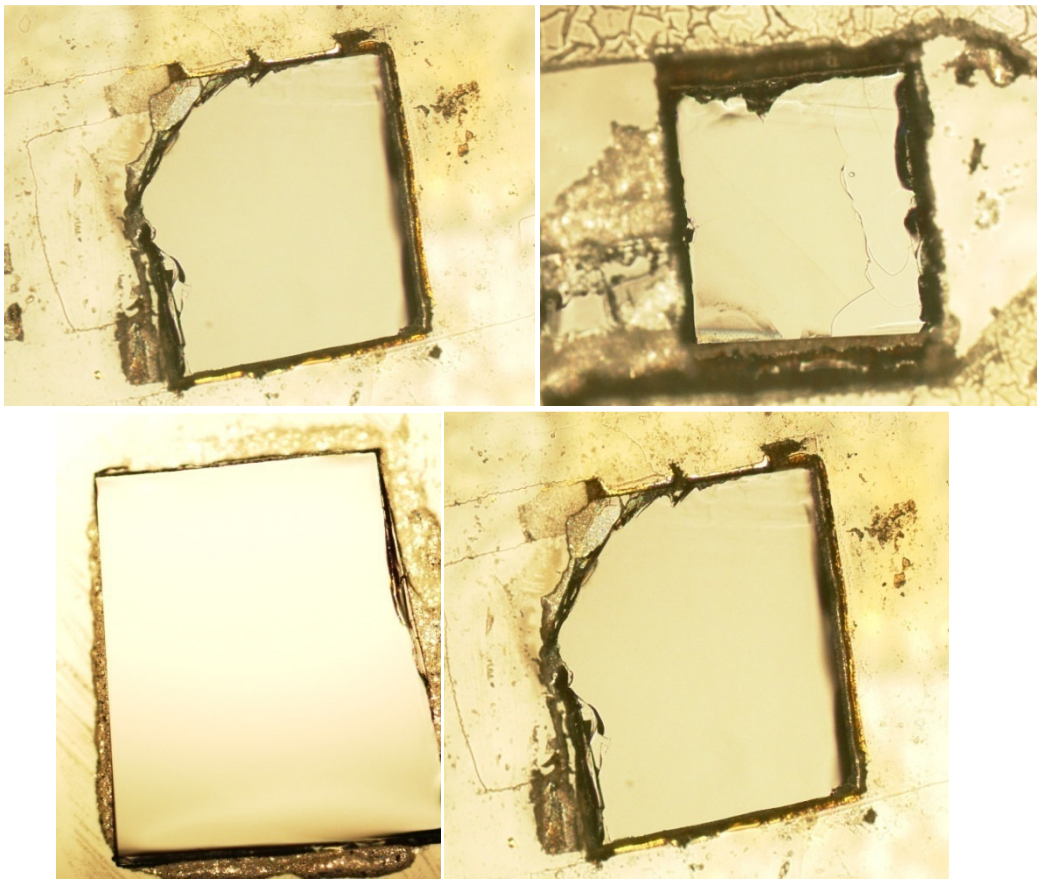

Figure 4.2. Optical image of crystals after the cleaving process

Figure 4.3. shows the fabricated single mesa structures by photolithography process with dimensions of respectively 60x300 µm and 30x300 µm. It is clearly observed from SEM pictures that although during the lithography procedures crystals sustained to many chemicals and other materials, surfaces are stil fresh and smooth.

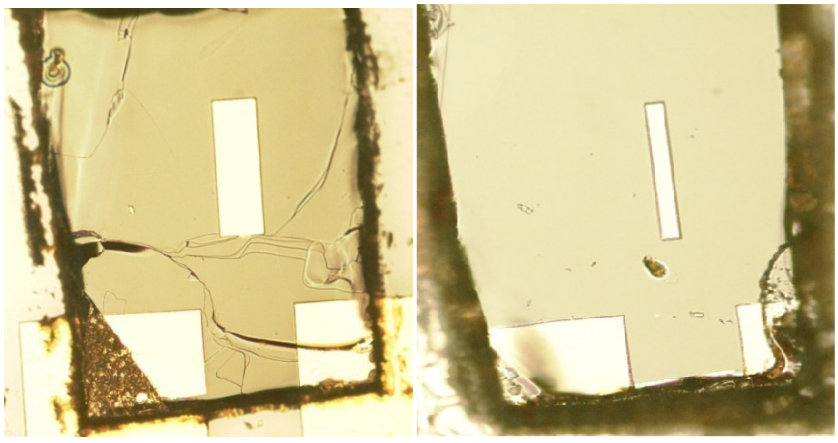

Figure 4.3. Optical image of crystals after single mesa fabrication

For electrical measurements, we compose gold stripes by electron beam lithograpy for 3 point contact method as observed in Figure 4.4. Also insulating CaF_2 layer at the top of the mesa structure and silver paint contacts are clearly seen.

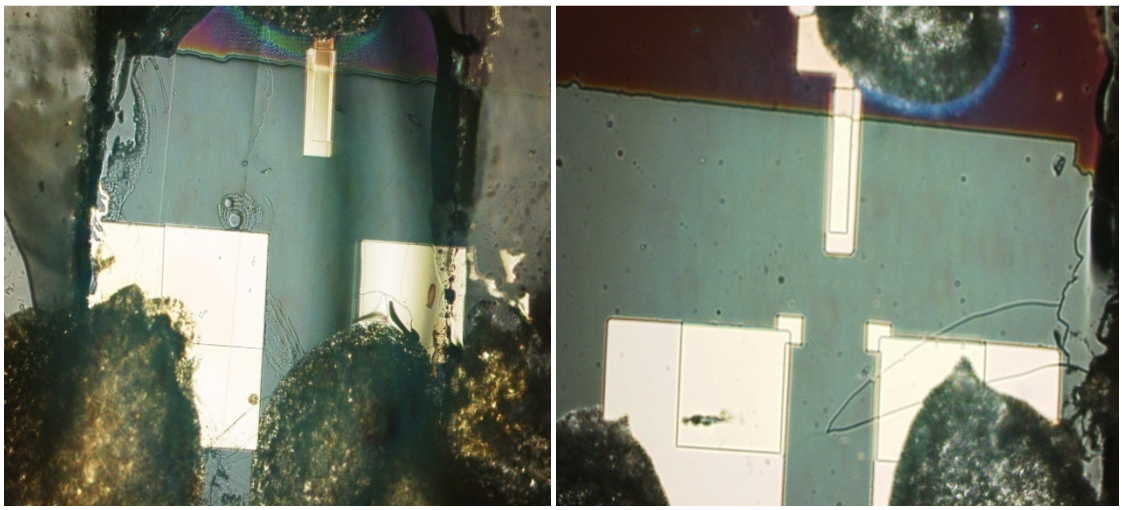

Figure 4.4. Optical image of crystals after gold stripe fabrication by lift off technique

4.1.2. SEM and Profilometer Results:

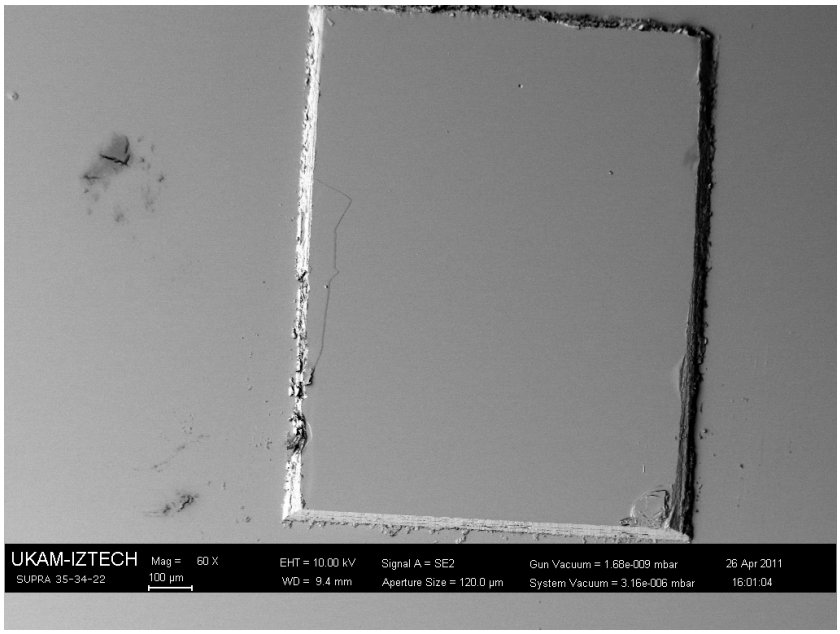

Figure 4.5. SEM image of a cleaved crystal before fabrication.

Figure 4.6. indicates the roughness and quality of the crystals after cleaving procedure.

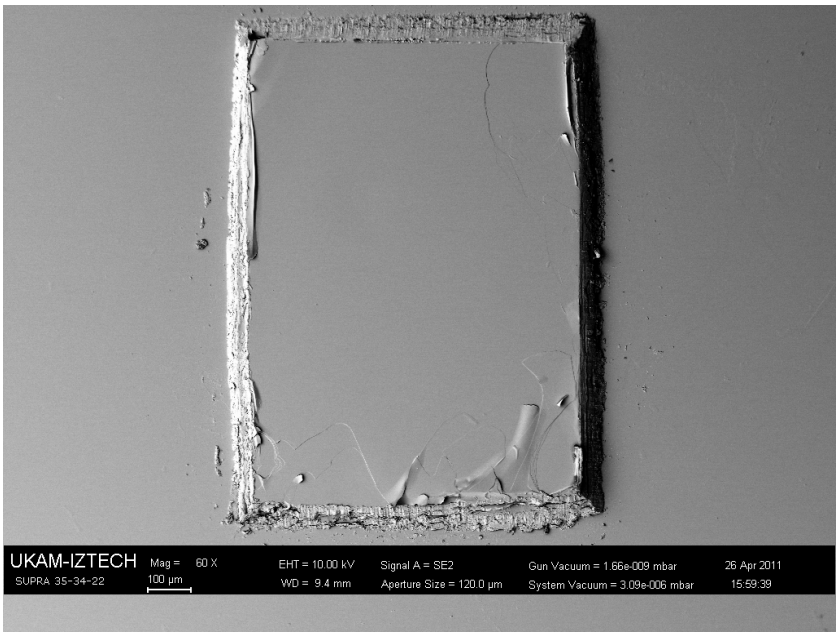

Figure 4.6. SEM image of a cleaved crystal before fabrication.

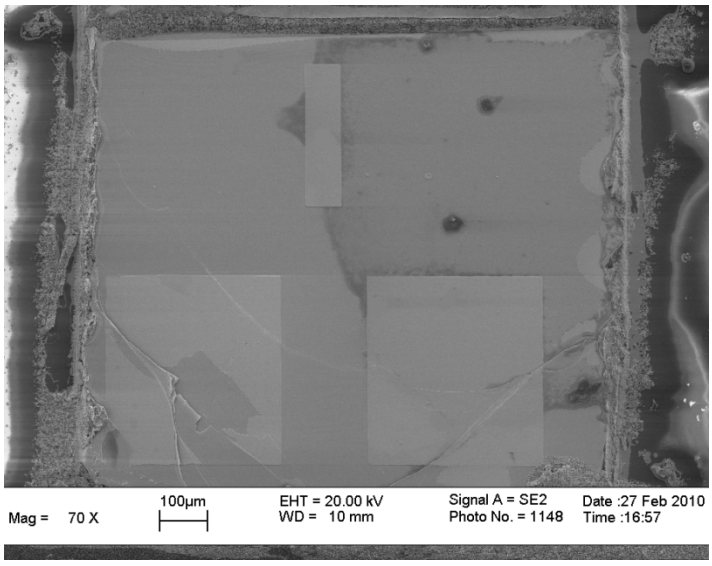

Figure 4.7. SEM image of YD 04 (single mesa)

From Figure 4.7. and Figure 4.8. it is clearly seen that the edges of the mesa structure of YD 04 are not sharp and straight.

Also the glass mask that we use for photolithography process may not be clean enough so we see some defects and semihole like structures on the lateral sides of the mesa.

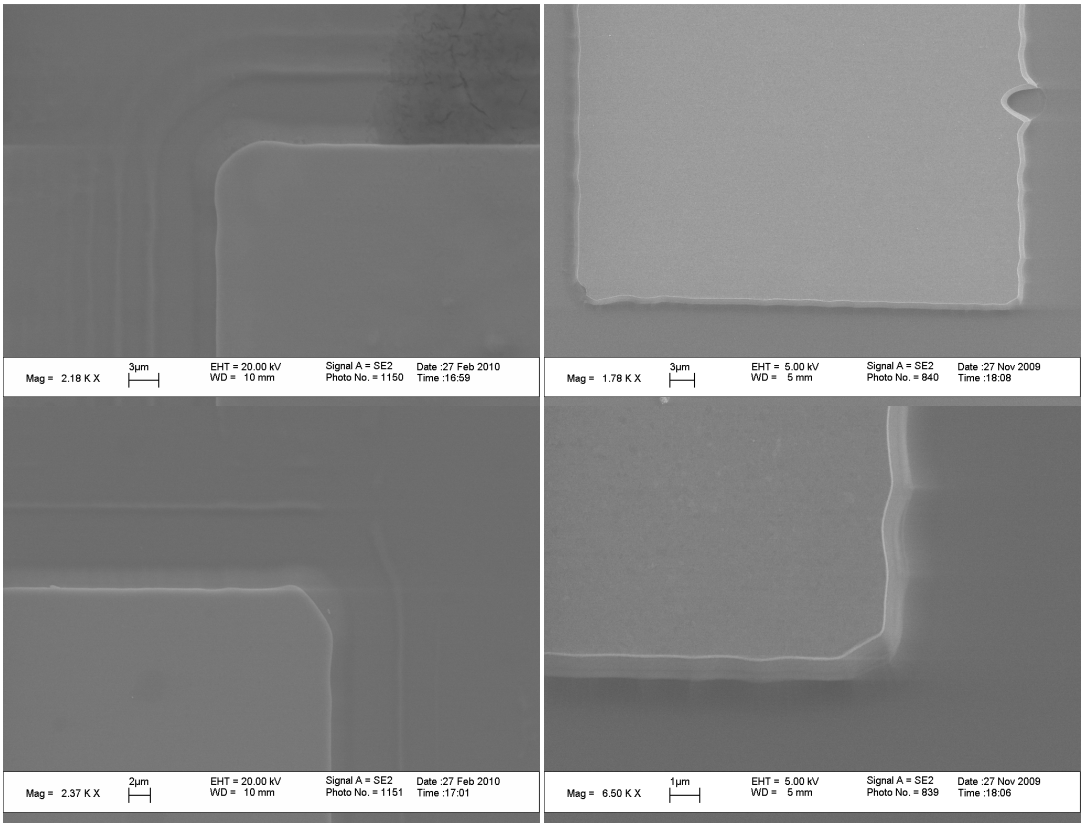

Figure 4.8. SEM images of YD 04 (single mesa) with different magnifications

For the sample YD 07 one of the gold square contact pads is not seen, because of the long etching duration photoresist layer can damage with the heat effect and gold layer on pad structure can be etched also. Especially around the mesa structures we observed the perfect surface of Bi2212 crystals.

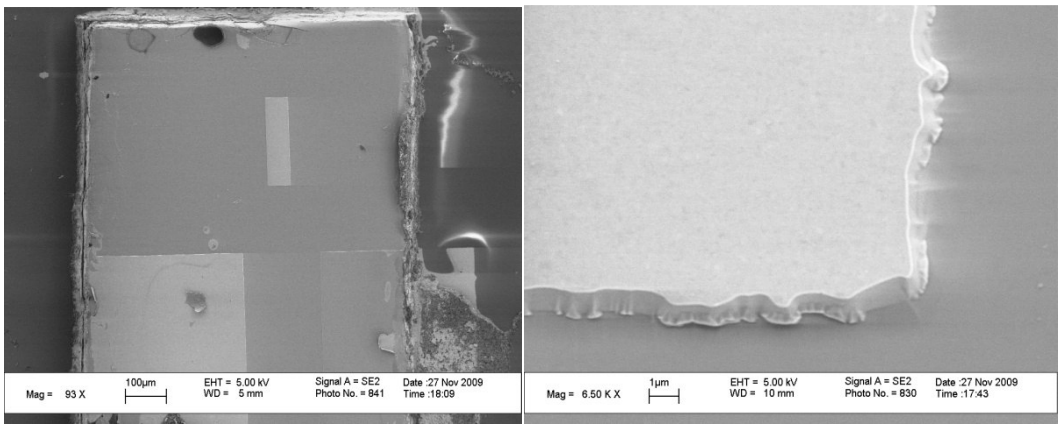

Figure 4.9. SEM images of YD 07 (single mesa) with different magnifications

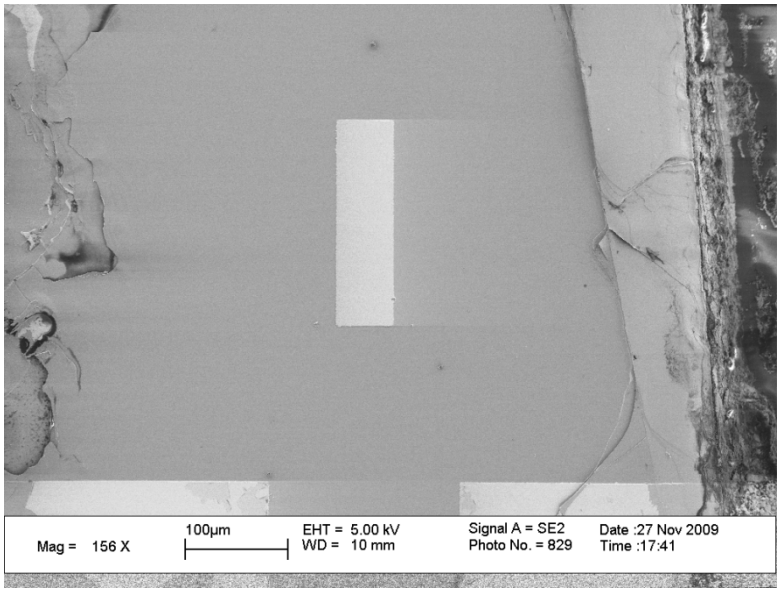

Figure 4.10. SEM images of YD 10 (single mesa) with different magnifications

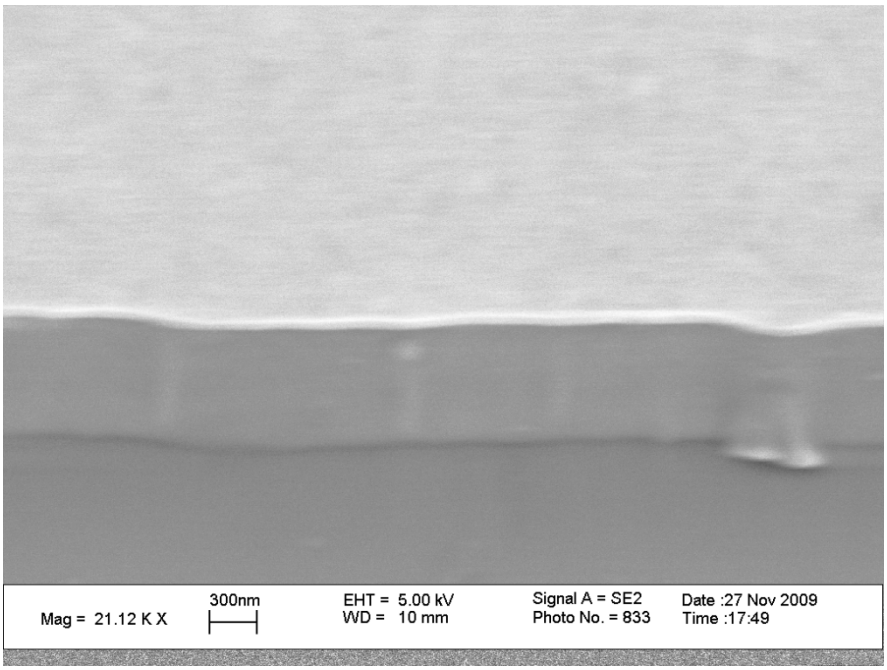

Figure 4.11. SEM images of YD 10 (single mesa) with different magnifications

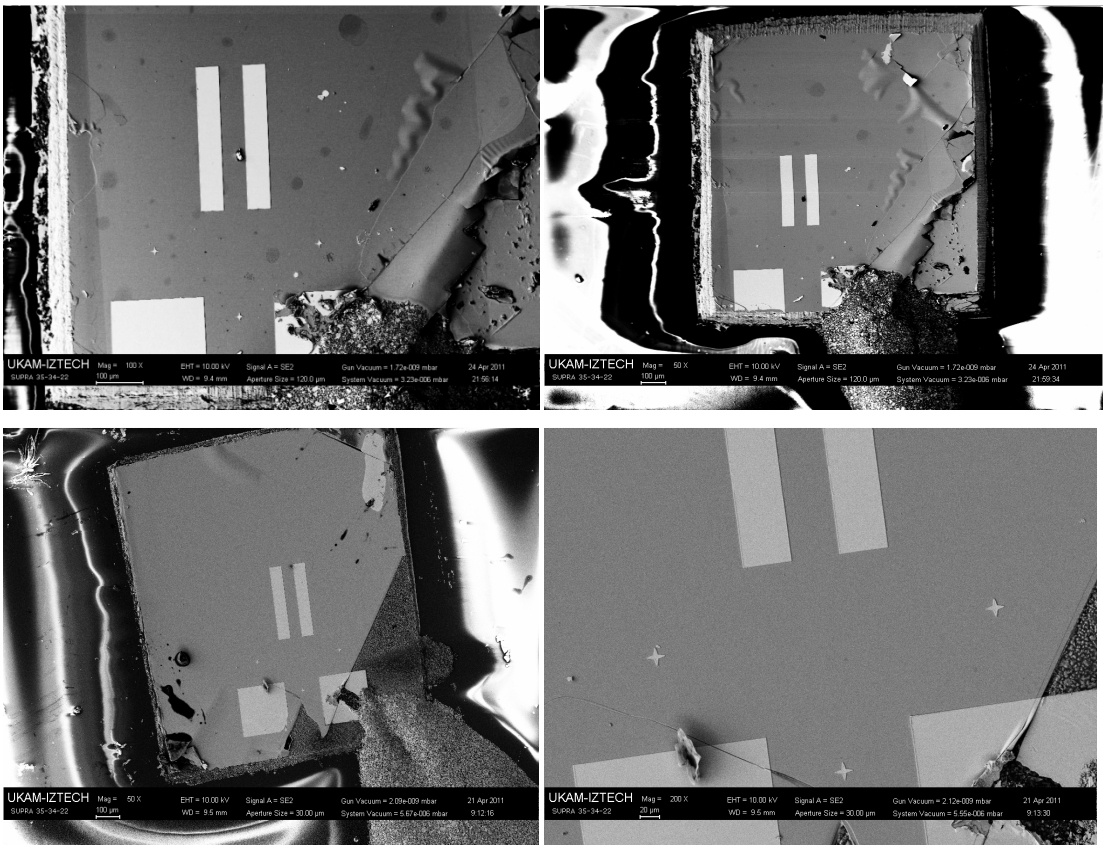

Figure 4.12. SEM images of a double mesa structure of YD 41

YD 41 is one of the samples that patterned by electron beam lithography, so from the SEM images from 4.13. double mesa structures and the stars between the mesas and pads that we use for allignment of gold stripes, are clearly seen. In electron beam system we design a software mask instead of glass mask which means we do not have problems about mask cleaning and so mesa edges are sharp and slight.

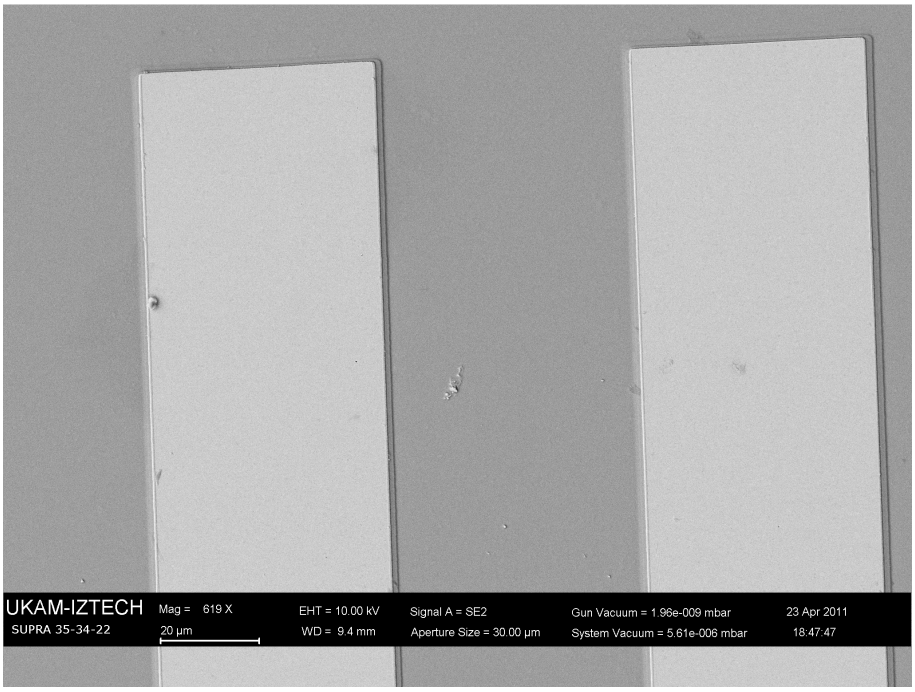

Figure 4.13. SEM images of a double mesa structure

In this work, surface profilometer was used to measure thicknesses of deposited Au film onto the Bi2212 single crystal surface and thickness of the Au/Bi2212 mesa structures. We employ SEM to image roughness of the side faces of the mesa and to image the condition of the mesa structures. Accuracy of profilometer is just for height (c-axis) measurements, so, slope of the long side faces characterized using both SEM and profilometer images.

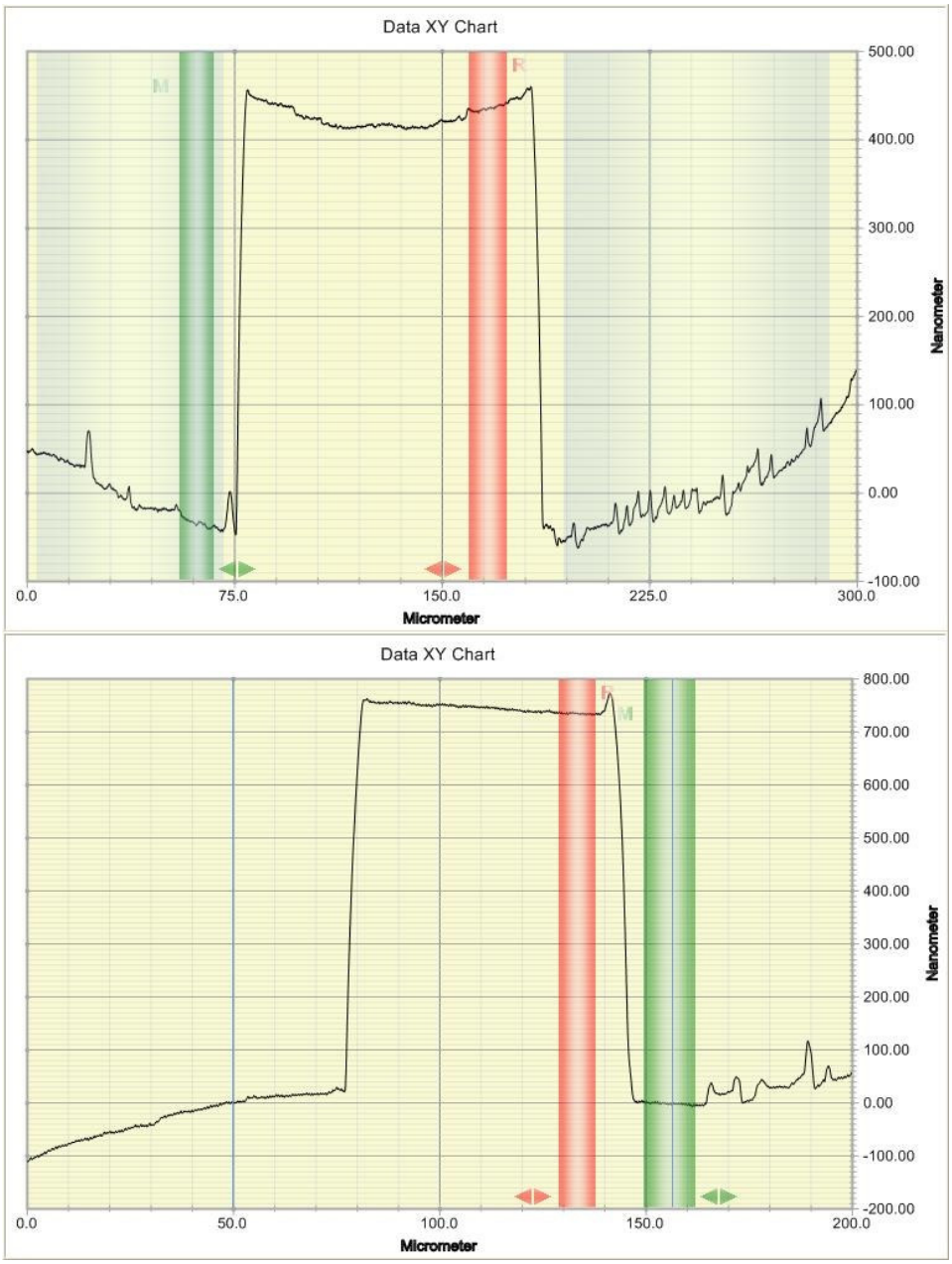

Figure 4.14. Step-height analyses of YD 10 and YD 11

The step-height analyses of two fabricated mesas are shown in Figure 4.14. which belong to YD 10 and YD 11. These heights include also thicknesses of deposited thin films. The height of the single crystal into the mesa can be obtained by subtracting thicknesses of deposited thin films from height of entire mesa. In order to determine the height of evaporated Au layer on the crystal surface, we use a thickness monitor. Thicknesses of deposited Au thin film and two different edges of mesa are shown in Table 4.1. For example, mesa with height of 1μm contains approximately 670 IJJs.

Figure 4.11. shows the SEM images of YD 10 with different magnifications. It displays a considerable surface roughness of the side faces of the mesa. SEM images of the mesas indicate that mesas are trapezoidal (narrow top, wide bottom). We can find the length difference between bottom and top of one edge of the mesa using SEM images. Using this length difference (SEM data (c-axis)) and the height of mesa (Profilometer data (a-axis)), the angle between the basal plane and the side of the mesa can be calculated by Equation 4.1.

$$\theta(lateral \quad angle \quad of \quad mesa) = \tan^{-1}\left(\frac{profilometer \quad data \quad (c-axis)}{SEM \quad data \quad (a-axis)}\right) \tag{4.1}$$

Table 4.1. Height of mesas and deposited thin films

Mesa type	**Mesa height**	**Au height**	**Mesa dimension**	**Doping time**
YD04-single	806nm	~100nm	60x300 μm^2	48hr 450^0C
YD07-single	752nm	~100nm	60x300 μm^2	48hr 450^0C
YD10-single	850nm	~100nm	80x300 μm^2	2hr 450^0C
YD12-single	600nm	~100nm	80x300 μm^2	2hr 450^0C
YD17-single	600nm	~100nm	80x300 μm^2	2hr 450^0C
YD21-single	810nm	~100nm	80x300 μm^2	2hr 450^0C
YD22-single	700nm	~100nm	80x300 μm^2	2hr 450^0C
YD23-single	613nm	~100nm	80x300 μm^2	2hr 450^0C
YD24-single	600nm	~100nm	60x300 μm^2	7hr 425^0C
YD25-single	2000nm	~100nm	60x300 μm^2	7hr 425^0C
YD27-single	1500nm	~100nm	60x300 μm^2	7hr 425^0C
YD38-double	615nm	~100nm	60x300 μm^2	4hr 450^0C
YD39-double	830nm	~100nm	60x300 μm^2	4hr 450^0C
YD40-double	847nm	~100nm	60x300 μm^2	4hr 450^0C
YD41-double	1500nm	~100nm	60x300 μm^2	4hr 450^0C

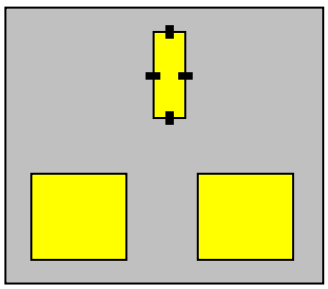

Figure 4.15. Labeled codes of mesa edges

4.2. Electrical Measurement Results

4.2.1. Temperature Dependence of c-axis Resistance in Bi2212

c-axis resistance versus temperature (R-T) characteristics of the as-grown Bi2212 mesas were measured in a He flow cryostat system. This measurement gives very useful information to check the condition of the mesa such as the contact resistance, the sample quality, the doping level. R-T measurements of some of the fabricated mesas are seen in Figure 4.17, Figure 4.18, Figure 4.19. and Figure 4.20, that are belong to samples YD 10, YD 12, YD 25, YD 27 and YD 41, respectively.

The sharp phase transitions to superconducting state are seen in all R-T graphs. The curves exhibit a typical temperature dependence of the c-axis resistance of as-grown Bi2212 single crystal, which exponentially increase with decreasing temperature from room temperature to Tc. The onsets of critical temperatures of the mesas are between 88 and 91 K. Both temperature dependence of the resistance and the superconducting transition temperatures of the mesas indicate that samples are in the near underdoped state of the Bi2212 crystals. The transition width, ΔTc, is mostly 4–7.5 K. Transition temperatures and their transition width values of the samples are shown in Table 4.2.

Table 4.2. Electrical properties of the mesas

	$R_{Tc(onset)}$	$R_{300\ K}$	$R_{contact}$	$R_{Tc}/R_{300\ K}$	$T_{c(onset)}$	ΔT_c
YD10	33.6 Ω	11.6 Ω	12.2 Ω	2.89	89 K	4.0 K
YD12	33 Ω	12 Ω	11.8 Ω	2.75	89 K	4.0 K
YD25	85 Ω	20 Ω	1.3 Ω	4.25	88 K	4.0 K
YD27	12.2 Ω	5.2 Ω	1.08 Ω	2.34	88 K	2.0 K
YD41	11.1 Ω	5.8 Ω	0.98 Ω	1.9	90.8	7.0K

As seen in all R-T graphs the mesa resistance is finite even below T_c. It is not a temperature dependent electrical behavior proper to superconducting crystal. This is because of the contact resistance due to three-point measurement configuration. This configuration is not generally preferred to four point contact method for accurate measurement because there is one contact probe on mesa which is used for both applying current and measuring voltage and it causes reading surface resistance at superconducting state. However four point contacts is very difficult to fabricate on small area of mesa. For all fabricated samples, contact resistance is usually smaller than a few ohms. Therefore, it seems not to influence the measurement, but it may contribute to the heating.

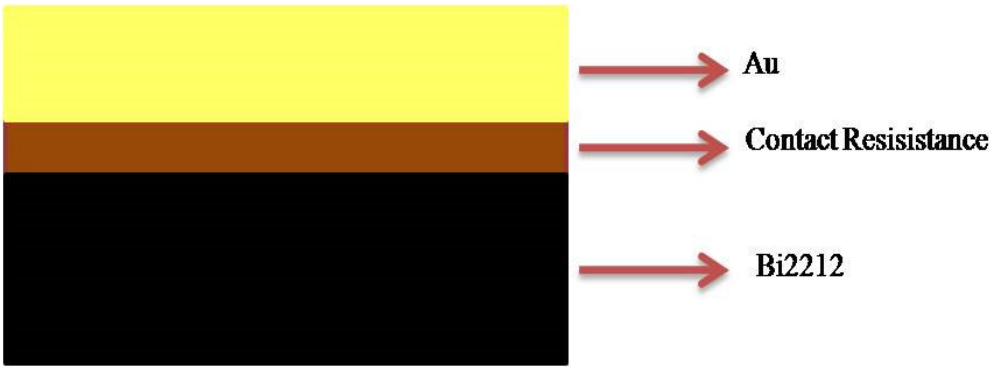

Figure 4.16. Side view of mesa to show the contact surface resistance between gold layer and surface of Bi2212

The reason of contact resistance is the interface between gold layer and surface of Bi2212 as shown in Figure 4.16. This kind of contact resistance increases at low temperatures, because the interface behaves like tunneling barrier. Assuming that the contact resistance is weakly dependent on temperature above T_c, the $R(T_c)/R(300\ K)$ values in Table 4.2 give at least a hint. For all fabricated mesas, the ratios of $R(T_c)/R(300\ K)$ are between 1.8 and 4.3. THz emitting mesas are below a certain underdoped level of Bi2212 and their $R(T_c)/R(300\ K)$ values are bigger than 4 (Ozyuzer, et al. 2007). As we can see from the table, only $R(T_c)/R(300\ K)$ value of YD 25 is bigger than 4. Since the oxygen doping level dependence of the c-axis resistivity of Bi2212 was systematically studied by Watanabe et al. 1997, $R(T_c)/R(300\ K) > 4$ indicates a necessity of a certain doping range of $\delta \sim 0.22$ for THz emission.

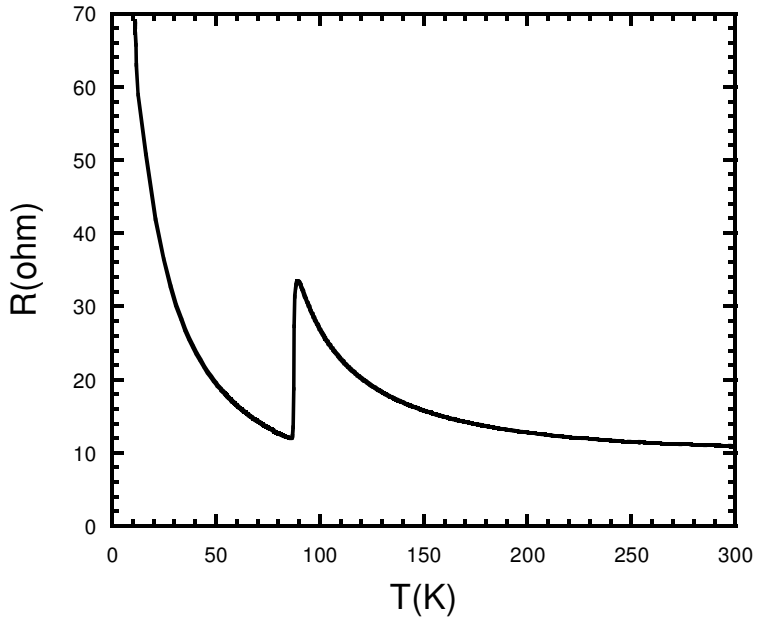

Figure 4.17. Resistance versus temperature behavior of YD 10

In R-T graph of YD 10, contact resistance is seen. In order to minimize contact resistance, samples can be annealed at, but it was not generally preferred since oxygen doping level in Bi2212 does not change. There are several reasons of contact resistance. Firstly it may be caused by resistance of silver epoxy connected gold wire to patterns on Bi2212, because this conducting adhesion is obtained by mixing two equal composites. If they are not mixed well, its conductance will be low. The other reason is the interface

between gold layer and surface of Bi2212. This kind of contact resistance increase at low temperature, because the interface behaves tunneling barriers and temperature dependence of barrier height is dominant in contact resistance. Therefore in R-T graphs, we see increasing in resistance from T_c to low temperatures.

R-T behavior of YD 12 with dimensions of 60x300 µm is seen, I=10 µA is used as a constant current we note that the resistance below T_c is due to the contact resistance.

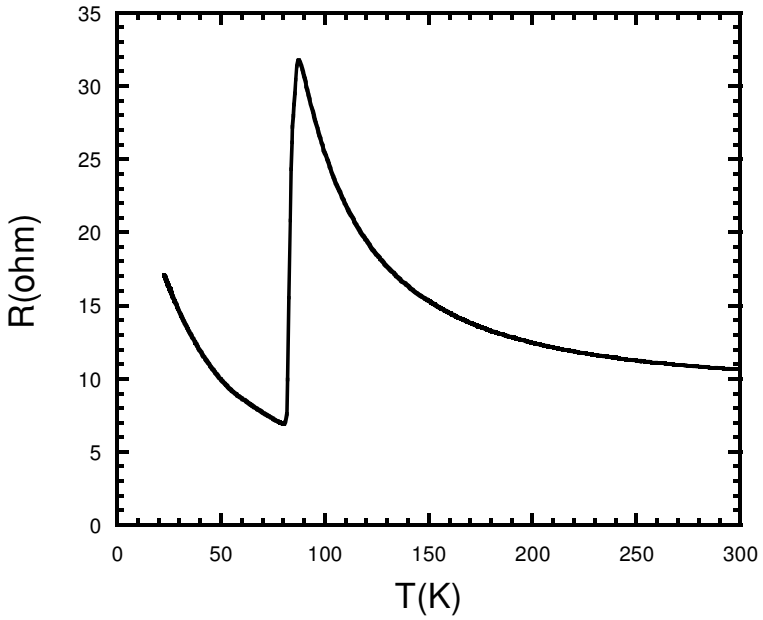

Figure 4.18. Resistance versus temperature behavior of YD 12

The most negligible contact resistance in our R-T measurements is belong to the YD 25 one of the 60x300 µm mesa structures patterned by photolithography process as observed in Fig. 4. 19. It is just a few ohms. We calculate the $R(T_c)/R(300\ K)$ value of the sample from the graph and compare it with out-of-plane resistivities with previous studies (Watanabe et.al.1996), we investigate that it matches with the σ=0,22 which corresponds to underdoped level.

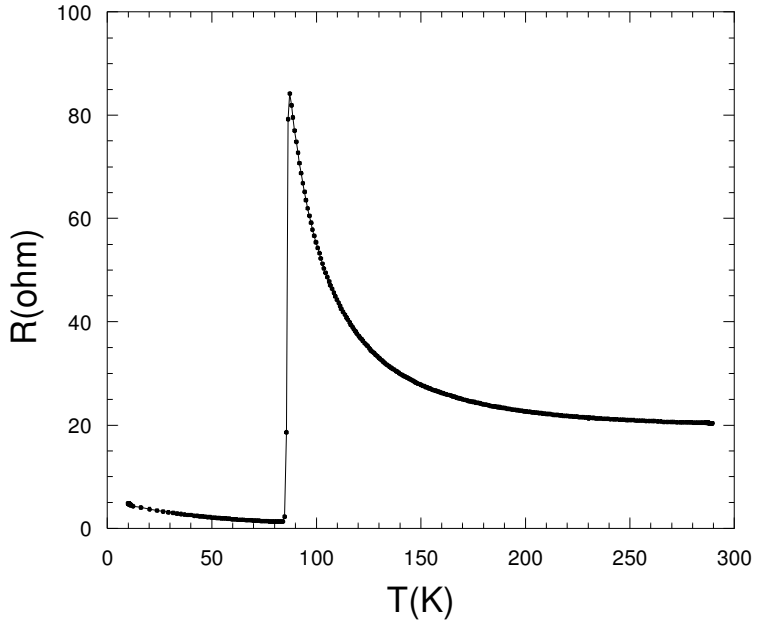

Figure 4.19. Resistance versus temperature behavior of YD 25

In Fig. 4. 20, we observe increase of the contact resistance at low temperatures, the sample has a critical temperature of 88 K.

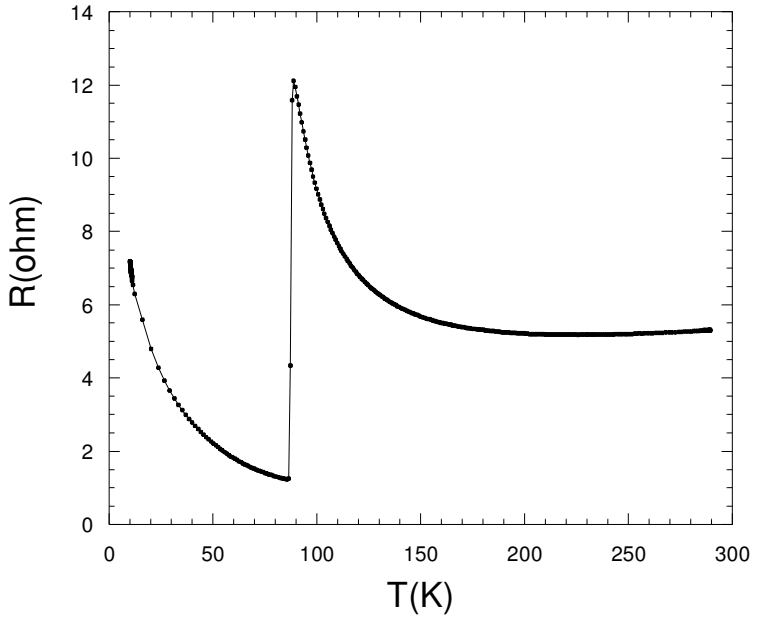

Figure 4.20. Resistance versus temperature behavior of YD 27

In Figure 4.21., critical temperature value of the 60x300 µm double mesa structure is 92 K, contact resistance is low and ıf we calculate the $R(T_c)/R(300\ K)$ and compare it with out-of-plane resistivities with previous studies (Watanabe et.al.1996), we investigate that it matches with the σ=0,20, slightly underdoped region.

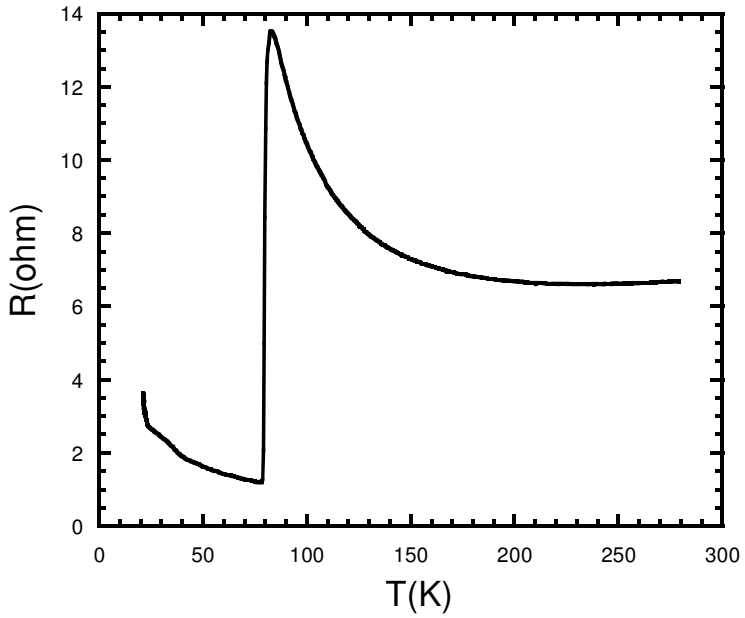

Figure 4.21. Resistance versus temperature behavior of YD 41

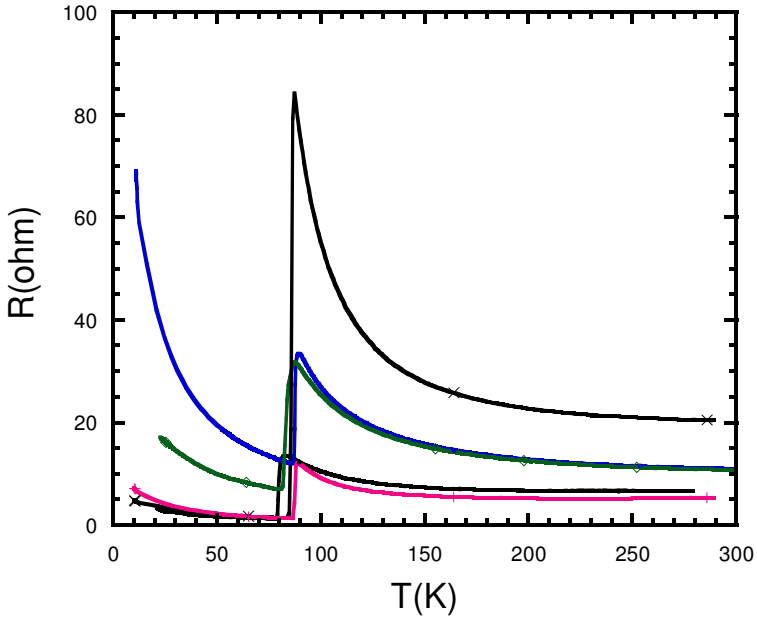

Figure 4.22. Resistance versus temperature behavior of all samples together

Figure 4.22. presents 60 µm width mesa structures annealed at various conditions, If we calculate the $R(T_c)/R(300\ K)$ values we can have an idea for the doping level. We observe that the overall magnitude of c-axis resistivity of the crystal increases with decreasing doping level. At variation of oxygen level from the optimally doped to overdoped, c-axis resistivity of the crystal gradually start to exhibit metallic behavior.

4.2.2. Tunneling Characteristic of Bi2212 Single Crystal

Figure 4.22. shows current voltage characteristics of YD 25. Measurements were taken at 10 K. I-V characteristic of Bi2212 mesas show a number of characteristic features of the multi stacked intrinsic Josephson junction. They includes several branches due to individual switching of each junction from Josephson state to quasiparticle state when the bias current exceeds the individual critical current of each junction (Yurgens 2000). Thus each of the junctions acts as one of the single branch. To obtain different quasiparticle branches, the bias voltage is continuously swept positively and negatively many times. While bias voltage increases, these branches appear such a

voltage jumps until all IJJs are completely in normal state. While decreasing bias voltage, I-V data does not trace these branches because there is a transition from normal state to superconducting state. This leads to hysteresis in the I-V characteristics.

From Figure 4.23., Temperature characteristics of a 60 µm mesa is seen, At 11K due to the heating effect a well-defined backbending is observed as the temperature rises up until 50 K, which has lose its robustness and we investigate that it is started to disappeared for the temperatures T≥50K.

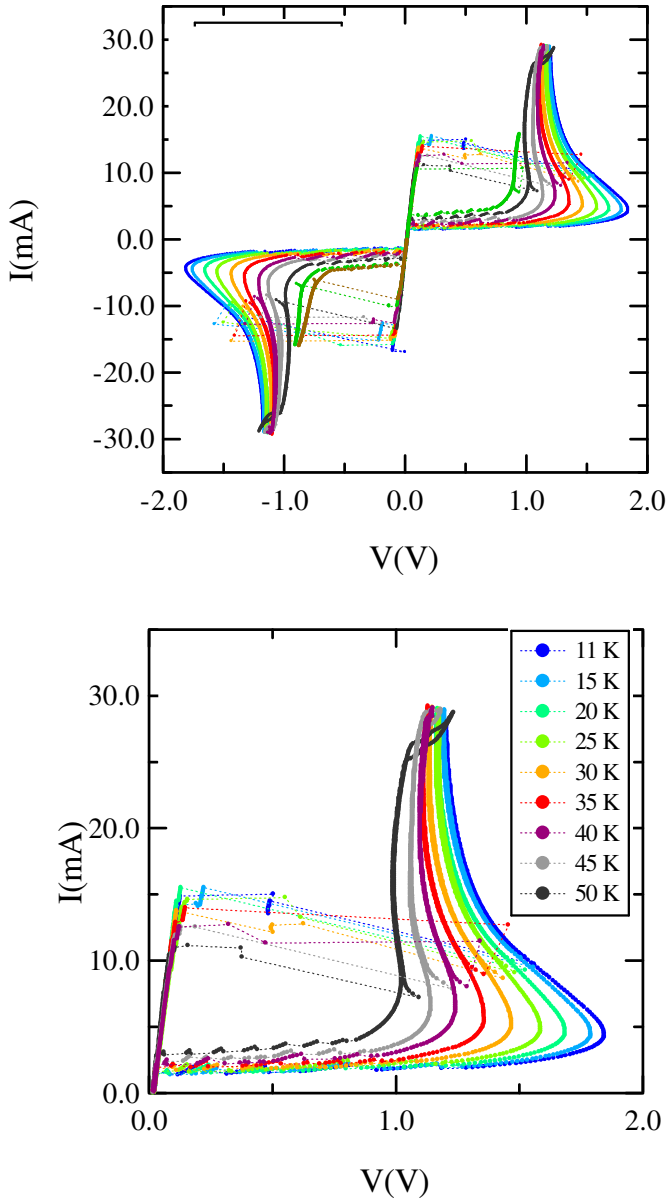

Figure 4.23. Temperature evolution of I-V measurement of YD 25 (a) and its detailed graph (b)

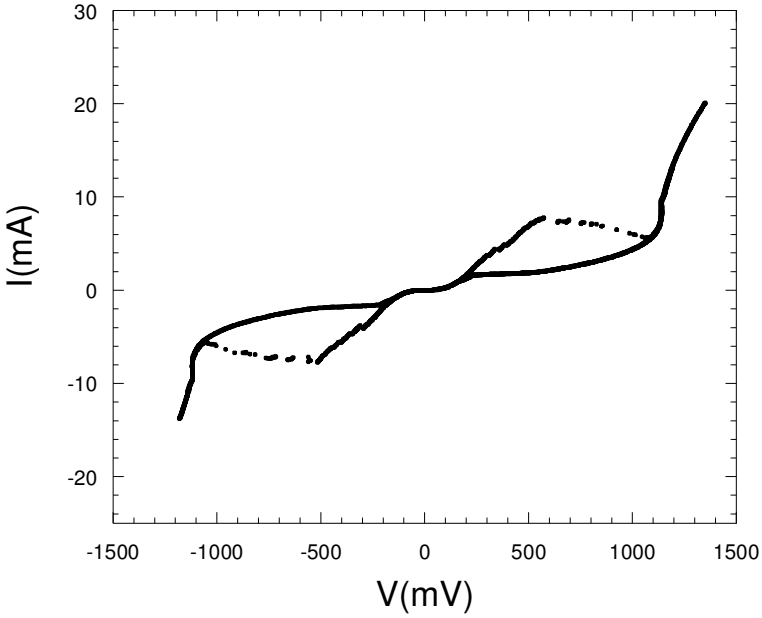

Figure 4.24. I-V measurement of YD 24 at 10K

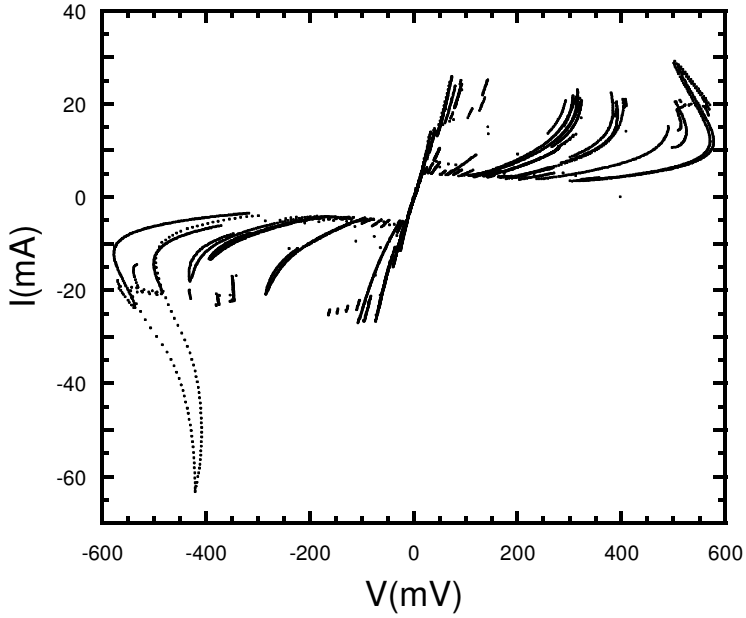

Figure 4.25. I-V measurement of YD 27 at 22 K

Josephson current with hysteresis behavior is seen at zero bias and it only occurs From cooper pair tunneling while all IJJs are in superconducting state. The hysteretic behavior of Josephson current results from switching the current from cooper pair tunneling to quasiparticle tunneling (Ozyuzer, et al. 2000). After exceeding of Josephson current, I-V data traces on quasiparticle branches that are one by one corresponding IJJs. The voltage value on which all of IJJs start to pass into normal state is called as total conductance peak of IJJs.

While decreasing bias voltage, I-V data does not trace these branches because there is a transition from normal state to superconducting state. There fore large hysteric I-V curve with many branches are obtained.

I-V measurements of YD 24 and YD 27 have been done at same temperature and their mesa sizes are almost same. However, ıf we compare the two graphs, it is seen that quasiparticle branches of YD 27 is more than YD 24. The critical current values are 7.6 mA and 26 mA respectively. Due to some measurement problems such as high swept frequency and quick increasing in amplitude of function generator output less quasiparticle branches are seen in some of our measurements. But general aspect reveals the heating effect. In order to obtain as much as more quasiparticle branches in I-V, the swept frequency should be low while ac bias current on mesa is swept negatively and positively by function generator.

Temperature dependence of c-axis tunneling characteristic of Bi2212 single crystals was analyzed by I-V measurements done at some constant temperatures. The tunneling behaviors from superconducting state to normal state are seen in figure 4.23 from the temperatures from 11 to 50 K which for the YD 25. In the superconducting I-V data, it is generally seen that total conductance peak value decreasing with increasing temperature. It is compatible with temperature dependence of energy gap of BCS theory mentioned in introduction part.

For this reason, decreasing in individual energy gap reveals reducing in total conductance peak of IJJ stacks. That could be intrinsically observed in spite of the presence of Joule heating in large number of IJJs.

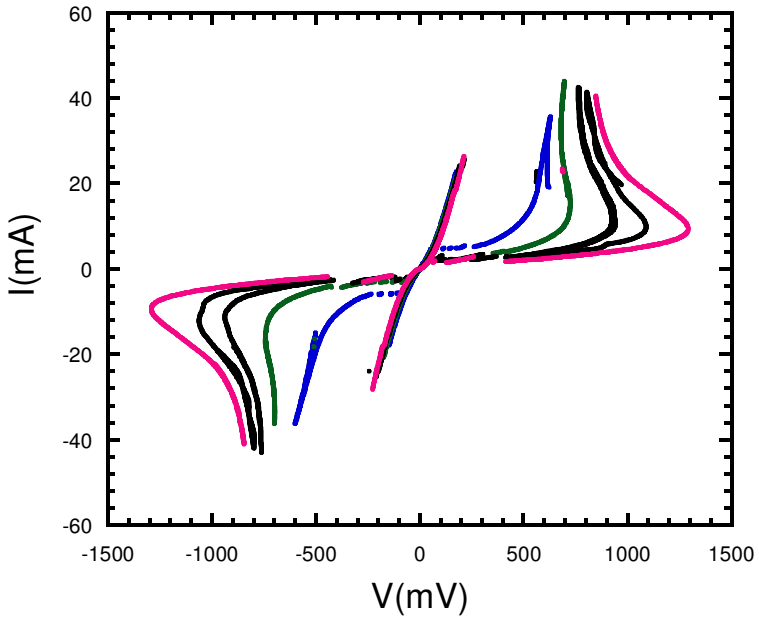

Figure 4.26. Temperature evolution of I-V measurement of YD 10

Above Tc, the energy gap feature and other superconducting behavior such a Josephson current are disappeared but there is an interesting result seen in I-V measurements of same mesa at different high temperatures. It is nonlinearities in I-V that is corresponds to increasing c-axis resistance with decreasing temperature. It is presented such pseudo-gap behaviors that are precursor of superconductivity and defines unusual pre-formed of pairs above T_c (Yurgens 2000). It has been observed in underdoped and overdoped Bi2212 single crystals. While it is very hard to observe presence of pseudo-gap in heavily doped Bi2212, feature of this gap is known as an underdoped behavior (Ozyuzer, et al. 2002).

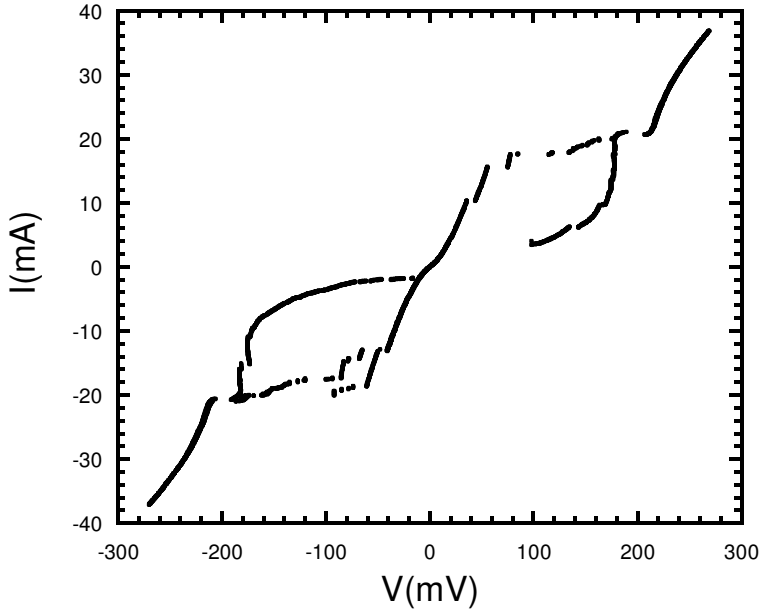

Figure 4.27. I-V measurement of YD 11

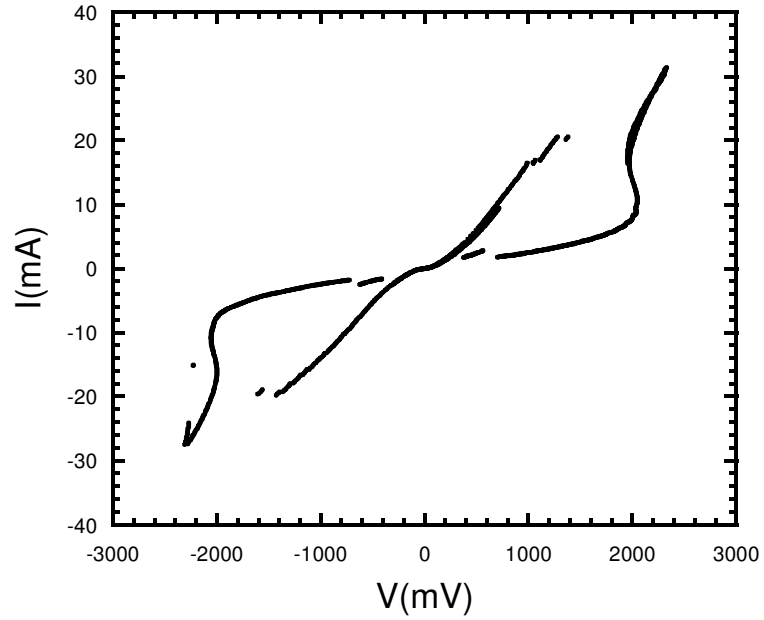

Figure 4.28. I-V measurement of YD 19

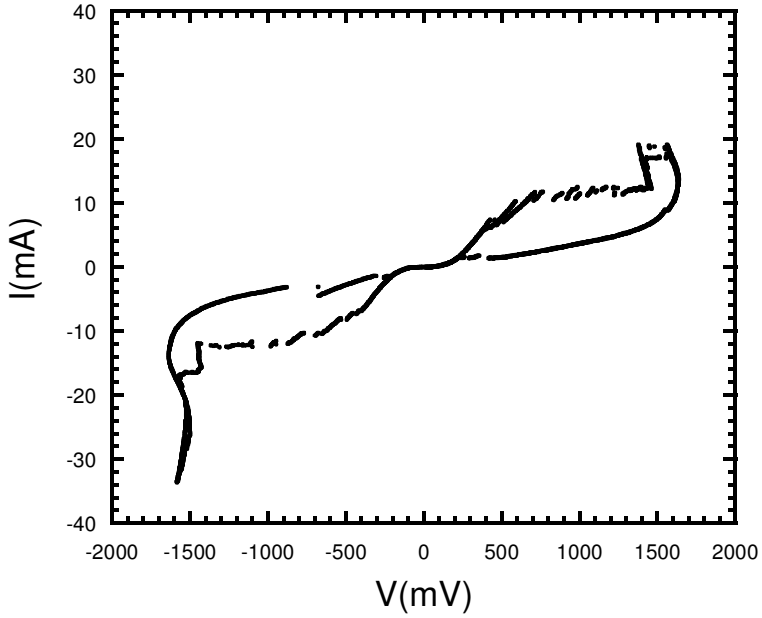

Figure 4.29. I-V measurement of YD 22

Figure 4.29. shows a typical I-V characteristics of one of the mesa patterned solid state device with 60x300 μm^2 at T=22 K. The backbending of the I-V curve at high voltages is due to self heating effects as indicated by the appearance of unpolarized blackbody radiation (Ozyuzer, et.al.2007).

CHAPTER 5

CONCLUSION

In this work, we work on a frequency tunable solid state device to meet the needs of continuous, coherent, powerful terahertz emission sources that fill practically important terahertz gap. In the previous studies, in our group we achieved to synchronize the Intrinsic Josephson junctions without any external source such as magnetic field, the designed rectangular mesa structures behave like cavity.

The most promising canditades of THz sources, high temperature superconductors have unfortunately poor thermal conductivity which causes heating problem and effect the emission negatively. From I-V graphs, backbending is observed as an obvious result of joule heating. By a pulsed emission or decreasing the number of Josephson layers we can decrease the heating effect but for practical applications we have to detect continous and powerful THz emission. Our approach for generation of powerful terahertz emission is to decrease the critical current density and reduce the heating effect so hole concentration was varied by changing the oxygen content of Bi2212.

Since doping dependence of Bi2212 is an important parameter, Bi2212 crystals are annealed in vacuum or purified argon gas flow at various temperatures for removal of oxygen. In mesa fabrication, mesa shaped PR mask was patterned by using either optical photolithography or electrom beam lithography processes and the rectangular mesa structures with required sizes were fabricated using Ar-ion beam etching. The lateral angles and heights of mesas were analyzed by SEM and Profilometer measurements. After the tunneling behaviors of natural layered structure of SIS junctions inside Bi2212 were characterized by R-T and I-V measurements, bolometric detection of emission from long lateral size of mesas were done.

We used Bi2212 single crystals grown by TSFZ method for the mesa fabrication. In long mesa fabrication processes, firstly, single crystal of Bi2212 is glued onto a sapphire substrate from its smooth a-b surface by silver epoxy. In order to get a fresh and smooth surface on Bi2212, the crystal was then cleaved with an adhesive tape and Au layer with the thickness of 100 nm was thermally deposited on the cleaved

crystal surface immediately to prevent the chemical reactions. 60-80x300 μm^2 mesa structures, their heights were up to 1500 nm, were fabricated on crystals by using standard optical photolithography or electron beam lithography and Ar ion beam etching techniques. Since the photoresist does not stand well and etched with ions rapidly, the samples were cooled by liquid N_2 during the etching process. Because of the difficulties in making a contact on small area of the mesa, firstly CaF_2 insulating layer is deposited by evaporation onto crystal and small area of the mesa then using lift-off technique with electron beam lithography a gold stripe with the width of 30 μm is deposited by evaporation on insulating layer and mesa. Finally three gold probe wires are connected to the two contact paths and mesa by silver epoxy. The contact on mesa was used as both the current and voltage leads.

In order to characterize the Bi2212 mesas, c-axis resistance versus temperature (R-T) and current-voltage (I-V) tunneling characteristics were investigated. R-T graphs of fabricated mesas exhibit a typical temperature dependence of the c-axis resistance of Bi2212 single crystal. The onsets of critical temperatures of the mesas are between 90 and 92.5 K. Both temperature dependence of the resistance and the superconducting transition temperatures are consistent with the near underdoped state of the Bi2212 crystals. In all R-T graphs, we observed contact surface resistance due to three-point measurement configuration. From the temperature evolution of the YD 25 we see that the critical current is decreasing with increasing temperature and also backbending is reduced at higher temperatures.

Some of the hysteretic quasiparticle branches are observed in the I–V characteristics of doped Bi2212 crystals. At high bias where heating severely affects the local mesa temperature, back bending of the I-V curve is observed because of high doping level and the large volume of the mesa. If we investigate the typical I-V characteristics of one of the mesa structures with 60x300 μm^2 at T=22 K, we observed the usual backbending of the I-V curve at high voltages is due to self heating effects as indicated by the appearance of unpolarized blackbody radiation.

To conclude up, in order to generate continuous and monochromatic THz radiation, the possible optimum doping level is searched. The measurements revealed distinct features of intrinsic Josephson junctions and the mesas exhibit usually underdoped behavior. Quite different from the process of photolithography, e-beam lithography requires higher efficiency for the fabrication of mesa structures. We observed hysteretic quasiparticle branches in the performed I-V measurements are all in

agreement with the mechanism of terahertz emission. Our results show a strong feasibility of developing high efficiency terahertz wave radiated devices that have non-ionizing nature and frequency tunability. Most importantly, electromagnetic emission in THz range may find many applications in near future.

REFERENCES

Akimitsu, J., A. Yamazaki, H. Sawa and H. Fujiki. 1987. Superconductivity in the Bi-Sr-Cu-O system. *Japanese Journal of Applied Physics* 26:2080.

Ambegaokar, V. and A. Baratoff. 1963. Tunneling between superconductors. *Physical Review Letters* 11:104.

Ambegaokar, V. and A. Baratoff. 1963. High temperature superconductors: Processing and science. *Physical Review Letters* 10:486.

Anderson, J. R. and J. M. Rowell. 1963. Probable observation of the Josephson superconducting tunnel effect. *Physical Review Letters* 10:230

Arnone, D. D., C. M. Ciesla, A. Coricha, S. Egusa, M. Pepper, J. M. Chamberlain,C. Bezant, R. Clothier and N. Khammo. 1999. Applications of terahertz (THz) tech-nology to medical imaging. Terahertz Spectroscopy and Applications II, ed. by J. M.Chamberlain. *Proceedings of SPIE* 3828:209–219

Bae, M. H., H. J. Lee and J. H. Choi. 2007. Josephson-vortex-flow terahertz emission in layered High-T_c superconducting single crystals. *Physical Review Letters* 98:027002

Barbara, P., A. B. Cawthorne, S. V. Shitov and C. J. Lobb. 1999. Stimulated Emission and Amplification in Josephson junction Arrays. *Physical Review Letters* 82:1963

Bardeen, J., L. N. Cooper and J. R. Schrieffer. 1957. The Theory of Superconductivity. *Physical Review Letters* 108:1175.

Batov, I. E., X. Y. Jin, S. V. Shitov, Y. Koval, P. Muller and A. V. Ustinov. 2006. Detection of 0.5 THz radiation from intrinsic $Bi_2Sr_2CaCu_2O_{8+x}$ Josephson junctions. *Applied Physics Letters* 88:262504.

Bednorz, J. G. and K. A. Müller. 1986. Possible high-Tc superconductivity in the Ba-La-Cu-O system. *Zeitschrift Physics B* 64:189.

Buckel, W. and R. Kleiner, eds. 2004. Superconductivity Fundamentals and Application. Tübingen: *Wiley-VCH* Verlag GmbH and Co. KGaA Weinheim.

Bulaevskii, L. N. and A. E. Koshelev. 2007. Radiation due to Josephson Oscillations in Layered Superconductors. *Physical Review Letters* 99:057002

Chu, C. W., P. H. Hor, R. L. Meng, L. Gao, Z. J. Huang and Y. Q. Wang. 1987. Evidence for superconductivity above 40 K in the La-Ba-Cu-O compound system. *Physical Review Letters* 58:405–407

Esaki, L. 1957. New Phenomenon in Narrow Germanium p-n Junctions. *Physical Review* 109:603.

Fischer, B., M. Hoffmann, H. Helm, G. Modjesch and P. U. Jepsen. 2005. Chemical recognition in terahertz time-domain spectroscopy and imaging. *Semiconductor Science and Technology* 20:S246–S253

Gaifullin, M. B., M. Matsuda, N. Chikumoto, J. Shimoyama and K. Kishio. 2000. Abrupt Change of Josephson Plasma Frequency at the Phase Boundary of the Bragg Glass in $Bi_2Sr_2CaCu_2O_{8+\delta}$. *Physical Review Letters* 84:2945

Gao, L., Y. Y. Xue, F. Chen, Q. Xiong, R. L. Meng, D. Ramirez, C. W. Chu, J. H. Eggert and H. K. Mao. 1994. Superconductivity up to 164 K in $HgBa_2Ca_{m-1}Cu_mO_{2m+2+\delta}$ (m=1,2 and 3) Under Quasihydrostatic Pressures. *Physical Review B* 50:4260

Giaever, I. 1960. Electron tunneling between two superconductors. *Physical Review Letters* 5:464.

Giaever, I. 1965. Detection of the ac Josephson Effect. *Physical Review Letters* 14:904.

Ginzburg, V. L. and L. D. Landau. 1950. On the theory of superconductivity. *Journal of Experimental and Theoretical Physics* 20:1064.

Gray, K. E. 1981. Plenum, New York. For a collection of review articles, see Nonequilibrium Superconductivity, Phonons, and Kapitza Boundaries, *Vol. 65 of NATO Advanced Study Institute, Series B: Physics*

Gray, K.E., L. Ozyuzer, A.E. Koshelev, C. Kurter, K. Kadowaki, T. Yamamoto, H. Minami, H. Yamaguchi, M. Tachiki, W.K. Kwok and U. Welp. 2009. Emission of Terahertz Waves from Stacks of Intrinsic Josephson Junctions. *IEEE Transactions on Applied Superconductivity* 19:886

Hazen, R. M., L. W. Finger, R. J. Angel, C. T. Prewitt, N. L. Ross, C. G. Hadidiacos, P.J. Heaney, D.R. Veblen, Z.Z. Shenh, A. El Ali and A.M. Hermann. 1988. 100 K superconducting phases in the Tl-Ca-Ba-Cu-O system. *Physical Review Letters* 60:1657.

H. B. Wang, S. Guenon, J. Yuan, A. Iishi, S. Arisawa, T. Hatano, T. Yamashita, D. Koelle and R. Kleiner. 2009, "Hot Spots and Waves in Bi2212 Intrinsic Josephson Junction Stacks: A Study by Low Temperature Scanning Laser Microscopy," *Physical Review Letters,* **102**, pp. 017006.

H. B. Wang, S. Guénon, B. Gross, J. Yuan, Z. G. Jiang, Y. Y. Zhong, M. Grünzweig, A. Iishi, P. H. Wu, T.Hatano, D. Koelle, and R. Kleiner. 2010. "Coherent Terahertz Emission of Intrinsic Josephson Junction Stacks in the Hot Spot Regime," *Applied Physical Letters.,* **105**, pp. 057002.

Irie, A., Y. Hirai and G. Oya. 1998. Fiske and flux-flow modes of the intrinsic Josephson junctions in Bi2Sr2CaCu2Oy mesas. *Applied Physical Letters* 72:2159

Ishibashi, T., K. Sato, K. Yonemitsu, K. Sato, K. Lee and S. Kim. 2001. Spin tunneling in Co/Au/I/BiSrCaCuO tunnel junctions. *Superconductor Science & Technology* 14:1014-1017

Jain, A. K., K. K. Likharev, J. E. Lukens and J. E. Sauvageau. 1984. Mutual phase-locking in Josephson junction arrays. *Physics Reports* 109:309

Josephson, B. D. 1962. Possible new effects in superconductive tunneling. *Physics Letter* 1:251-253.

Josephson, B. D. 1964. Coupled Superconductors. *Review of Modern Physics* 36:216–220

Josephson, B. D. 1974. The discovery of tunnelling supercurrents. *Review of Modern Physics* 46(2):251-254

Kadowaki, K., I. Kakeya, T. Yamamoto, T. Yamazaki, M. Kohri and Y. Kubo. 2006. Dynamical properties of Josephson vortices in mesoscopic intrinsic Josephson junctions in single crystalline $Bi_2Sr_2CaCu_2O_{8+d}$. *Physica C* 437-438:111-117

Kadowaki, K., H. Yamaguchi, K. Kawamata, T. Yamamoto, H. Minami, I. Kakeya, U. Welp, L. Ozyuzer, A. Koshelev, C. Kurter, K. E. Gray and W. K. Kwok. 2008. Direct observation of terahertz electromagnetic waves emitted from intrinsic Josephson junctions in single crystalline $Bi_2Sr_2CaCu_2O_{8+d}$. *Physica C* 468:634-639

Kadowaki, K., M. Tsujimoto, K. Yamaki, T. Yamamoto, T. Kashiwagi, H. Minami, M. Tachiki and R. A. Klemm. 2010. Evidence for a Dual-Source Mechanism of Terahertz Radiation from Rectangular Mesas of Single Crystalline $Bi_2Sr_2CaCu_2O_{8+\delta}$ Intrinsic Josephson Junctions. *Journal of the Physical Society of Japan* 79:023703

Kamihara, Y., H. Hiramatsu, M. Hirano, R. Kawamura, H. Yanagi, T. Kamiya and H. Hosono. 2006. Iron-based layered superconductor: LaOFeP. *Journal of the American Chemical Society* 128, 10012–10013

Kawase, K. 2004. Terahertz imaging for drug detection & large scale integrated circuit inspection. *Optics & Photonics News* 15:34–39

Kleiner R., F. Steinmeyer, G. Kunkel, and P. Müller. 1992. Intrinsic Josephson effects in $Bi_2Sr_2CaCu_2O_8$ single crystals. *Physical Review Letters* 68:2394.

Kleiner, R. 1994. Two-dimensional resonant modes in stacked Josephson junctions. *Physical Review B* 50:6919.

Koshelev, A. E. and I. Aranson. 2001. Dynamic structure selection and instabilities of driven Josephson lattice in high-temperature superconductor. *Physical Review B* 64:174508

Koshelev A. E. and L. N. Bulaevskii. 2008. Resonant electromagnetic emission from intrinsic Josephson junction stacks with laterally modulated Josephson critical current. *Physical Review B* 77:014530

Krasnov, V. M. 2006. Quantum Cascade Phenomenon in $Bi_2Sr_2CaCu_2O_{8+\delta}$ Single Crystals. *Physical Review Letters* 97:257003

Kume, E. I., Iguchi, and H. Takahashi. 1999. On-chip spectroscopic detection of terahertz radiation emitted from a quasiparticle-injected nonequilibrium superconductor using a high-T_c Josephson junction. *Applied Physics Letters* 75:2809

Kurter, C., K. E. Gray, J. F. Zasadzinski, L. Ozyuzer, A. E. Koshelev, Q. Li, T. Yamamoto, K. Kadowaki, W. K. Kwok, M. Tachiki and U. Welp. 2009. Thermal Management in Large Bi2212 Mesas Used for Terahertz Sources. *IEEE Transactions on Applied Superconductivity* 19:428

Langenberg, D. N., D. J. Scalapino, B. N. Taylor, and R. E. Eck. 1965. Investigation of Microwave Radiation Emitted by Josephson Junctions. *Physical Review Letter* 15:294.

Lin, S. and X. Hu. 2008. Possible Dynamic States in Inductively Coupled Intrinsic Josephson Junctions of Layered High-T_c Superconductors. *Physical Review Letters* 100:247006.

Lukens, J. 1990. Superconducting Devices, *Plenum Press* p-135

Maeda, H., T. Tanaka, M. Fukutomi and T. Asano. 1988. A New high-Tc oxide superconductor without a rare earth element. *Japanese Journal of Applied Physics* 27:L209.

Madsen, S., G. Fillatrella, and N. F. Pedersen. 2004. Interaction between a BSCCO-type intrinsic Josephson junction and a microwave cavity. *European Physical Journal B* 40:209

Maxwell, E. 1950. Isotope Effect in the Superconductivity of Mercury. *Physical Review* 78:477.

Meissner, W. and R. Ochsenfeld. 1933. Ein neuer effect bei eintritt der supraleitfahigkeit. *Naturwissenschaften* 21(44):787

Minami, H., I. Kakeya, H. Yamaguchi, T. Yamamoto and K. Kadowaki. 2009. Characteristics of terahertz radiation emitted from the intrinsic Josephson junctions in high-T_c superconductor $Bi_2Sr_2CaCu_2O_{8+\delta}$. *Applied Physics Letters* 95:232511

Miyakawa, N., P. Guptasarma, J.F. Zasadzinski, D.G. Hink and K.E. Gray. 1998. Strong dependence of the Superconducting gap on oxygen doping from tunneling measurements on $Bi_2Sr_2CaCu_2O_{8+x}$. *Physical Review Letters* 80:157.

Mott, N. F. 1936a. The electrical conductivity of transition metals. *Proceedings of the Royal Society* 153:699–717

Nagamatsu, J., N. Nakagawa, T. Muranaka, Y. Zenitani and J. Akimitsu. 2001. Superconductivity at 39 K in magnesium diboride. *Nature* 410:63-64

Onnes, H. K. 1911. Disappearance of the electrical resistance of mercury of Helium temperature. *Akad. Van Wetenschappen* (Amsterdam) 14:113.

Ozyuzer, L., A. E. Koshelev, C. Kurter, N. Gopalsami, Q. Li, M. Tachiki, K. Kadowaki, T. Tamamoto, H. Minami, H. Yamaguchi, T. Tachiki, K. E. Gray, W. K. Kwok and U. Welp. 2007. Emission of coherent THz radiation from superconductors. *Science* 318:1291

Ozyuzer, L., Y. Simsek, H. Koseoglu, F. Turkoglu, C. Kurter, U. Welp, A. E. Koshelev, K. E. Gray, W. K. Kwok, T. Yamamoto, K. Kadowaki, Y. Koval, H. B. Wang, and P. Müller. 2009. Terahertz wave emission from intrinsic Josephson junctions in high-T_c superconductors. *Superconductor Science & Technology* 22:114009

Poole, C. P., A. F. Horacio and J. C. Richard. 1995. Superconductivity, *Academic Press*, California

P. Barbara, P., A. B. Cawthorne, S. V. Shitov and C. J. Lobb. 1999, " Stimulated Emission and Amplification in Josephson junction Arrays, " *Physical Review Letters.,* **82** , pp. 1963.

Reynolds, C. A., B. Serin, W. H. Wright, and L. B. Nesbitt. 1950. Superconductivity of Isotopes of Mercury. *Physical Review* 78:487.

Romano, P., J. Chen and J. F. Zasadzinski. 1998. Josephson and Quasiparticle Tunneling in SIS Junctions $Bi_2Sr_2CaCu_2O_8$ and $Bi_2Sr_2CuO_6$. *Physica C* 295:15

Saldin, E. L., E. A. Schneidmiller and M. V. Yurkov. 2000. The Physics of Free ElectronLasers, Advanced Texts in Physics. New York: *Springer-Verlag*, Berlin.

Schilling, A., M. Cantoni, J. D. Guo and H. R. Ott. 1993. Superconductivity above 130 K in the Hg-Ba-Ca-Cu-O System. *Nature* 363:56.

Schmid, A. and G. Schön. 1975. Linearized kinetic equations and relaxation processes of a superconductor near T_c. *Journal of Low Temperature Physics* 20:207

Shapiro, S. 1963. Josephson currents in superconducting tunneling: the effect of microwaves and other observations. *Physical Review Letters* 11:80

Suziki, M., T. Watanabe and A. Matsuda. 1999. Short pulse tunneling measurements of intrinsic Josephson junction in Bi-Sr-Ca-O. *IEEE Transactions on Applied Superconductivity* 9:4507

Suzuki, M., T. Hamatani, Y. Yamada, K. Anagawa and T. Watanabe. 2009. Significantly doping-dependent Josephson critical current–Inhomogeneity in real space or heterogeneity in k-space. *Journal of Physics: Conference Series* 150:052252

Tachiki, M., S. Fukuya and T. Koyama. 2009. Mechanism of Terahertz Electromagnetic Wave Emission from Intrinsic Josephson Junctions. *Physical Review Letters* 102:127002

Taillefer, L., B. Lussier, R. Gagnon, K. Behnia, and H. Aubin. 1997. Universal heatconduction in YBa_2Cu_3O6. *Physical Review Letters* 79:483–486

Takahashi, H., K. Igawa, K. Arii, Y. Kamihara, M. Hirano and H. Hosono. 2008. Superconductivity at 43 K in an iron-based layered compound LaO1-xFxFeAs. *Nature* 453(7193): 376–378

Tanabe, K., Y. Hidaka, S. Karimoto and M. Suzuki. 1996. Observation of both pair and quasiparticle tunneling in intrinsic junction stacks fabricated on $Bi_2Sr_2CaCu_2O_{8+x}$ single crystals. *Physical Review B* 53:9348

Tinkham, M. 1996. Introduction to Superconductivity, 2nd ed. *McGrawHill*, New York

Tonouchi, M. 2007. Cutting-edge terahertz technology. *Nature Photonics* 1:97-105

Wade, A., G. Fedorov, D. Smirnov, S. Kumar, B. S. Williams, Q. Hu and J. L. Reno 2009. Magnetic-field-assisted terahertz quantum cascade laser operating up to 225 K. *Nature Photonics* 3:41

Wang H. B., S. Guenon, J. Yuan, A. Iishi, S. Arisawa, T. Hatano, T. Yamashita, D. Koelle and R. Kleiner. Hot Spots and Waves in $Bi_2Sr_2CaCu_2O_8$ Intrinsic Josephson Junction Stacks: A Study by Low Temperature Scanning Laser Microscopy. 2009. *Physical Review Letters* 102:017006

Wesche, R. 1998. High Temperature Superconductor Materials, Properties, and Application. Boston: *Academic Publishers*

Wu, M. K., J. R. Ashburn, , C. J. Torng, P. H. Hor, R. L. Meng, L. Gao, Z. J. Huang, Y. Q. Wang and C. W. Chu. 1987. Superconductivity at 93 K in a New Mixed-Phase Y-Ba-Cu-O Compound System at Ambient Pressure. *Physical Review Letters* 58:908

Yurgens, A., D. Winkler, N. V. Zavaritski and T. Claeson. 1996a. Strong temperature dependence of the c-axis gap parameter of $Bi_2Sr_2CaCu_2O_{8+x}$ intrinsic Josephson junctions. *Physical Review B* 53:R8887.

Yurgens, A. 2000. Intrinsic Josephson junctions: Recent developments. *Superconductor Science and Technology* 13:R85-100.

Yurgens, A., D. Winkler, T. Claeson, S. Ono and Y. Ando. 2004. Yurgens et al. Reply. *Physical Review Letters* 92:259702

Zasadzinski, J. 2002. Tunneling spectroscopy of conventional and unconventional superconductors: The Physics of Superconductor, Edited by Bennemann, K., H. and Ketterson, J. New York: Springer

Zhi-An, R., L. Wei, Y. Jie, Y. Wei, S. Xiao-Li, Z. Cai, C. Guang-Can, D. Xiao-Li, S. Li-Ling, Z. Fang and Z. Zhong-Xian. 2008. Superconductivity at 55 K in Iron-Based F-Doped Layered Quaternary Compound $Sm[O_{1-x}F_x]FeAs$. *Chinese Physics Letters* 25(6):2215

Zhu, X. B., Y. F. Wei, S. P. Zhao, G. H. Chen, H. F. Yang, A. Z. Jin, and C. Z. Gu. 2006. Intrinsic tunneling spectroscopy of $Bi_2Sr_2CaCu_2O_{8+\delta}$: The junction-size dependence of self-heating. *Physical Review B* 73:224501